SECONDARY FLOW IN COMPRESSOR CASCADES

Thesis by

Charles A. Lindley

In Partial Fulfillment of the Requirements

For the Degree of

Doctor of Philosophy

California Institute of Technology

Pasadena, California

1956

ACKNOWLEDGEMENTS

I wish to express my sincere gratitude to Dr. W. D. Rannie for his guidance, many important ideas, constructive criticism, and encouragement in this research. I also wish to thank Dr. F. E. Marble for his advice and continuing interest in the problem.

I wish to express my appreciation to Mr. F. T. Linton for his aid in the design, construction, and operation of the cascade tunnel and equipment, and for his help in preparing the thesis.

Of considerable aid in the large job of reduction of data and preparation of diagrams and plots were Miss Janet Chandler and Miss Ann Wayland. The typing was done by Miss Ruth Winkel, and the majority of the final figures by Mrs. Barbara Dixon. Many others at the California Institute of Technology contributed aid or advice to the success of the project.

The project was sponsored by the Air Research and Development Command under Contract No. AF 18(600)-178, and the author received financial assistance from a Daniel and Florence Guggenheim Foundation Fellowship in Jet Propulsion.

ABSTRACT

An experimental study was made of the secondary flow in a compressor cascade. Detailed surveys of the entire flow channel at various operating conditions are presented. The chief difference of the experimental results from those predicted by linearized theory was the presence of a turbulent separation region at the corner of the wall and the low pressure surface of the blade. While the actual losses involved were small, the effects on the succeeding stages of a turbomachine might be more severe.

TABLE OF CONTENTS

SYMBOLS

b = half-width of channel in stagger direction

P = pressure

Q = dynamic head

R_n = Reynolds number, based on blade chord length

V = velocity

v = velocity component in stagger direction

w = velocity component in span direction

y = distance in stagger direction

z = distance in spanwise direction

α = angle of attack

ϵ = channel turning angle

δ = total boundary layer thickness

ζ = vorticity component in flow direction

Γ = circulation

ψ = perturbation stream function of secondary flow

ϕ = perturbation velocity potential of secondary flow

Subscripts

1 = inlet

2 = outlet

T = total

s = static

SUMMARY

There has been in recent years, great interest in "secondary flow" in turbomachines. In the simplest model, these result from a velocity gradient in a flow approaching a bend in a passage such that the vorticity vector initially is normal to the incoming flow direction and in the plane of turning. Downstream of the bend, a vorticity component appears in the direction of the main stream flow, giving rise to the secondary flows. Such conditions occur when the boundary layer on a wall enters a row of turning vanes or airfoils perpendicular to the wall.

The secondary flow velocity distribution has been calculated with simplifying linearizations by a number of investigators. The calculated kinetic energy of the secondary vorticity, which must be assumed as lost in a turbomachine, is small in most examples. On the other hand, the overall losses that have been measured in turbomachines are appreciably higher than can be accounted for by the friction of two-dimensional flow on blades and end walls. The few detailed measurements of the secondary flow in compressor cascades that have been made in the past have indicated large losses, but have not established the mechanism of these losses. Hence it was decided to carry out such measurements in a large cascade with adequate Reynolds number, to determine whether the secondary flow theory was satisfactory, and to attempt to trace the source of the losses.

The experimental results obtained showed that the losses were not appreciably greater than would be expected from surface friction

alone. However, a three-dimensional, turbulent separation was found to occur at the corner of the end wall and the low pressure surface of the blade. This separation resulted from the adverse pressure gradient, combined with the low velocity of the boundary layer air. The direct losses involved in this separation, however, were quite small.

The pressure gradients under which this separation developed, and its variation with angle of attack, were studied experimentally. It was found that the separation was not present for angles of attack somewhat lower than the design angle of the cascade, but appeared rather abruptly at an angle of attack just above the design value, and steadily increased in size with increasing angles up to the positive stall. A similar separated region appeared on the opposite side of the blade for negative angles of attack just before the negative stall.

The secondary flow velocities obtained experimentally were compared with those obtained from a linearized model based on Squire and Winter's work. The analytical model is of some value, in that it gives secondary flow velocities of the right order of magnitude, and in the right general direction over most of the channel. However, this simple model takes no account of the three-dimensional boundary layer effects that are responsible for the corner separation. These latter effects are not amenable to analysis.

Another and entirely different model of the secondary flow based on a lifting line theory has sometimes been proposed. In such a model the circulation around the blade is shed in a strong vortex near the wall. Although previous observers have found indications of such a flow, no

definite trailing vortex could be produced in the present cascade.

In the course of the experiments, it was found that a very small amount of flow leakage through the clearance space between the blade tip and the wall resulted in rather drastic changes in the flow patterns near the separation region. The size of the clearance space and the amount of leakage involved were such as to make the severity of the effect most surprising. Apparently very small quantities of leakage had a large effect on the three-dimensional separation. This effect could be prevented only by positive sealing.

The actual losses occurring in the wall boundary layers passing through the cascade were found to be quite small, despite the presence of the separation region. In an actual turbomachine, however, the effects on the performance of succeeding blade rows operating in the wakes of the observed separation regions may be significant. Unfortunately, it is an extremely difficult task to simulate in a cascade the effects resulting from relative motion of successive blade rows. Although moving belts, and similar devices have been tried, the resulting models are not very satisfactory. The effects of the flow pattern leaving one cascade on the performance of succeeding cascades in relative motion will probably have to be determined in rotating machinery, despite the difficulty of such tests.

I. INTRODUCTION

The development of turbomachinery has been largely paced and controlled by improvements in the efficiency of its components. In particular, the specific fuel consumption and the specific output of the gas turbine are quite sensitive to the efficiencies of the compressor and turbine. This sensitivity results from the fact that the majority of the work of the turbine is required to drive the compressor, so that a small increase in the efficiency of either results in a larger increase in the margin of useful work available from the machine.

Improvements in the design of the compressor and turbine have been based, for the most part, on general theories of the overall flow in the machine, without any real understanding of the details of the flow. This approach has been necessary because of the tremendous complexity of the actual internal flows involved. The efficiencies of well designed components are now running in the neighborhood of 90 $^{o}/o$ at design operating conditions. However, efficiencies usually fall off quite rapidly at off-design operating conditions, especially for axial flow compressors.

Since these off-design operating conditions are encountered by most turbomachines in practical operation, they must be given some consideration in the design of the components. In order to improve off-design performance significantly, it will almost certainly be necessary to study the details of the flow around the individual blades. It appears possible that small improvements in design performance may also be obtained from more detailed study.

In a typical axial flow compressor, with which this report is chiefly concerned, the losses associated with the boundary layers

created by flow around the blades are actually quite small. Expressed in terms of loss of adiabatic compressor efficiency, they may amount to only about 4 °/o. Since hub and tip casings are required to contain and guide the flow, a small additional loss in case skin friction here is unavoidable, perhaps to the extent of 1 - 2 °/o in adiabatic efficiency. The remaining efficiency losses at design flow are not so clearly unavoidable. However, the question of whether they can be greatly reduced or eliminated cannot be answered until we understand the details of their nature and causes much more clearly than we do at the present time. At off-design conditions, the losses which can be attributed to simple blade and casing boundary layers increases, but the total actual losses increase much more, leaving an even larger proportion of the actual losses to be explained in terms of other mechanisms.

Among the flow mechanisms that may cause additional losses in the compressor are; flow leakage through clearance spaces (either blade tips or shrouds), unsteady flow through succeeding stages caused by the passage of the wakes of preceeding blades, off-design flow on the blades near the casings caused by distortions of the flow direction and velocity in the case boundary layers, and secondary flows, a term sometimes used to describe the whole class of three-dimensional flows induced by the interaction of the "design" two-dimensional flow with the blade, casing, and inlet boundary layers. It is generally believed that these phenomena account for the discrepancies between losses estimated on the basis of simple blade and casing boundary layer losses, and the losses that actually occur. Attempts have been made by various

authors[1, 2, 3] to sort out the approximate magnitude and importance of these various phenomena. Unfortunately it is not possible to isolate the exact contribution of each. As a matter of fact, they are probably inseparable, in the sense that there is considerable interaction between them.

Nevertheless, there is a serious need to gain, by some combination of experimental and analytical efforts, a better estimate of the relative magnitude, and an understanding of the mechanism of each. Only after gaining such a basic understanding can we hope to obtain significant improvements in both design and off-design performance of axial flow turbomachinery. The present work is concerned with the effects of the secondary flow in compressor blade passages.

In recent years, a number of attempts have been made to describe analytically the secondary flow in a channel or cascade passage. These attempts have met with only moderate success, and have not clearly shown the mechanism of any large losses associated with secondary flow. The problem is inherently a very difficult one of rotational flow.

Early attempts were based on theories analogous to those successfully used in the induced drag problem for a finite wing, in which the lifting airfoil is represented by a bound line vortex or "lifting line". Theodore von Karman and H. S. Tsien[4] made the necessary extension of the lifting line theory to the case of a general, non-uniform entrance velocity. In this extension, however, the lifting line was still assumed to be lightly loaded, so that the flow differs only slightly from a uniform parallel flow. This linearization is not applicable to most cascades.

Carter and Cohen[5] used as an analytical model a series of lifting lines, with trailing vortices at a distance from the wall proportional to the average of the boundary layer thickness before and behind the cascade. They set up a system of vortices and images to represent this model, and calculated the induced angle of incidence at the center of the cascade, and an "induced drag coefficient" for the cascade. George Hausman[6] uses a similar system to calculate the induced deflection angles, with some effort to include the details of the circulation disturibution on the line vortex in the wall boundary layer.

The weakness of all such solutions lies in the failure of typical cascade flows to satisfy the fundamental requirement that the span be large compared with the chord, or that the variation of the velocity in the spanwise direction be small compared with that in the plane normal to the span. However, the frequent experimental observation (for instance, see Reference 5) that a rolled-up core of losses, sometimes referred to as a "passage vortex", may appear trailing downstream of the blade near the wall gave some support to the lifting line theory. This phenomenon, which did not occur in the present tests, will be discussed further in the body of this paper.

A different analytical approach was used by Squire and Winter[7]. Their model was an inviscid, incompressible flow through a channel of large turning angle with the incoming boundary layer considered as a field of vorticity normal to the flow. As the flow passes through the cascade, a component of the vorticity is turned into the flow direction, and this vorticity component causes the secondary flow. In their treat-

ment, the secondary flow was treated as a perturbation on the two-dimensional "design" flow, making possible a linearization of the problem. The secondary vorticity was obtained as an integral along the streamline through the cascade, and was then integrated along the streamlines of the "design" flow, giving the result

$$\zeta = -2\epsilon \frac{\partial U}{\partial z}$$

where ϵ is the cascade turning angle, and $\frac{\partial U}{\partial z}$ is the incoming vorticity strength. This result is strictly applicable only for a curved channel with small velocity gradient $\frac{\partial U}{\partial z}$ into the channel. The authors then gave an approximate solution for the secondary velocities and stream function in a bend of high aspect ratio and rectangular cross-section, and compared the results with experimental results taken from a study of the turning vanes in a wind tunnel. Unfortunately, the approximate solution is not generally applicable. Nevertheless, the secondary vorticity solution is correct, within the limits of the assumptions, and is a result of the utmost importance. The result is applicable to a wide range of practical problems to which the incoming rotational layer is of considerable extent and the channel turning is moderate.

Following up the work of Squire and Winter, Hawthorne[8] developed a more general theory for the flow of an inviscid, incompressible, rotational fluid in three dimensions, concentrating on the component of vorticity in the direction of flow. His result was a relatively simple equation expressing the rate of change of secondary vorticity along a streamline in terms of a line integral of quantities along the

streamline. This expression reduces to the result of Squire and Winter when applied to that linearized case. Hawthorne went on to work out an approximate solution for the secondary flow in a pipe with an entrance velocity profile varying in only one direction. His solution predicted a secondary flow of an oscillatory nature, which he confirmed with experimental results. He concluded with an experimental study of the secondary flow in a rectangular pipe bend, and showed that this too, is of an oscillatory nature if the turn continues long enough. The period of this oscillation, however, is so long that it is of no practical interest in typical compressor cascades such as that studied in the present report.

Eichenberger[9], working with Hawthorne, made an experimental study of the secondary flow in a 90^{o} bend of rectangular cross-section. He concluded that the energy lost in the kinetic energy of secondary flow leaving the cascade, was less than 1 $^{o}/o$ of the energy entering the bend and that the actual energy dissipation in the bend was small. He stated that the cores of high losses observed in cascade tests were not losses due to trailing vorticity, but actually displaced wall boundary layers, and that the major part of the secondary losses in compressors occurs in the following stages, because of bad angle of attack variations resulting from secondary flow.

Eichenberger also solved an analytical model for his experimental case. He got a Poisson's equation equivalent to that of Squire and Winter, and an approximate solution for the equation within a square boundary. This solution checked his experimental data very well.

A similar study on a bend of circular cross-section was made by Detra[10] at about the same time. His experimental work included total pressure surveys at the bend outlet for several inlet velocity profiles, and for turning angles of 21° and 42°. In the analytical parts of his paper, he set up a Green's function for the flow velocities in a circular boundary, resulting from any given distribution of vorticity, and worked out a simple example. He then tried a new theoretical approach to the secondary flow problem, in which he replaced the "centrifugal forces" in a curved flow by equivalent "body forces" in a straight flow. He resorted to essentially the same perturbation assumption as Squire and Winter, and got a partial differential equation that could be solved only numerically. For an axisymmetric inlet velocity distribution, the differential equation reduced to an ordinary one, which was solved by numerical methods for several inlet distributions. The solutions compared favorably with experiment up to the point where the self-transport was rather large.

One of the chief weaknesses of the previous analytical models is that, in order to linearize the problem, the self-transport of the secondary vorticity has been neglected, that is, the secondary vorticity has been assumed to be carried with the two-dimensional flow, but not affected by the perturbation velocities which the vorticity itself induces. While this is a reasonable approximation for a number of cases in which either the channel turning or the initial boundary layer gradient is small, in a large number of cases of practical interest the self-transport is sufficient to remove most of the boundary layer from the wall on which it entered, and carry it to the low pressure side of the blade

near the wall. It seems evident that the secondary flow velocities resulting from such a secondary vorticity distribution will be noticeably different from those resulting from the linearized assumption. In order to correct for this self-transport effect, it is necessary, in principle, to follow the displacement of the secondary vorticity as it passes through the passage.

Loos[11] developed a model to take approximate account of vorticity self-transport. He assumed the secondary vorticity at the cascade outlet to be uniformly distributed over two rectangular regions at the intersections of the low pressure surface of the blade and the end walls. The proportions of these rectangles were determined from a rather artificial condition of constancy of kinetic energy. The model was inadequate, in that it contains no criteria for deciding when to assume no self-transport, when to assume self-transport to the prescribed position, and when the self-transport may be assumed to have exceeded that described by the model. However, it seems likely that with the substitution of some empirical, experimentally based rules for determining the dimensions of the rectangles, the model could be extremely useful.

Several other items worthy of notice were covered in Loos's report. He pointed out the fact that the inverse hodograph plane is useful in evaluating the integral in Hawthorne's formula for the growth of secondary vorticity. He also applied Hawthorne's formula to the logarithmic spiral flow of a source-vortex combination, and obtained a simple correction factor to be applied to Squire and Winter's result,

for the secondary vorticity in a converging or diverging channel. An estimate was made of the losses caused in succeeding cascades by unsteady flows resulting from displacement of the low velocity fluid by secondary flows. The estimated loss was large, but it is difficult to judge its validity.

The self-transport of the boundary layer in the secondary flow process was discussed in some detail by Ehrich and Detra[2]. A simple graphical procedure was shown, whereby, given the perturbation stream function of the secondary flow, the transport of the boundary layer during passage through the cascade could be traced. In principle, using this method, one could calculate alternately the secondary flow stream function and the new secondary vorticity distribution at successive positions through the cascade, and so solve the complete problem including self-transport. However, since neither solution was done analytically in this paper, the method would be exceedingly long and tedious. Expression of either or both solutions in analytic form might reduce the necessary labor to a reasonable level.

The present experimental study was intended to compare the actual secondary flow with the predictions of the two principal perfect fluid models, the lifting line model, and the channel flow model of Squire and Winter. It was hoped to determine the significance of diffusion, self-transport, and other effects not properly accounted for in the analytical models, in order to clarify their range of applicability.

A second purpose of the tests was to determine whether large losses occur in the wall boundary layer of a cascade, and, if so, to

determine the mechanism of these losses. It was hoped that the source of some of the unexplained losses that actually occur in axial flow compressors might be located by this study.

II. EXPERIMENTAL EQUIPMENT AND TECHNIQUE

The cascade wind tunnel used in these tests was designed and built specifically for the study of secondary flow and critical Reynolds number effects in conventional subsonic compressor cascades. It is a large low-speed, open-return tunnel of wooden construction. The general size and layout are shown in Figure 1. Photographs of the tunnel are shown in Figures 2 and 3.

Because of the intention to study critical Reynolds number effects in addition to the present subject, special attention was given to producing a uniform, steady, low-turbulence flow at the inlet to the test section, with a very thin wall boundary layer. The inlet bell has an area contraction ratio of 16:1, and the inlet to the bell is faced with a layer of honeycomb paper, followed by two layers of screening. The resulting flow is quite steady, and the turbulence level is probably quite low compared to most cascade tunnels. The loss of total head caused by this inlet arrangement was of the order of 10 $^{o}/o$ of the total head at the test section, and, to the accuracy of the measurements, constant over the entire flow.

The test section of the tunnel is 2' x 3', with five blades of 8-1/2" chord length. The general layout of the test section is shown in Figure 4, and a photograph in Figure 5. It may be noted that the aspect ratio and number of channels are both far below those recommended by Howell[13] for valid "two-dimensional" data, but there is no desire to get "two-dimensional" data in the present tunnel.

Since the natural boundary layer of the tunnel was quite thin, it

was necessary to use a "fence" to create a thick, turbulent boundary layer on the lower wall for the secondary flow studies. This fence was set at the exit of the nozzle, as shown in Figure 6. A survey of the boundary layer created at the cascade position when there was no cascade in the tunnel, is shown in Figure 7. The correspondence with a 1/7 power law profile can be seen to be good. However, with the blades in place, the velocity profile in the survey made one blade chord length ahead of the leading edges was more nearly linear, as shown in Figure 8. Part of the change probably occurred because some of the cascade pressure rise was propagated ahead of the blades at the wall. Part of the change may have been caused by advancing the survey point nearer to the boundary layer fence, although it is still nearly three chord lengths behind it. It is felt that this velocity profile is reasonably typical of the profiles encountered in actual compressors. The boundary layer at the top of the test section inlet was not artificially thickened, and had a total thickness of not more than 1/4". The resultant cascade flow was of course, not symmetrical.

The tunnel was powered by a 30 hp., 3-phase, AC220 v, electric motor driving a fan, with speed control by a drum switch and grid resistor box. This system only allowed the operator a number of discreet speed settings, with no fine adjustments, so that fluctuating line voltages necessarily caused small fluctuations in speed. Variations in experimental data caused by these speed fluctuations were corrected for in the following manner. The propellor RPM was read from a tachometer and recorded with each data point. This RPM was divided

by a standard value for that speed setting. All tunnel velocities were then corrected by this ratio, and all pressure differences by its square. Various experimental checks have shown this correction method to be entirely satisfactory over a considerable speed range.

The cascade blades were mounted in the test section on large pivoting pins with a linkage that allowed simultaneous rotation of all blades to any desired angle of attack. It will be noted that this method of variation of angle of attack changed the geometry of the cascade slightly at the same time, but it was considered a reasonable expedient for these tests.

The cascade blade drawing is shown in Figure 9. Coordinates of the airfoil are given in Table I. The cascade geometry at an angle of attack of $14^{\circ}\ 59'$ was identical to the mean section of the free-vortex stator of the experimental compressor described in Reference (14). This cascade had a solidity of 0.920, a blade camber angle of $29^{\circ}\ 59'$, a design turning angle of $21^{\circ}\ 51'$ at $14^{\circ}\ 59'$ angle of attack, with a parabolic mean line, 10 $^{o}/o$ thickness and an entrance flow angle of $46^{\circ}\ 13'$ measured from the stagger line.

The survey mechanism used can be seen in Figure 5. It was basically a "barn door hanger" suspension parallel to the cascade stagger plane, held in place by its own weight, and rolling on ball bearings on machined rails. The probes were clamped to a small fixture, with the tip at the desired depth in the channel. Hand cranks then moved the carriage in a direction parallel to the stagger line, and the probe clamping fixture in a direction parallel to the blade span. Positions were read from counters geared to the cranks, which could

be read in thousandths of an inch. Repeatability of the probe positions was at least within .002". This survey mechanism, along with a variety of sting mounted probes, made it possible to survey the entire volume of the cascade, with the possible exception of certain small regions near the leading edges of the blades.

Total pressure surveys, with few exceptions, were made with the shielded total pressure tube shown in Figure 10a. The proportions of this tube were taken from Reference (15) with the exception of an increase of the shield outlet flow area. This probe was found to read true total pressure over a range of approach angles up to about 45^{o} from the probe axis. The reduction of range from that quoted in Reference (15) was probably attributable to the reduction in Reynolds number. Because of the insensitivity of this probe to flow angle, it was simply pointed in the mean flow direction and read directly. Its readings were valid everywhere except very near the wall, where it reads a bit high, and in separated regions. The wall effect was quite small and only detectable when the probe touched the wall (center .078" off). To avoid the effect on the inlet surveys, small boundary layer total tubes (Figure 10b) were used for this part of the surveys. Also, it was possible to get closer to the wall with small tubes. Unfortunately, because of the unpredictable nature of the flow direction, it was not practicable to use these simple total tubes on the surfaces inside the cascade. Therefore the total pressure readings within 0.090" of the wall inside the cascade were made with the shielded probe, and are probably slightly high. It was not considered necessary for the purposes

of this study to get total pressures inside the cascade closer to the wall than .078", the radius of the shielded probe tip.

The double claw and pitot probe shown in Figure 10c, was used to get static pressures and flow directions inside the cascade. Calibration of this probe was accomplished in the inlet portion of the test section of the tunnel. Checks were made on the uniformity, steadiness, and direction of the local flow in that region.

Flow direction was checked by inverting the probe, uniformity by surveying a volume surrounding the calibration zone for variations in total pressure, static pressure and flow direction, and steadiness by observation of tufts, very large total pressure tubes, and hot wire probes. Probes for reference during calibration were inserted into the calibration zone from a mount on the side instrument slot shown in Figure 4. All reference probes were kept far enough from the probe being calibrated to avoid interference effects. The calibration of the combination claw and pitot probe was such as to make the readings not very trustworthy outside a flow angle of about 20° to the axis of the probe, and the probe was set at various angles during surveys to minimize errors from this source.

The standard pitot tube shown in Figure 10d was used to get a reference static to calibrate the claw probe, and for various other incidental uses. The validity of its readings were checked against a static tap in the tunnel wall well ahead of the blades.

Static pressure distributions on the surface of the blade were surveyed by means of the instrumented sliding blade and cuff arrange-

ment shown in Figure 11. The blade is a standard wooden blade with a series of static pressure taps along both surfaces on approximately the same chord line. The taps are .020" in diameter and carefully made flush with the blade surface. The cuff is made of brass shim stock, rolled and fitted to the contour of the airfoil. In testing, the joint between the cuff and the blade was sealed with masking tape, and the slot through which the blade passes in the bottom wall was sealed with moulding clay before taking data at each survey position. Although the cuff was not a perfect replica of the blade contour, it is believed to be sufficiently good to cause no noticeable change in the pressure distribution near the bottom wall, where most data was taken. At none of the angles of attack tested did the cuff cause any severe disturbance such as local stalling or separation.

Pressures were read by means of a bridge circuit and a Statham pressure transducer, as described in Reference (14). Because of the low range of pressures involved, however, the 0.05 psi., Model P97 Statham pressure transducer was used. It was found possible to calibrate this unit for ranges down to 0.1" of water full scale, allowing the reading of pressure differentials down to 0.0001" with probable errors of the order of 0.0003". In actual use of this low range, considerable difficulty was experienced because of "air thermometer" effects. Any sudden change of temperature of the gage or connected tubing caused expansion or contraction of the enclosed volume of air, which caused a pressure change which was not immediately equalized by the flow through the small orifice in the probe being used. There

was also a small effect due to gradients of temperature in the gage itself. These effects were minimized by thermally insulating the transducer, avoiding bodily contact or proximity to the tube connections, and making all probe orifices as large as practicable. Disturbances were also noted from air conditioning fluctuations, opening and closing of doors in the room, and wind gusts outdoors. These difficulties were minimized by choice of running times, and by simply waiting for disturbances to settle out. Fortunately, all these effects were only appreciable in the lowest range of operation, and therefore only in the few runs taken at the minimum speed of the tunnel.

A battery of pressure switches was installed for use where several pressure differences had to be read successively, as with the combination claw probe. These switches were sealed by internal "O" rings, and were checked for leakage from time to time during the test program.

The tuft probe shown in Figure 10e was the last and most successful of a number of tuft probes used for visual studies and checks of the flow angles for probe settings. The chief difficulty encountered in using the earlier tufts was that at the low velocities encountered in this work the usual types were not light enough or flexible enough. The probe shown was made of a needle, a loop of .001" dia. wire, and a dandelion seed with the seed weight removed. For the low speed ranges, it was far more sensitive than any tuft that was manufactured.

Smoke studies were also carried out during the test program. The smoke generator used was a simple device drawing air at low

gage pressure from the laboratory compressed air supply, and burning cigars soaked in light machine oil. Unfortunately, because of the turbulent nature of the flow in the regions of interest, the resulting smoke patterns were not sufficiently dense for useful photographic recording.

Liquid evaporation tests were carried out using a special grade of kerosene prepared for viscosimeter use. This liquid was chosen after unsuccessful tests of many other volatile liquids, as the only one drying in a reasonable time, but not too fast for application and observation, and not adversely affecting the lacquer finish on the blades or leaving an oily residue. The blades had a dull, non-reflecting gray surface, and the presence of a liquid film on the surface could be determined by the specular reflection of a light source where the surface was wet. To study the resulting patterns, it was necessary to move both the light source and the observer to various positions, and study the reflections. This precluded the possibility of photographing the liquid film patterns, so they were recorded by rapid sketching of outlines and density symbols. The sketches were used to make the drawings presented in this report. Since the presence of the observer and light source in the airstream upset the cascade flow considerably, it was necessary to stop the tunnel during examination of the liquid film patterns, to prevent their distortion during observation.

III. PRESENTATION OF EXPERIMENTAL RESULTS

A. Surveys Ahead of Cascade Inlet

The inlet velocity distribution is believed to be one of the key factors in determining the secondary flow pattern. Accordingly, a number of surveys of the inlet velocity profiles were made in the course of these experiments. With no cascade installed, the total pressure was found to be uniform within less than 1 $^{o}/_{o}$ of dynamic head over all of the tunnel test section outside the wall boundary layers. The undisturbed wall boundary layers were everywhere of the order of .250" thick. The fence described in the previous section (Figure 6) was very quickly and simply developed to give a good approximation to a 1/7 power law turbulent velocity profile. A board was tried to gain some idea of the size of obstacle needed. The resulting profile was almost right, but a bit full just above the height of the board. A similar board was made up, carefully fitted and fastened to the wall, for the sake of reproducibility of the results, and a piece of drill rod was mounted at approximately the height of the undesired "bulge" in the original velocity profile. The resulting velocity profile, at the plane in which the cascade leading edges would lie when installed, is shown in Figure 7. This velocity profile was considered a sufficient approximation to a "natural" turbulent boundary layer profile, and no further changes were made. The relative ease with which this development was accomplished was taken to indicate that the distance of the boundary layer run after the fence was sufficient to produce a fully developed turbulent boundary layer profile.

When the cascade blades were installed, it was necessary to survey a little farther ahead of the cascade in order to avoid the local disturbances to the boundary layer caused by the blade leading edges. Accordingly, the survey shown in Figure 8 was taken one chord length ahead of the cascade. At this point the total pressure distribution was still constant in the direction of the cascade stagger line. The static pressure distribution was also constant, but had risen about 1 $^{o}/_{o}$ of the inlet dynamic head from the value near the tunnel inlet. It will be noticed that the boundary layer profile at this point had changed to an almost linear form, typical of those encountered in actual compressors. It is believed that this change of profile was caused chiefly by the adverse wall pressure gradient affecting the boundary layer ahead of the cascade. There is probably also some effect due to the survey point being closer to the boundary layer fence, but since it is still almost three chord lengths downstream of the fence, this effect is believed to be small.

B. Surveys Inside and Behind Cascade

A large number of surveys were made inside and behind the cascade. The results are shown in various figures at the end of the report. The following brief summary is intended to introduce the reader to these results, and describe the manner of taking and presenting them.

Using the shielded total pressure probe described earlier, a large number of total pressure surveys were made in planes parallel to the stagger plane of the cascade. These surveys were made at

several different angles of attack of the cascade, and at several successive planes in the flowwise direction for each angle of attack. Figures 12 - 16 show the cascade configuration at each of the angles of attack tested, and the manner of designation of the survey planes. This designation is carried throughout the report. The total pressure survey results are presented as contour plots of constant total pressure, with the bottom wall of the cascade represented by a line at the bottom of the plot, and the blade surface intersections represented by vertical lines, with the low pressure side of the channels always to the left. Where the blade surface does not actually intersect the survey plane, as at the inlet, or down-stream of the outlet, the approximate blade position is represented by a dashed line. The numbers designating the contours are the loss of total pressure from the uniform inlet value, expressed as a percentage of the midstream inlet dynamic pressure. Throughout the report, all velocities and pressure differences are divided by the inlet velocity, and inlet dyanmic pressure, respectively, measured at midstream. The survey results, presented on this basis, are shown in Figures 17 - 36.

The cascade channel was surveyed with the combination claw probe described under Instrumentation, for the free stream distribution of static pressure and local flow direction. This survey was carried out only at an angle of attack of $13\text{-}1/2^{\circ}$, which is very near the cascade design angle of attack of $14^{\circ}\ 59'$. The spanwise projections of the actual velocity vectors at various spanwise positions are shown superposed on scale drawings of the cascade in Figures 37 - 40. In

Figures 41 - 45, profile maps of the free-stream static pressure at various spanwise positions are shown superposed on the same cascade drawing. The numbers used represent the difference between the inlet total pressure and the local static pressure, expressed as a percentage of the inlet dynamic pressure.

In order to present a diagram of the "secondary flow velocities", it was necessary to define exactly the "design flow direction" in the plane of the cascade turning, at all points through the cascade. The "design flow" was defined as follows:

1. Design flow ahead of the cascade, and at the cascade inlet, (OC) is parallel to the tunnel axis, and undistorted by the presence of the cascade.

2. Within the cascade, along each line parallel to the stagger line, the flow at each end is parallel to the blade surface locally, and the flow angle is linearly interpolated between these end angles.

3. At the cascade outlet plane and behind, the design flow angle is constant at $20\text{-}1/2^{\circ}$.

4. The design flow, of course, has no component in the spanwise direction.

The components of the actual flow velocity vectors normal to this "design flow direction" were then considered to be the components of the "secondary flow velocity", and were plotted as vectors at the points of survey for successive planes in the flowwise direction in Figures 48 - 51. Simple contour plots of the static pressure distribution in the same planes of survey are given in Figures 52 - 56.

Surveys of the static pressure distribution on the surface of the blade were made at several angles of attack with the sliding blade and cuff arrangement described under Instrumentation. The results of these surveys are presented as individual chordwise plots in Figures 57 - 66.

All the above listed data was taken at the same tunnel speed; about 38 fps. inlet velocity, and a Reynolds Number of 160,000 based on the blade chord length. Tests were also run at lower tunnel speeds to show the effects of sub-critical Reynolds number, and under various special conditions of tunnel sealing, etc. These miscellaneous experimental results are shown in Figures 70 - 88.

IV. EXPERIMENTAL RESULTS AND DISCUSSION

A. Flow at Design Angle

The plot of secondary flow velocities at the 3/4C survey plane in the cascade at design angle of attack (Figure 49), shows that a definite secondary flow pattern existed. However, comparing this pattern with Figure 67, which shows the results of applying Squire and Winter's theory, as explained in a later section, it can be seen that there are some significant differences. The actual secondary flow pattern was definitely asymmetric, with the center of rotation shifted toward the high pressure side of the channel, and the largest velocities near the low pressure side. Part of this asymmetry may be explained by the self-transport of vorticity to the low pressure corner at the wall. However, this will not explain the fact that the secondary flow velocities 1/2 chord from the bottom wall show a very definite net upward flow. No possible simple vortex distribution can give this result; it can only be caused in a two dimensional potential flow model by the addition of a source distribution in the lower part of the channel (and a distributed sink distribution in the upper part to satisfy continuity). Further examination of the flow pattern will indicate that at least the majority of this source distribution must be concentrated near the low pressure corner of the channel.

There are two possible causes of this effective source distribution. One is a separation in the low pressure corner, which would allow no mass flow through this region, and would thus act as a strong concentrated source distribution. The other is the disproportionate

thickening of the flow layers near the wall, caused by the adverse pressure gradient and the fact that they have a lower total pressure than the main flow far from the wall. This thickening of the low velocity layers is not purely a boundary layer phenomenon. It will occur at any time when two adjoining flows of different total pressure are diffused in the same channel, and will become so marked as to prevent further effective diffusion whenever the static pressure in the channel closely approaches the total pressure of the lower energy stream. A simple illustration of this effect for a non-viscous, incompressible, quasi-one-dimensional flow is shown in Figure 68.

By comparing the secondary flow patterns at successive stations through the cascade, (Figures 46 - 51) it can be seen that the secondary flow velocities connected with the secondary vorticity begin slowly at the 1/4C survey plane and increase steadily to the cascade outlet, while those connected with boundary layer growth begin rather abruptly at the 1/2C survey plane, and decrease after the cascade outlet. (The effects at the OC and 1/4C stations are somewhat obscured by the local effects of the round nose of the blade, the stagger angle of the survey planes, and the high curvature on the low pressure surface just behind the leading edge, of which the "design flow" assumption does not take account properly). The diagrams of the flow directions in the plane of two-dimensional turning (Figure 39 for example) show that the channel turning is well begun at the 1/4C survey plane, so that the secondary vorticity in the flow direction would be expected to have appeared before this point in the channel, and to be increasing steadily

in the flow direction. The static pressure profile map in the same plane, however, (Figure 43) shows that most of the static pressure rise occurs in the region from the 1/2C to the 3/4C survey planes, especially near the low pressure side of the channel. Therefore, separation and thickening of the low velocity stream tubes would be expected to occur near the lower wall and low pressure corner with resultant displacement of the main flow as seen in the secondary flow patterns.

The surveys of total pressure in the low pressure corner and near the wall, (Figures 27 - 30) show how the typical outlet total pressure pattern developes in the cascade. At the 1/2C survey plane, (Figure 27) the profiles of total pressure in the wall boundary layer are very similar to those entering the cascade (Figure 8). The large difference between the lowest total pressure that can be read near the wall with the shielded total pressure probe and the local static pressure (Figure 63) indicates that the part of the boundary layer nearest the wall is still subject to strong viscous shear and not of the typical separation profile. In the 3/4C survey, (Figure 28) the total pressure profiles have become distorted considerably. All profiles show a general slope to the left, caused by their displacement by the secondary flow. In addition, the lowest part of the total pressure profile, with losses more than about 70 $^{o}/o$ of inlet dynamic head, has been distorted considerably, thrown almost entirely into the low pressure corner, and increased several times in area.

This last effect cannot be explained in terms of the model of

secondary flow used by Squire and Winter[7]. Since the local velocities are less than half the through flow velocity, and the local flow deflection angles are quite large, the perturbation treatment is not valid in this small region. Also, the effect of viscosity is not negligible in this region. The problem is essentially that of a three-dimensional turbulent boundary layer with large cross-flow components. The general solution of this problem has not yet been accomplished, (see discussion in introduction of Reference 16) so only a general discussion of the expected results is possible. This discussion is given in a later section. Fortunately, for the cascade geometry tested here, the region occupied by this flow of very low total pressure is small, so that it can be disregarded in an analytical description of the secondary flow, and corrected for later, if necessary.

Referring again to the static pressure plots, it will be seen that the total pressure read from the probe is so near the local static pressure that it is not clear whether or not local separation has taken place over an area from the low pressure corner about two inches up the blade. Since neither reading is very trustworthy in this region, it is necessary to refer to other evidence to confirm the existence of the separation. Such evidence is forthcoming in the flow visulization studies to be described later.

The survey at the 1C plane, with the probe passing just behind the trailing edge of the blade, (Figure 29), shows a triangular loss region of moderate size in the low pressure corner, and distortion of the total pressure profiles in the remainder of the channel by the

secondary flow as would be expected. At about this point, the whole loss region must become subject to strong turbulent mixing, because at the 1-1/2C survey plane (Figure 30), the loss region is considerably shallower, showing no losses greater than about 65 °/o of inlet dynamic head.

Visual studies with a tuft indicate that strong turbulent mixing begins, and the edge of the loss region becomes rather poorly defined, at about 80 - 90 °/o of the blade chord length. An attempt was made to outline the edge of a "separation" region with various tuft probes, but this proved to be impossible. Throughout the region, the tuft blows erratically in all directions. Deep in the region, near the corner, the tuft spends most of its time pointing upstream, indicating a definite reverse flow of the mean velocity. As the tuft is moved toward the outer edges of the mixing region, it spends a progressively larger percentage of its time pointing in generally downstream directions. Because of the unsteadiness of the flow, however, it is impossible to determine a definite limiting surface below which there is no net through flow. Because of this uncertainty as to the definition and limits of the region of actual separation, the general region will usually be referred to hereafter as the "mixing region".

In a further attempt to determine the character of the mixing region, a heavy stream of smoke was introduced at the rear of the region to determine how far forward it could move under the action of the reverse flow in the corner. Although the resulting coloration was too faint to be photographed, it permeated the entire mixing region, as

outlined in Figure 69. The fact that the smoke was able to move forward to the upstream end of the mixing region confirms the existence of a mean reverse flow velocity at the base of the region. It is interesting to note that when smoke was introduced into the flow on the high pressure side of the blade, near the wall, a small portion of it still managed to work forward into the mixing region on the opposite side of the blade.

There was no evidence in these tests of the presence of a "passage vortex" such as that reported in Reference (17). Nor was it possible to obtain such a phenomenon by removing the boundary layer fence, and testing with the resulting thin wall boundary layer, nor by testing at lower speeds. However, it was not possible under any of these conditions to produce a laminar wall boundary layer at the cascade inlet with the present equipment. It is believed that it is impossible to maintain a smooth smoke trace, such as those shown in Reference (17), for any appreciable distance unless the surrounding flow is laminar. It seems possible, then, that the "passage vortex" phenomenon may occur only in the presence of laminar wall boundary layers. This phenomenon may also be associated with the presence of large "loss cores" somewhat removed from the walls, as reported in Reference (5). In neither of these reports were the Reynolds numbers clearly stated, but the velocities appear to have been such that extensive laminar boundary layers were possible. It should be noted that in Reference (17) the smoke tests were all made at low speeds, while many of the other tests in the same report were made

at much higher speeds. On the other hand, results that compare favorably with the present picture of a triangular mixing region in contact with the wall were reported in References (14), (18), and elsewhere. It may be noted that Reference (8) showed no change in the character of the secondary flow in a square pipe leak over a wide range of Reynolds numbers, but at all Reynolds numbers tested in that report, the flow entering the bend was stated to be a "fully developed pipe flow", and since there were no blades in the bend to form fresh boundary layers, there was no laminar boundary layer involved anywhere in those experiments. The conclusion is reached that the laminar or turbulent character of the boundary layers in a cascade or bend may be a decisive factor in determining the character of the secondary flow.

B. Flow at Low Speed; Reynolds Number and Turbulence Level Effects

Since the character of the boundary layer may have a crucial effect on the type of flow resulting in a given cascade, it might be well to consider such effects briefly. The laminar boundary layer is characterized by steady flow parallel to the surface, a moderate shear force on the wall and a low rate of momentum exchange throughout the boundary layer. The turbulent boundary layer is characterized by irregular eddying motions with velocity components in all directions, which greatly increase the rate of momentum exchange. Consequently, the turbulent boundary layer has a much larger shear force at the surface. A laminar boundary layer can proceed only a short distance against an adverse pressure gradient before the flow at the surface is

brought to a halt and separation occurs. In a turbulent boundary layer, on the other hand, the more rapid exchange of momentum between the surface and outer layers by the process of turbulent mixing, allows the flow to proceed much farther against an adverse pressure gradient before separating.

When a flow which is initially steady passes over a body or through an internal passage, such as those in a compressor or cascade, the boundary layers initially formed on the surfaces are usually laminar. If no adverse pressure gradients are encountered, the laminar boundary layer normally persists for a certain distance, beyond which it becomes unstable to any infinitesimally small disturbance present, and breaks down into turbulent flow in a "transition region".

When a laminar boundary layer encounters an adverse pressure gradient, either of two things may occur. If the adverse gradient is strong, the flow will probably separate and remain detached from the surface. If the adverse gradient is mild, however, the separation may be slight, and because the free streamline after the separation is very unstable, it breaks down almost immediately into a turbulent motion which reattaches to the surface and becomes a turbulent boundary layer. This phenomenon is commonly referred to as a "bubble separation". Whether or not the flow will reattach after a laminar separation, apparently depends upon whether the turbulent mixing after transition in the shear layer spreads rapidly enough to touch the surface again behind the bubble.

If the flow striking the body or entering the flow passage is not

initially steady, but carries turbulence or disturbances, these disturbances will cause early transition in the boundary layers. If the disturbances are sufficiently strong, the boundary layers will be turbulent everywhere, if the Reynolds number is moderately high.

Local roughness of the surface may also cause earlier transition of the boundary layer to turbulent flow. Various artificial devices have been used to "trip" the boundary layer to speed transition where this is desirable, and the whole class of such devices, wires, notches, vanes, holes, grooves, etc., are generally known as "turbulators".

Because of the different character of the two types of boundary layers, it would be desirable in flow machinery to have laminar boundary layers wherever the pressure gradient is favorable to the through flow, to reduce the losses in skin friction, and turbulent boundary layers wherever the pressure gradients oppose the through flow, to avoid separation with its accompanying losses. However this rather ideal state of affairs is rarely attainable in practice. The usual situation in a machine such as a subsonic axial flow compressor of ordinary size is that all stages after the first are subject to such large disturbances from the upstream blades that the boundary layers are expected to be almost entirely turbulent. The character of the boundary layers on the first stage, and especially on the inlet guide vanes, is much more uncertain, and may depend largely on the inlet configuration.

In order that a cascade tunnel may be a valid representation of the flow in a subsonic compressor cascade, it is not enough that the geometries should be similar. It is also necessary that the Mach

number and Reynolds number of the two flows be similar, and, for some purposes, that the disturbance level in the incoming flows should be similar. This latter requirement must be given careful consideration.

If the entire flow entering a diffusing cascade, including the wall boundary layers, is laminar, then boundary layer transition to turbulent flow is essential before any appreciable diffusion can occur in the cascade. If the Reynolds number of the cascade, based, say, on the chord length, is less than a certain critical value, transition to turbulent flow in the boundary layer on the low pressure surface of the blade may not occur before the point where the strong adverse pressure gradient begins. The boundary layer will then separate from the low pressure surface and may not reattach before leaving the cascade. The result is a large increase in the total pressure loss and a reduction of the turning and diffusion accomplished by the cascade.

A closely related situation is encountered in tests run in the present tunnel at the lowest speeds. Figures 70 - 84 show the results of tests on the present cascade at design angle of attack and an inlet velocity of 16 fps. The flow outside the wall boundary layer at the test section inlet had a low turbulence level, and the Reynolds number of the blades was so low (about 67, 000) that transition did not occur on the low pressure side of the blades before the flow reached the beginning of the adverse pressure gradient. At this point (about 30 $^{o}/_{o}$ of the chord length from the leading edge) the flow separated and left the cascade without reattaching, as illustrated by the total pressure

surveys in Figures 70 and 71.

It is interesting to note that the secondary flow velocities (see Figures 78 - 81) were relatively small in this case, as would be expected from the linearized theory for the small turning accomplished.

However, the flow in the wall boundary layer entering the cascade was turbulent. Therefore, at a point on the cascade blades just inside the wall boundary layer, the total head and velocity were still practically the same as in the free stream, but the turbulence level was considerably higher. The local turbulence caused the blade boundary layer to become turbulent before reaching the strong adverse gradient, and therefore it did not separate. As a result, the total pressure wake of the blades was very wide and deep at mid-span, but became much narrower and shallower at the outer edge of the boundary layer, as can be seen from the total pressure map in Figure 71.

At the next higher speed of the tunnel, an inlet velocity of 26 fps., the cascade was still operating at a subcritical Reynolds number (120, 000), and the flow pattern was very similar. A series of total pressure surveys across the blade wake at different distances from the wall are shown in Figure 85. This flow, however, was obtained only so long as there was no loud noise, vibration, or other disturbance in the room in which the tunnel was installed. When such disturbances occurred, transition occurred in the blade boundary layer outside the region of wall disturbances, the separation disappeared, and the blade wake became much narrower, as illustrated in Figure 86. When sounds of definite frequency were produced in the tunnel, transi-

tion was found to occur most readily for a frequency near 150 cycles per second. At this frequency, only a tone scarcely audible above the tunnel noise was required, while at higher frequencies a greater intensity was required to insure transition and at lower frequencies, transition could not be induced with the sound intensity available. This observation is in accord with the existing theory of the stability of the laminar boundary layer. Apparently the tunnel noise is not loud enough in the sensitive frequencies to effect transition at this Reynolds number. From the fact that transition can be induced so readily, it is inferred that the cascade is operating very slightly below its critical Reynolds number.

At the next higher tunnel speed, with an inlet velocity of 38 fps. and a blade Reynolds number of 160,000, the flow was clearly supercritical, and the blade wakes at midspan were quite narrow. However, a close examination of the flow over the low pressure surfaces of the blades showed that there was a bubble separation from about 30 ^{o}/o to 60 ^{o}/o chord on the blade outside of the wall boundary layer. In Figure 94, the liquid film evaporation pattern for the blade at the design angle of attack is shown. The dry surface from the leading edge to about 30 ^{o}/o chord indicates that the boundary layer was attached there. The layer of liquid from about 30 - 60^{o}/o chord indicates the extent of the laminar separation bubble, and the dry area behind it represents the turbulent reattachment after the bubble. The heavy bead of liquid near the front of the separation bubble probably indicates the forward limit of a trapped vortex on the blade surface. Study of the chordwise

static pressure distribution on the surface of the blade (Figure 67) also showed the typical indication of a bubble separation; a region of nearly constant surface static pressure just behind the point of minimum pressure, followed by an abrupt rise of static pressure at the point of reattachment. Such evidence is necessary to confirm the presence of the bubble separation, because it was so shallow in height that the shielded total pressure probe would not detect total pressures as low as the local static pressure.

On the part of the blade immersed in the wall boundary layer, the separation bubble probably vanished. It could be detected in the surface static pressure distribution. The evaporation tests showed less liquid near the wall, which may have indicated reduced surface shear without actual separation. Because of the slightly greater flow loss where the bubble was present, the blade wake was still somewhat larger at mid-span than at the edge of the wall boundary layer (see Figure 29). At higher speeds, up to 45 fps. (Reynolds number of 200,000), the bubble separation became a little smaller and the increase of losses at midstream a little less noticeable, but it was certainly still present.

To confirm the significance of the boundary layer condition, tests were made with the addition of a turbulator at the nose of the airfoil. This turbulator consisted of a length of .020" piano wire on the low pressure side of the blade at about 2 $^{o}/_{o}$ chord, taped down at both ends but free to vibrate in the airflow over the middle of its length. This type of turbulator had previously been found in many cases

to be extremely effective without adding a great deal of airfoil drag in the wall boundary layer where it is not needed, provided the wire is small and properly located. In this case, it reduced the size and depth of the blade wake slightly at midstream and increased it slightly in the edge of the wall boundary layer, eliminating the anomaly discussed above. Its effect in one instance, can be seen by comparing Figures 25 and 26.

The turbulator wire was not used in any of the tests described in this paper. All tests except those specifically noted were run at the third speed of the tunnel, at an inlet air speed of about 38 feet per second, and a Reynolds number of about 167,000, which is the lowest reliably supercritical speed. It should be remembered that the bubble separation, though rather large in its chordwise extent, causes a flow displacement of less than 1/16 " normal to the blade surface. Despite the large size of the blades it was difficult to detect it without surface static pressure measurements and liquid evaporation tests. Therefore its total effect was probably only that of an effective thickening of the blade outside the wall boundary layer, by about 1/2 $^{o}/_{o}$ of the chord length. Because of its isolation from the wall, in addition to its small thickness, the bubble separation is believed to have no appreciable effect on the secondary flow or on the behavior of the flow near the wall.

To summarize, then, the validity of the test conditions of the cascade for their applicability to similar cascades in an actual turbomachine:

1. The flow within the wall boundary layers was turbulent, and

the velocity profile of the wall boundary layers were typical of axial flow compressors. The Reynolds number of the blade was clearly supercritical in this region, and therefore the test conditions here were probably quite a representative model of the flow in a typical axial compressor cascade, except for the absence of the gross disturbances caused by the passage of upstream blade wakes.

2. The turbulence level in the flow outside the wall boundary layers was much too low to be representative of a typical turbomachine. However, the blade Reynolds number was supercritical, in that the laminar separation reattached, and the bubble was very thin normal to the surface so that design turning and diffusion are very nearly attained. Therefore, it is believed that the separation bubble does not seriously affect the proper cascade representation of typical compressor blading. On the whole, the model is thought to be a valid one for secondary flow studies.

C. Discussion of the Mixing Region and Related Phenomena

Let us now return to consideration of the flow in the test cascade, particularly that in the lowest velocity portions of the wall boundary layer. Figure 45 shows the static pressure distribution about 0.7" off the wall in the free stream, which must closely approximate that on the end wall itself. The static pressure distribution on the high and low pressure sides of the blade at the angle of attack of 13-1/2°, is given in Figures 61 and 62.

While the cross-channel static pressure gradient at the wall, which is usually considered in discussions of secondary flow, is quite

appreciable, it should be noted that over most of the channel the adverse pressure gradient in the direction of flow is of very nearly the same magnitude. The effect of this adverse pressure gradient on the secondary flow is not considered in any of the secondary flow theories available to date except that of Loos[11]. In Loos's work, its effect is shown to be very small so long as the velocity variations are small preturbations. Indeed, substituting the area ratio of this cascade in Loos's expression, the result is simply a 1 $^{o}/o$ increase in all secondary flow velocities at the cascade outlet. Thus the signifigance of this adverse pressure gradient is quite small for that part of the incoming wall boundary layer for which the perturbation treatment can be expected to hold, namely, where the flow velocity is greater than about half the free stream velocity.

However, for that small portion of the boundary layer very near the wall, for which the linearized theory does not apply, and which probably is responsible for the turbulent mixing region at the low pressure corner of the channel, the adverse pressure gradient has a much greater significance. In particular, there is a portion of the boundary layer, however small, whose total pressure is less than the static pressure at the outlet of the cascade. The flow of this air through a diffusing cascade cannot be described by inviscid flow theory, since without the aid of viscosity it cannot ever leave the channel. Ignoring the effects of viscosity for a moment for the sake of discussion, the through-flow velocity component of this air would go to zero at some point, say, between the 1.00 and 0.80 static pressure coefficient

contours in Figure 44. The cross-channel gradient would then force this flow to the low pressure corner of the channel, where the mixing region actually forms. Note that without viscous shear there is no question whatever of whether the flow would go entirely across the channel before reaching the channel outlet. The through-flow velocity component would be stopped, and the flow would remain in the channel, and go directly to the low pressure corner.

The factor that allows this low velocity fluid to be removed from the channel is the transfer of momentum to the fluid by the laminar or turbulent shearing action of the faster moving layers of fluid farther from the wall. However, the rate of this momentum transfer will be quite varied, and will depend chiefly upon the thickness of the low velocity layers, and their character, i.e. laminar or turbulent.

If the incoming wall boundary layer is laminar, then because of the velocity profile normally associated with the laminar boundary layer, there will be considerable fluid flow near the wall which does not have the necessary total pressure to pass through the channel unaided. Because the shearing forces are small in a laminar boundary layer, the through-flow component of a relatively large portion of fluid will be stopped rather early in the channel. Unless transition to turbulent flow, with its greater mixing rates, occurs almost immediately, the separated region will fill a large volume, and the design diffusion and turning will both be seriously reduced at the wall. This separation at the wall may or may not be associated with a stall of the remainder of the blade. In either case, the losses can be

expected to be high in the separated regions near the wall. The severe loss of lift on the blade near the wall, if the remainder of the blade did not stall, would cause a strong trailing vorticity in the wake of the blade near the wall, and could well be the explanation of the "tip vortex" loss core frequently observed in other tests of diffusing cascades.

If, on the other hand, the incoming wall boundary layer is turbulent, the velocity profile will be such that only a small portion of the flow very near the wall has too low a total pressure to pass through the cascade without momentum transfer from the outer stream. Also, the prevailing rates of momentum exchange are much higher in a turbulent boundary layer than in a laminar one, both in the turbulent outer layer and in the laminar sublayer that is always present at the wall. Therefore the turbulent boundary layer will tolerate much larger adverse, or cross-channel pressure gradients without separating or being thrown to the low pressure corner. However, even with a turbulent boundary layer, both possibilities still exist if the adverse and cross-channel gradients are strong enough.

Therefore, with a turbulent boundary layer entering the cascade, there are several possible results, depending upon the strength of the pressure gradients. If both the turning and the diffusion are sufficiently mild, it is to be expected that the cross-flow at the bottom of the boundary layer will be so mild that no noticeable mixing zone will form at the low pressure corner of the channel. The boundary layers will then pass through without difficulties. If the adverse and cross-

channel pressure gradients are somewhat stronger, the low velocity fluid will be turned sharply into the low pressure corner of the passage. Since this fluid is already turbulent, a turbulent mixing zone will be formed in or near this corner, which will grow until it entrains sufficient fluid from the higher velocity flow above it so that the low velocity fluid can be carried out of the mixing region as fast as it enters. If the adverse and cross-channel gradients are still stronger, the amount of air thrown into the low pressure corner mixing region will be so great that sufficient high velocity flow cannot be entrained to carry it out of the cascade. In this case the mixing region will grow, and will either cause the entire blade to stall, or will block sufficient area at the outlet of the cascade to reduce the channel turning and diffusion to levels that the turbulent mixing process can cope with.

It will be noticed that in the above discussion it was always assumed that the diffusion and channel gradients were increased simultaneously. In any two-dimensional cascade the overall diffusion and the overall channel turning are uniquely related through the cascade geometry. The relative local rates of turning and diffusion are, of course subject to some adjustment by the designer.

The relationship between the overall turning and diffusion is different, however, when the angle of attack is changed by changing the incoming flow angle, as in an actual flow machine, and when it is changed by changing the angle setting of the individual blades, as was done in these cascade tests, and as might be done in a turbomachine

with variable angle blading. Despite this difference, it was hoped that some indication of the behavior of the mixing region at various combinations of diffusion and turning could be gained by testing the present cascade at various angles of attack, and studying the mixing region by total pressure surveys. The results of these tests are described in the next section.

It might be well to remark in passing, that another type of secondary flow is possible, associated with the strong turning in the region of the stagnation point on the part of the blade in the wall boundary layer. This type of secondary flow was described by Hawthorne in Reference (19), with experimental evidence confirming its existence. It is, however, a very small effect when the leading edge radius is small compared to the distance along the edge in which a significant inlet velocity change occurs. The question could be asked, whether such a secondary flow occurs in the present cascade, and, if it does, whether this flow causes, or significantly affects the formation of the corner mixing region.

A special series of spot checks were made to determine whether any strong flow of this kind occurred at the intersection of the blade leading edges and the wall, and whether any local separations resulted, either upstream or downstream of the corner "stagnation point". No separated region could be found by any technique, and any secondary flow velocities of this type were of negligible magnitude at any points far enough from the walls to be reached by the instrumentation used.

D. Effect of Variation of Angle of Attack

A series of tests were run in which the cascade was set at various angles of attack to determine whether the resulting changes in overall channel turning and diffusion affected the position, size, and character of the turbulent mixing region. It should be recalled that since the blades are rotated about their individual mounting pins, instead of the cascade being rotated as a unit, the cascade geometry is necessarily changed with the angle of attack. The adjustable end walls were used to equalize the flow conditions over the various cascade blades. For this purpose, the static pressure was read from a pitot tube in the same relative positions just ahead of the first and fourth blades. The end walls were adjusted until the static pressures were the same at corresponding pairs of points. All data was taken with this setting.

The data taken consisted of total pressure surveys in the regions of interest near the corners of the channel, and static pressure distribution over the surface of the blade. The total pressure surveys were taken with the shielded total pressure probe at several stations through the cascade. The surveys were made at the same set of survey planes relative to the test section, and the relations of the blades to the survey planes, as well as the cascade geometries at the various angles of attack, are shown in Figures 12 - 16. The contour plots of total pressure are shown in the following figures.

The static pressure distributions on the high pressure and low pressure sides of the blades were taken with the instrumented blade

and cuff arrangement described in the previous section. The results are presented as chordwise plots, in terms of the percent of dynamic head, in Figures 57 - 66.

The surveys were made at five angles of attack, ranging from 21-1/2° to -1° . These limiting angles are about 2 - 3° from the positive and negative stall, respectively. They were chosen to be far enough from stall so that stable and repeatable flow could be obtained.

At the 21-1/2° and 13-1/2° angles of attack, the turbulent mixing region occurs in the low pressure corner as in the previous data. The general character of the flow is the same in both cases, although the mixing region is somewhat larger at the higher angle of attack. At the 9° angle of attack, however, there is practically no region of high loss in the corner. The distortion of the total pressure profiles in the higher velocity portion of the stream is less than in the previous cases, as would be expected from the lower channel turning of the cascade at this angle of attack. But the disappearance of the mixing region is a much more noticeable change.

At the 5° angle of attack, there is no detectable mixing region at the corner, and only a very small secondary flow distortion of the total pressure profiles, which begins rather late in the channel, as does the channel turning. At an angle of attack of -1°, approaching the negative stall, a very small mixing region appears on the opposite side of the blade from what was normally the low pressure corner. This region, however, is much smaller than those encountered at the high angles of attack.

It will be noticed, from Figure 17, that at the angle of attack of -1° there is a separation bubble of considerable size in the concave "high pressure" surface of the blade. This separation is brought on by the severe adverse pressure gradient present on the low pressure side of the blade at negative angles of attack. It seems likely that the negative stall is brought on by the rearward growth of this separation region, while the positive stall may be brought on by spreading of the corner mixing region.

In terms of the descriptions given in Section C of wall boundary layer conditions considered likely to occur in cascades, the situation at angles of attack of 5° and 9° would fit the case of turbulent incoming wall boundary layer with mild adverse and cross-channel pressure gradients, so that the boundary layer is not seriously turned, or separated. The results at $13-1/2^{\circ}$ and $21-1/2^{\circ}$ show the effect of increasing gradients, with a mixing zone appearing and growing with increasing angles of attack until it may result in separation of the whole cascade blade. At negative angles of attack, it appears that in this cascade the entire blade may separate because of the bad two-dimensional adverse pressure gradients, before the mixing zone on the opposite side grows to any great size.

E. Effect of Tip Clearance Leakage

In all the tests described so far, the tip clearance spaces at the bottom end of the blade being tested were sealed by forcing in a small fillet of moulding clay, and then removing all clay outside the crack with a sharp wooden tool. In a couple of instances where this sealing

was omitted, some very striking differences in the flow resulted. Since not all experimenters have been careful about clearance sealing, and its significance in cascade testing seems to be generally underrated, a few brief comparative studies made during the present tests will be reported here.

The top and bottom walls of the test section were constructed of 1" plywood and were flat and free from warps. The blades were well constructed of mahogany, and the ends were cut off about as flat and square as is possible in wood. To allow insertion, the blades were about .030" shorter than the tunnel height, and when installed, this gap was placed at the top of the blade, to avoid disturbing the lower portion of the channel where the surveys were to be made.

The clearance remaining at the bottom of the blade was quite small, and was due mostly to lack of squareness between the blade and the wall. At the worst places, one could get the edge of a razor blade between the blade and the wall. The maximum clearance was about 0.015" with the average about 0.010". Considering the large size of the blades and the velocities and pressure differentials involved, this clearance is quite small, and of approximately the same proportion as in most tunnels of more typical construction.

The dimensions and pressure differentials across the clearance space were such that the leakage flow would be definitely expected to be laminar in the slot. In the terms used by Rains[20], the value of $\lambda^2 R_e \epsilon$ was only 2.2, or the Reynolds number of the flow, based on the slot height and the mean velocity was about 15. The mean velocity

of the leakage flow would be expected to be about 3 fps., and the amount of mass flow that would get through is so small as to seem insignificant. However, its effects were quite noticeable.

To make a direct comparison of the size and shape of the mixing region with and without the clearance sealed, two consecutive total pressure surveys were taken at the 1C survey plane at an angle of attack of 13-1/2° with no changes other than sealing the clearance space, and with particular care that no fillet was made of the moulding clay seal. The unsealed blade was pushed down firmly against the lower wall before running. The results of the two comparitive surveys are shown in Figure 87. The mixing region is considerably larger in the unsealed case. The increased size seems out of all proportion to the amount of leakage flow that caused it.

As a further indication of the magnitude of the effect of this separation, Figure 88 shows the secondary flow velocities at the 3/4C survey plane in the unsealed condition. Clearance leakage is the only difference between this diagram and that shown in Figure 49. The increased size of the mixing region is indicated by the greater displacement of the flow away from the corner.

The explanation of this tremendous reaction to a very small amount of flow probably lies in the fact that the channel is diffusing, and in the basic explanation of the existence of the mixing region. The mixing region is formed because a very small portion of the incoming stream at the base of the boundary layer does not have sufficient energy to leave the cascade without undergoing a mixing process which

entrains considerable flow from the higher velocity fluid above it. The tip clearance leakage has the effect of adding an even smaller portion of additional flow to the mixing region, with no useful energy whatever. Furthermore, most of the leakage flow is added in the region of very low pressure near the nose of the blade, so that its total pressure is even below that of the base of the inlet boundary layer. Thus, although the leakage mass flow is considerably smaller, even, than the amount of mass flow in the inlet wall boundary layer whose total pressure is below the outlet static pressure, this small amount of mass flow is added at the lowest possible energy and chiefly in the worst possible place. This gives it a "triggering action" in encouraging the formation of a large mixing region.

All the data reported here, except that described in the previous paragraphs, was taken with the clearance sealed on the low pressure side of the channel being surveyed. However, the clearance spaces elsewhere in the cascade were not generally sealed. When all clearance spaces were sealed, the cascade diffusion more nearly approached the theoretical value.

F. Estimates of the Various Cascade Losses

An attempt was made to determine the order of magnitude of the various losses occurring in the cascade. It was hoped from this to determine the magnitude of the losses caused by the secondary flow. These losses were found to be quite small.

In order to gain a better feeling for the significance of the losses, they were put on a basis of equivalent compressor efficiency.

To do this, the velocity triangles of the compressor from which the cascade was taken[14] were assumed, and the total pressure loss of the cascade was related to the loss of adiabatic efficiency of a actual compressor stage made up of two such cascades as the rotor and stator. This change actually consists of simply multiplying the cascade percentage total pressure loss by a factor of 1.94 to get the equivalent adiabatic efficiency loss.

Furthermore, since the losses with which we are concerned are those losses in excess of the two dimensional losses, at the ends of the cascade, these losses will depend directly upon the aspect ratio of the blades. That is, the excess losses associated strictly with the flows at the end wall, will become less significant as the aspect ratio of the blade is increased. To handle this on a reasonable basis, the losses associated strictly with the flows at the ends of the channel were reduced to an "effective aspect ratio" of 2.0 and then reduced to compressor equivalents.

On this basis, the outlet energy deficit, weight flow averaged, and related to the inlet mid-stream total pressure, represents a loss of adiabatic efficiency of 23.5 $^{o}/o$. But most of this loss merely represents the energy deficit in the wall boundary layers entering the cascade. This inlet energy deficit is about 15.7 $^{o}/o$ on the same basis. The net loss of the cascade, then is represented by a loss in equivalent compressor adiabatic efficiency of about 7.8 $^{o}/o$. The equivalent compressor would thus have an efficiency of about 92 $^{o}/o$ which is a reasonable figure, considering that no clearance losses or

unsteady flow losses occur in the cascade as tested.

Of the 7.8 °/o losses charged to the cascade, a certain portion must result from the "two-dimensional" losses of the blades themselves. From surveys of the blade wakes far from the wall, the integrated "two-dimensional" loss amounts to about 4.9 °/o in adiabatic efficiency. This figure is based on the assumption that the losses of a two-dimensional nature should be proportional to the square of the velocity in the wall boundary layer. Some loss is also to be expected in skin friction on the wall between the inlet and outlet survey stations. An estimate of this loss, based on the flow conditions at the inlet and a two-dimensional boundary layer flow, gives an adiabatic efficiency loss of 0.7 °/o.

Subtracting these two losses, which would be expected on a two-dimensional basis, from the total losses which occurred, we get a remainder of about 2.2 °/o. This amount must be charged to excessive losses caused by non-two-dimensional effects associated with the flow in the neighborhood of the wall, such as losses due to local separation, and excessive viscous dissipation.

This loss is somewhat lower than that usually charged to secondary flow effects, but it must be remembered that it includes only the losses that actually occur in the cascade. Among other things, it does not include the energy contained in the "secondary velocities" leaving the cascade. These are generally assumed to be unconvertable by the succeeding blade rows, although this assumption is probably quite pessimistic. This loss cannot quite honestly be reduced to a

different aspect ratio than that at which the tests were made because the secondary flow pattern depends somewhat upon the channel proportions. However, it is true that most of the energy is concentrated in the portion of the channel near the wall, and that the flow here would not be greatly affected by a change of the aspect ratio of the blades. Therefore the secondary flow energy up to a height equal to the blade chord length will be taken as representative of the losses of this type for a channel of aspect ratio 2.0. On this basis, the kinetic energy of the secondary flow is about 1 $^{o}/_{o}$ expressed in compressor adiabatic efficiency, in addition to the losses mentioned previously.

In addition to these losses, further losses would be expected in an actual turbomachine that cannot be estimated from these cascade tests. These additional losses include the unsteady flow losses due to the passage of blade wake, bad flow conditions caused by off-design angles and velocities near the walls, and losses caused by leakage through the clearance spaces at the blade tips.

Returning to the excess loss of 2.2 $^{o}/_{o}$ which actually occurs inside the cascade, there are several flow mechanisms which may contribute to this loss. They may be explained in terms of mixing losses, separation losses, and other excessive losses caused by the three-dimensional character of the flow near the corner.

To put these figures in proper perspective, it must be realized that the necessary limitations on the accuracy of the surveys, and the methods of integrating the losses, make exact figures arrived at by subtracting off successive parts, as above, subject to some

uncertainty. Therefore, the exact numbers should be considered as only a guide to the orders of magnitude. Considered in this light, the following statements seem justified:

1. A considerable part of the energy deficit at the cascade outlet represents only losses that had occurred in the boundary layers upstream of the cascade inlet. These losses should be properly accounted before the remainder is charged to secondary flow.

2. Of the energy losses properly chargeable to the cascade, and that actually occur in the cascade, by far the largest part can be accounted for by the simple two-dimensional blade loss and the skin friction loss on the end wall. This is true even for the relatively low aspect ratio of 2.0, to which these cascades have been reduced, therefore even more true for the higher aspect ratios common in turbomachine practice. Thus the losses commonly charged to "secondary flows" are much higher than those that occur in the cascade itself and immediately behind it.

3. The energy involved in the "secondary velocities" leaving the cascade is also quite small, being a small fraction of one percent of the dynamic head entering the cascade. This result would be anticipated, either from direct application of Squire and Winter's result, or by comparison with Eichenberger's results[9] in a bend of much greater turning angle. If this energy is largely unconverted by the succeeding cascades, the resulting compressor efficiency loss would be expected to be about 1 $^{o}/_{o}$.

4. There are direct losses of rather small magnitude in the

cascade channel itself, associated with the secondary flow. These losses probably are of the nature of mixing losses, losses due to small local separations, and other three-dimensional boundary layer effects. For cascades of which the present design is typical, these losses may amount to 1 - 3 $^{o}/_{o}$ on the adiabatic efficiency.

5. No judgement can presently be made of the magnitude of the losses resulting from running one cascade in the wakes of another. However, it seems quite clear that the presence of mixing regions at the walls, as reported here, would increase these losses. In addition to the unsteady flow effects, the design velocities and flow angles may be seriously altered, causing off-design operation of the succeeding stages.

G. Analytical Description of the Secondary Flow Based on Linearized Theory

From the linearized theory of secondary flow as developed by Squire and Winter (see Introduction), it is possible to get a simple analytical prediction of the secondary flow velocities in a turning cascade. This simple theory does not predict the existence of a mixing region, and does not account for the effects of vorticity self-transport, diffusion, and large velocity variations. Nevertheless, the solution is of considerable interest, both as an approximation, to indicate trends, and as a possible starting point, on which it may be possible to superpose various corrections for higher order effects.

Under the assumptions that the secondary flow and the velocity variations are small perturbations on the design flow, Squire and

Winter[7] obtain the result that the secondary vorticity at the channel outlet is

$$\zeta = -2\epsilon \frac{\partial U}{\partial z} \tag{1}$$

where ϵ is the total angle of channel turning and z is the spanwise direction. This equation is equally applicable for any plane normal to the flow within the channel if ϵ is the channel turning up to this plane. To obtain the stream function and secondary velocities at any plane in the channel normal to the flow, it is then necessary to solve the Poisson equation,

$$\frac{\partial^2 \psi}{\partial y^2} + \frac{\partial^2 \psi}{\partial z^2} = 2\epsilon \frac{\partial U}{\partial z} \tag{2}$$

subject to the boundary conditions imposed by the channel geometry. This problem is essentially that of the two-dimensional flow in a bounded region due to a vorticity distribution described by Equation (1). Squire and Winter's paper gives an approximate solution to this problem for a passage of width small compared with the height, which should describe the case of greatest interest, namely bends and cascades of moderate to high aspect ratio. Unfortunately, this approximate solution is not generally applicable, and gives an unreasonable result for the present configuration. In order to apply the theory, an exact solution was found, using the Green's function of a general infinitesimal vorticity in a semi-infinite strip. This resulted in an

integral expression for the stream function of the secondary flow, which was readily evaluated for the present case of a linear inlet velocity profile.

It is necessary first to obtain the stream function for a single concentrated vortex at an arbitrary point in a semi-infinite strip. This is most easily obtained by solving first for the velocity potential of a vortex at an arbitrary position along the y-axis in an infinite strip, as illustrated in Figure 89. The differential equation is still the Laplace equation in the velocity potential, and because of the symmetry of the problem and the nature of the velocity potential, the boundary conditions on ϕ are particularly simple in this arrangement. They are shown in Figure 89. A series solution is assumed, of a form exponential in z multiplied by a sine series in y. Constants are evaluated to meet the boundary conditions at the walls, at $z=0$, and at $z=\infty$. The resulting expression for the velocity potential is:

For $z>0$;

$$\phi=\sum_{n=0}^{\infty}\frac{\Gamma}{\pi(2n+1)}\, e^{-(2n+1)\frac{\pi}{2}\frac{z}{b}} \sin(2n+1)\tfrac{\pi}{2}\tfrac{y}{b}\, \cos(2n+1)\tfrac{\pi}{2}\tfrac{\eta}{b}$$

For $z<0$; (3)

$$\phi=\sum_{n=0}^{\infty}\frac{\Gamma}{\pi(2n+1)}\, e^{+(2n+1)\frac{\pi}{2}\frac{z}{b}} \sin(2n+1)\tfrac{\pi}{2}\tfrac{y}{b}\, \cos(2n+1)\tfrac{\pi}{2}\tfrac{\eta}{b}$$

This velocity potential is then converted to a stream function, transposed to an arbitrary $z=S$, and added to an equal and opposite

image vortex at $z=-\zeta$, giving the stream function for a vortex at an arbitrary position in a semi-infinite strip;

For $z>\zeta$;

$$\psi=-\sum_{n=0}^{\infty} 2ab\Gamma\left[e^{-a(z-\zeta)}-e^{-a(z+\zeta)}\right](\cos ay)(\cos a\eta)$$

For $0<z<\zeta$; (4)

$$\psi=-\sum_{n=0}^{\infty} 2ab\Gamma\left[e^{+a(z-\zeta)}-e^{-a(z+\zeta)}\right](\cos ay)(\cos a\eta)$$

where

$$a=(2n+1)\frac{\pi}{2}\frac{1}{b}$$

The geometry and coordinates of this configuration are shown in Figure 90. To obtain a Green's Function, we substitute an infinitesimal area distribution of vorticity $\zeta\, d\eta\, d\zeta$, for the single concentrated vortex Γ. The resulting expression is to be integrated over the entire distribution of secondary vorticity to obtain the stream function of the secondary flow. The integral expression for this stream function is:

$$\psi=-\sum_{n=0}^{\infty}\left\{\int_{0}^{z}\int_{-b}^{b}\frac{\zeta}{2ab}\left[e^{-a(z-\zeta)}-e^{-a(z+\zeta)}\right]\cos ay\cos a\eta\, d\eta\, d\zeta\right.$$

$$\left.-\int_{z}^{\infty}\int_{-b}^{b}\frac{\zeta}{2ab}\left[e^{+a(z-\zeta)}-e^{-a(z+\zeta)}\right]\cos ay\cos a\eta\, d\eta\, d\zeta\right\} \quad (5)$$

where;

$$a=(2n+1)\frac{\pi}{2}\frac{1}{b}$$

This expression is perfectly general, and can be used to calculate the stream function resulting from any vorticity distribution within the

prescribed boundaries. It is also, of course, a good approximation for channels of moderate to high aspect ratios, where the distant wall has little effect on the secondary flow.

We will be chiefly interested in the case where the distribution is constant in the y-direction, zero above the inlet boundary layer height, δ, and below this height given by Squire and Winter's result,

$$\zeta = -2\epsilon \frac{\partial U}{\partial z}$$

For this case, the expression for the stream function reduces to;

For $z > \delta$;

$$\psi = \sum_{n=0}^{\infty} \frac{2\epsilon}{a^2 b} [\cos ay][e^{-az}] \int_0^{\delta} \left(\frac{\partial U}{\partial z}\right)[e^{+a\varsigma} - e^{-a\varsigma}]\, d\varsigma$$

For $0 < z < \delta$; (6)

$$\psi = \sum_{n=0}^{\infty} \frac{2\epsilon}{a^2 b} [\cos ay][e^{-az}] \left\{ \int_0^{z} \left(\frac{\partial U}{\partial z}\right)[e^{+a\varsigma} - e^{-a\varsigma}]\, d\varsigma + \right.$$

$$\left. + \int_z^{\delta} \left(\frac{\partial U}{\partial z}\right)[e^{+a(2z-\varsigma)} - e^{-a\varsigma}]\, d\varsigma \right\}$$

where

In many cases, including the present configuration, the inlet velocity profile is very nearly linear, and the distribution of can be well represented as a constant over the entire boundary layer region. Then can be removed from the integral and the general integration carried out. The resulting stream function of the

secondary flow for a linear inlet velocity profile is:

For all $z > \delta$;

$$\psi = \sum_{n=0}^{\infty} \frac{2\epsilon \frac{dU}{dz}}{a^3 b} \left[\cos ay\right]\left[e^{-az}\right]\left[e^{-a\delta} + e^{+a\delta} - 2\right]$$

For all $0 < z < \delta$; (7)

$$\psi = \sum_{n=0}^{\infty} \frac{2\epsilon \frac{dU}{dz}}{a^3 b} \left[\cos ay\right]\left[2(1 - e^{-az}) + e^{-a\delta}\left(e^{-az} - e^{+az}\right)\right]$$

where

$$a = (2n+1)\frac{\pi}{2}\frac{1}{b}$$

This gives for the secondary flow velocity components;

For all $z > \delta$;

$$v = \sum_{n=0}^{\infty} \frac{-2\epsilon \frac{dU}{dz}}{a^3 b} \left[\cos ay\right]\left[e^{-az}\right]\left[e^{a\delta} + e^{-a\delta} - 2\right]$$

(8)

$$w = \sum_{n=0}^{\infty} \frac{-2\epsilon \frac{dU}{dz}}{a^3 b} \left[\sin ay\right]\left[e^{-az}\right]\left[e^{a\delta} + e^{-a\delta} - 2\right]$$

where

$$a = (2n+1)\frac{\pi}{2}\frac{1}{b}$$

For all $0 < z < \delta$;

$$v = \sum_{n=0}^{\infty} \frac{-2\epsilon \frac{dU}{dz}}{a^2 b} \left[\cos ay\right]\left[2e^{-az} - e^{-a\delta}\left(e^{-az} + e^{+az}\right)\right] \qquad (8a)$$

$$w = \sum_{n=0}^{\infty} \frac{-2\epsilon \frac{dU}{dz}}{a^2 b} \left[\sin ay\right]\left[2(1 - e^{-az}) + e^{-a\delta}\left(e^{-az} + e^{+az}\right)\right]$$

where

$$a = (2n+1)\frac{\pi}{2}\frac{1}{b}$$

These expressions fit all the boundary conditions on the velocity including the exponential reduction to zero velocity for large z . Also, they match correctly at the edge of the vorticity layer, $z = \delta$. The v-component of velocity above the vorticity layer is of the same sign everywhere, as would be expected if the distributed vorticity is all of the same sign. The terms of the above series for v and w possess an upper bound that dies off at least as fast as $\frac{1}{(2n+1)^2}$, so that for all practical purposes, only the first term is needed. These expressions were evaluated for a set of numbers approximating the present case. The streamlines of the predicted secondary flow are shown in Figure 95. The secondary flow velocity diagram is given in Figure 67, and was compared earlier to the actual secondary flow from the experimental surveys. Although there were some very definite differences, the general character of the secondary flow is predicted. Also, the predicted velocities are of the correct order of magnitude, so that an estimate of the energy of the secondary flow velocities based on this analytical model would be reasonably near to the actual value.

The above solution is strictly applicable, only for a channel of infinite aspect ratio. However, it can be seen from the vector diagram of the secondary flow velocities, that the velocities are practically zero for this case at a distance from the end wall equal to the channel width. Therefore, it probably is very nearly correct for channel aspect ratios down to about 2.0. Since this covers most of the range of practical

interest, there is little need for solutions for channels of finite aspect ratios. However, if such solutions were needed, they could be obtained easily; either by altering the Green's function to include an infinite series of images in the $\bar{z}$ -direction to satisfy the new end wall boundary condition, and integrating the resulting expression, treating the limits carefully, or by forming an infinite series from the solution of the appropriate case. The resulting expression would be a double summation, and for most practical cases, only the leading term, identical with the present expression, would be of significant magnitude.

Since the linearized theory gives the general character of the actual flow, it would seem that this could be treated as a first approximation to the complete solution, and corrections could be developed for approximations of higher order. Of first importance among these corrections would be the behavior of the three-dimensional boundary layer flow at the end wall. It would be desired, in particular, to find criteria for determining whether a mixing zone will form, and its expected size. Since the boundary layer of interest is three-dimensional, turbulent, and in an adverse gradient, this problem is extremely difficult. Some guidance to the expected behavior may be found in the present experimental results. Other corrections of lesser importance would be the correction of the vorticity distribution for self-transport, for the increased local turning near the wall, and for the variation in radius of the channel turn across the channel. Superposition of these effects upon the linearized solution, might account for most of the observable characteristics of the flow in a conventional compressor cascade.

V. CONCLUDING REMARKS

The laminar or turbulent character of the boundary layer on the cascade blades and end walls was found to be a decisive factor in determining the cascade performance. The behavior of the two types of boundary layers is distinctly different when exposed to the adverse pressure gradients encountered in a diffusing channel. Separation of a laminar boundary layer, either on the blades or on the wall, can lead to unique flow patterns in the cascade. However, at the Reynolds numbers at which most turbomachines operate, the high disturbance level practically insures that all stages after the first will have entirely turbulent boundary layers. Therefore, those flow patterns resulting from laminar boundary layers are of extremely limited practical interest at the present time.

Cascade end clearance leakage also was found to have serious effects on the three-dimensional flow near the wall of the cascade. These effects were disproportionately strong for leakage in very small amounts. This information is significant, both in the interpretation of cascade results for application to turbomachinery, and in the turbomachinery itself.

The most significant observation of these experiments was the presence of a three-dimensional separation, or mixing region, at the corner of the low pressure surface of the blade and the wall, which appeared at high angles of attack, both positive and negative, and grew rapidly as the cross-channel and adverse pressure gradients increase with increasing angles of attack. While the direct losses associated

with this mixing region appeared to be small, the regions would be expected to have a serious effect on the performance of succeeding stages in a turbomachine. This effect would be present in the off-design performance of a conservatively designed turbomachine, and even at the design operating point of a machine designed for larger channel turning and diffusion. Because very small amounts of flow appear to be responsible for these mixing regions, it would appear that the application of boundary layer control in this region is of more than usual interest.

These mixing regions differ from the channel vortices often reported. They are not displaced from the wall, and their vorticity appears to be much less than that expected of a channel vortex, although the presence of the wall confuses the issue. In any case, the lift of the blades remains large at the wall.

An exact solution for the secondary flow velocities, based on Squire and Winter's linearized result for the secondary vorticity, was compared with the experimental results. The velocities and directions predicted were generally of the right order. The predicted kinetic energy of the secondary flow is also satisfactory. The chief deviation from theory for the present cascade was the presence of the mixing region. It does not appear to be possible, at present, to predict either its presence or its magnitude, since the problem is essentially three-dimensional and non-linear.

It should be noted that the discrepancy between the present cascade representation and the secondary flow in the rotor of a turbo-

machine is not only a matter of the passage of wakes from the upstream blade row. Another matter of particular interest in the secondary flow in a rotor is that in a typical axial flow machine, the vorticity vector in the wall boundary layers entering the rotor will point nearly parallel to the incoming relative velocity entering the rotor passage, instead of normal to it, as in the stator cascade considered here. The secondary flow resulting from this incoming vorticity will be generally in the opposite direction to that which we have so far discussed, and will be a somewhat stronger effect, since it will depend, not on the component of vorticity turned out of the direction of flow, but on practically the full magnitude of the vorticity vector. If no separation occurs at the channel inlet, due to the distortion of the design relative velocities by the various effects of the inlet wall boundary layer, this rotor secondary flow might be successfully treated by the analytical model used in this report, assuming the inlet secondary vorticity distribution to be known. However, it is impossible to judge from the information presently available whether this analytical model would be satisfactory. It should be noticed that after a few stages, similar effects might be induced in the following stators by the boundary layers leaving the rotors.

It would be an extremely difficult task to study this aspect of the secondary flow problem in a cascade. Attempts have been made to simulate the effects of relative motion of successive blade rows in a cascade, by the use of moving belts and similar devices, but the resulting models are not very satisfactory. The effects of the flow pattern leaving one cascade on the performance of succeeding cascades in

relative motion will probably have to be determined in rotating machinery, despite the difficulty of such tests.

REFERENCES

1. Ainley, D. G.: Performance of Axial-Flow Turbines, War Emergency Issue No. 41, published in Proceedings, the Institution of Mechanical Engineers (London). Reprinted in U.S. by ASME, (April 1949), pp. 230-244.

2. Carter, A. D. S.: Three-Dimensional Flow Theories for Axial Compressors and Turbines, War Emergency Issue No. 41, published in Proceedings, The Institution of Mechanical Engineers (London). Reprinted in U.S. by ASME, (April 1949), pp. 255-268.

3. Wu, Chung-Hua: Survey of Available Information on Internal Flow Losses Through Axial Turbomachines, NACA RM E50J13, (1951).

4. von Karman, Theodore and Tsien, H. S.: Lifting Line Theory for a Wing in Non-Uniform Flow, Quarterly of Applied Mathematics, Vol. III, (April 1945).

5. Carter, A. D. C. and Cohen, E. M.: Preliminary Investigation into the Three-Dimensional Flow Through a Cascade of Aerofoils, Aeronautical Research Countil Reports and Memoranda No. 2339, (1949).

6. Hausmann, G. F.: The Theoretical Induced Deflection Angle in Cascades Having Wall Boundary Layers, Journal of the Aeronautical Sciences, Vol. 15, No. 11, (November 1948).

7. Squire, H. B. and Winter, K. G.: The Secondary Flow in a Cascade of Airfoils in a Non-Uniform Stream, Journal of the Aeronautical Sciences, Vol. 18, No. 4, (April 1951).

8. Hawthorne, W. R.: Secondary Circulation in Fluid Flow, Proc. of the Royal Society of London, Series A, Vol. 206, No. A1086, (May 1951).

9. Eichenberger, H. P.: Sear Flow in Bends, Office of Naval Research, Contract N5ori07848, Tech. Rept. No. 2, (1951).

10. Detra, Ralph W.: The Secondary Flow in Curved Pipes, Mitteilungen aus dem Institut fur Aerodynamic, Nr. 20, (1953).

11. Loos, Henk G.: Analysis of Secondary Flow in the Stator of an Axial Turbomachine, Office of Scientific Research, ARDC, Tech. Rept. No. 3, (September 1953).

12. Ehrich, F. F. and Detra, R. W.: Transport of the Boundary Layer in Secondary Flow, Journal of the Aeronautical Sciences, Readers Forum, Vol. 21, No. 2, (February 1954).

13. Howell, A. R.: The Present Basis of Axial Flow Compressor Design, Part I. Cascade Theory and Performance, R and M No. 2095, (1942).

14. Rannie, W. D., Bowen, John F., and Sabersky, Rolf H.: Theoretical and Experimental Investigations of Axial Flow Compressors, Part I. Summary Report, California Institute of Technology, Mechanical Engineering Laboratory, (1949).

15. Russel, Walter R., Gracey, William, Letko, William, and Fournier, Paul G.: Wind Tunnel Investigation of Six Shielded Total-Pressure Tubes at High Angles of Attack, NACA TN 2530, (1951).

16. Mager, Artur: Three-Dimensional Laminar Boundary Layer with Small Cross-Flow, Journal of Aeronautical Sciences, Vol. 21, No. 12, (December 1954).

17. Hansen, Arthur G., Herzig, Howard Z., and Costello, George R.: A Visualization Study of Secondary Flows in Cascades, NACA TN 2947, (1953).

18. Erwin, John R. and Emery, James C.: Effect of Tunnel Configuration and Testing Technique on Cascade Performance, NACA TN 2028, (1950).

19. Hawthorne, W. R.: Secondary Flow About Struts and Airfoils, Journal Aeronautical Sciences, (September 1954).

20. Rains, Dean A.: Tip Clearance Flows in Axial Flow Compressors and Pumps, California Institute of Technology, Hydrodynamics and Mechanical Engineering Laboratories Report No. 5, (1954).

Table I. Airfoil Coordinates in Inches.

X_u	Y_u	X	Y	X_{nom}
0.024	.081	.061	-.059	.0425
0.059	.123	.111	-.078	.0850
0.134	.182	.205	-.093	.1700
0.212	.238	.298	-.106	.2550
0.293	.279	.387	-.104	.3400
0.374	.318	.476	-.102	.4250
0.456	.354	.564	-.101	.5100
0.538	.394	.652	-.098	.5950
0.621	.428	.739	-.094	.6800
0.705	.461	.825	-.089	.7650
0.788	.493	.912	-.083	.8500
1.212	.628	1.340	-.048	1.275
1.640	.738	1.760	-.012	1.700
2.071	.826	2.179	+.027	2.125
2.505	.895	2.595	+.060	2.550
2.941	.941	3.009	+.094	2.975
3.378	.965	3.422	+.127	3.400
3.814	.970	3.836	+.157	3.825
4.250	.953	4.250	+.185	4.250
4.684	.916	4.666	+.211	4.675
5.117	.861	5.083	+.231	5.100
5.547	.791	5.503	+.245	5.525
5.974	.705	5.926	+.251	5.950
6.399	.604	6.351	+.249	6.375
6.822	.499	6.778	+.229	6.800
7.243	.389	7.207	+.191	7.225
7.663	.273	7.637	+.137	7.650
8.082	.154	8.068	+.062	8.075
8.502	.033	8.498	-.033	8.500

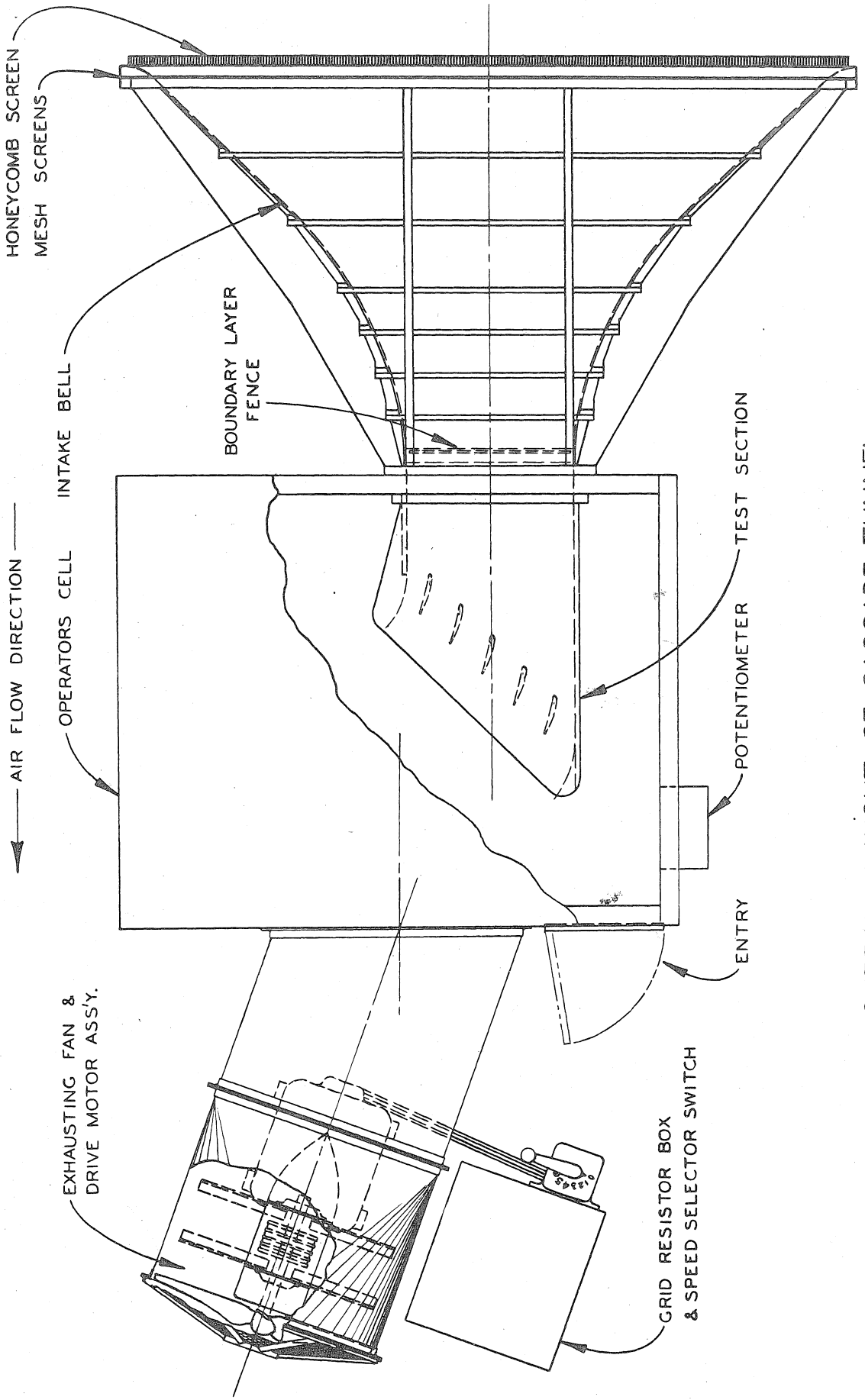

OVERALL LAYOUT OF CASCADE TUNNEL

FIGURE 1

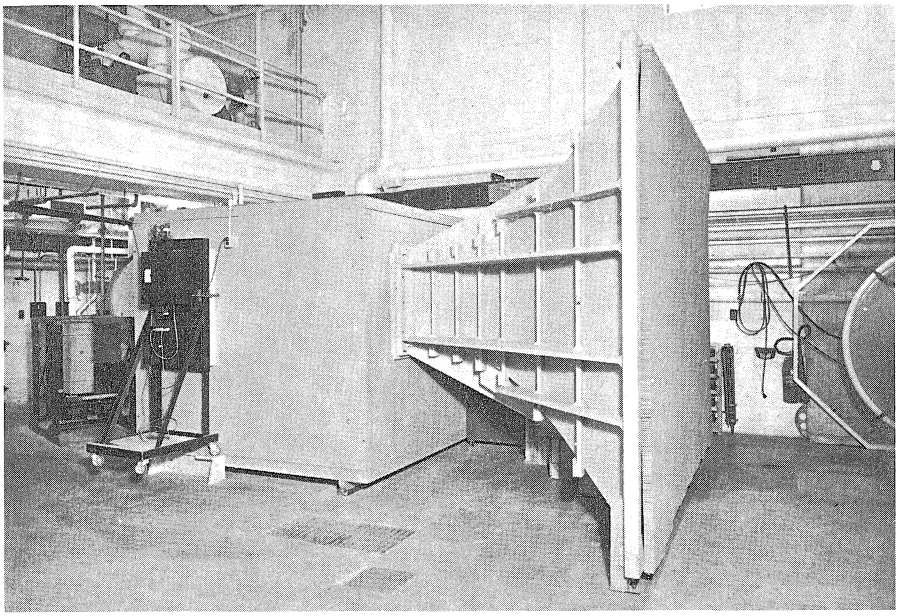

VIEW OF CASCADE TUNNEL FROM INLET

FIGURE 2

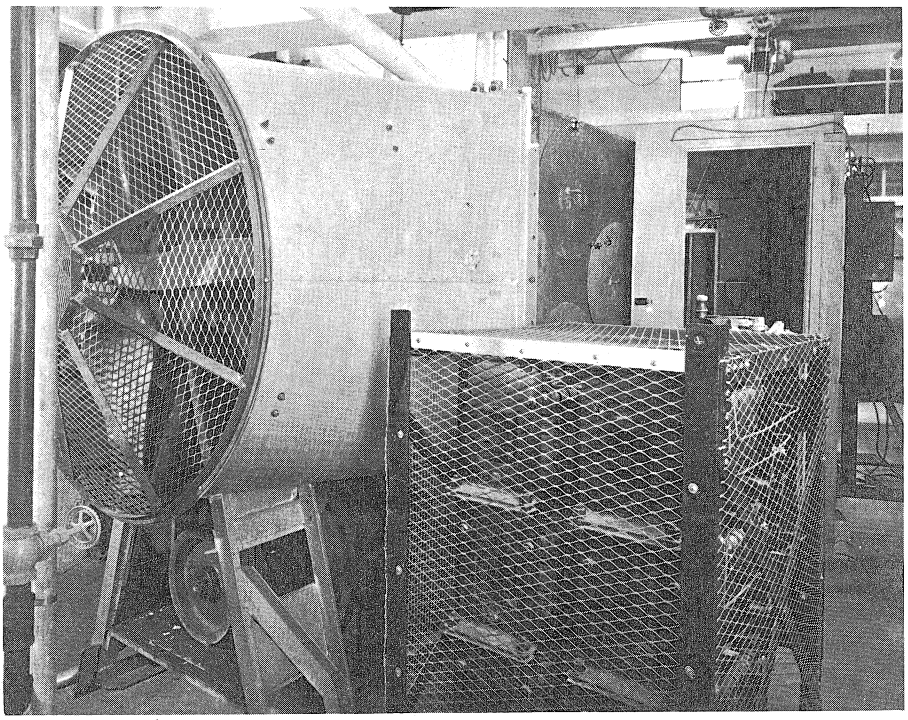

CASCADE TUNNEL OUTLET

FIGURE 3

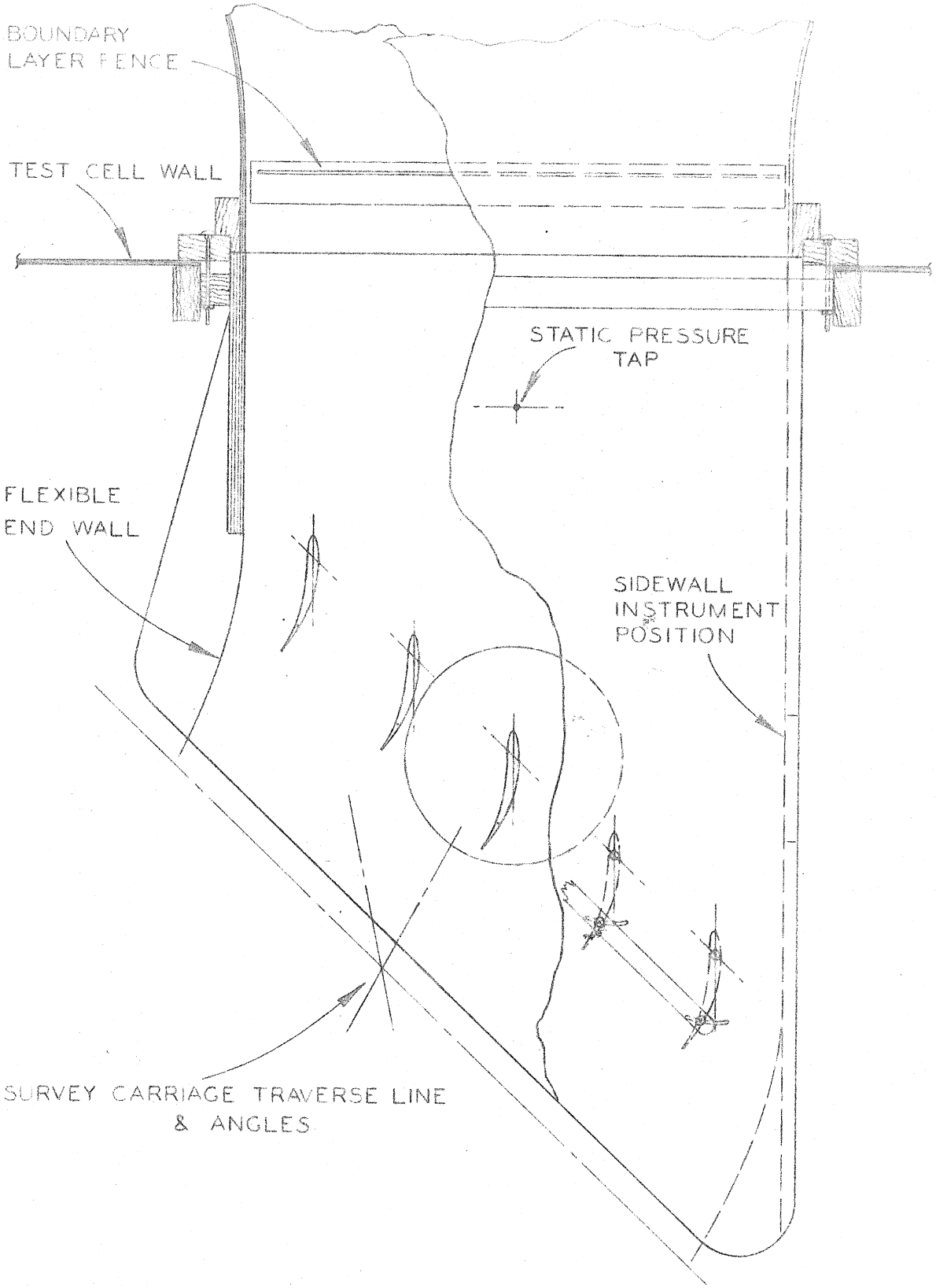

TEST SECTION LAYOUT

FIGURE 4

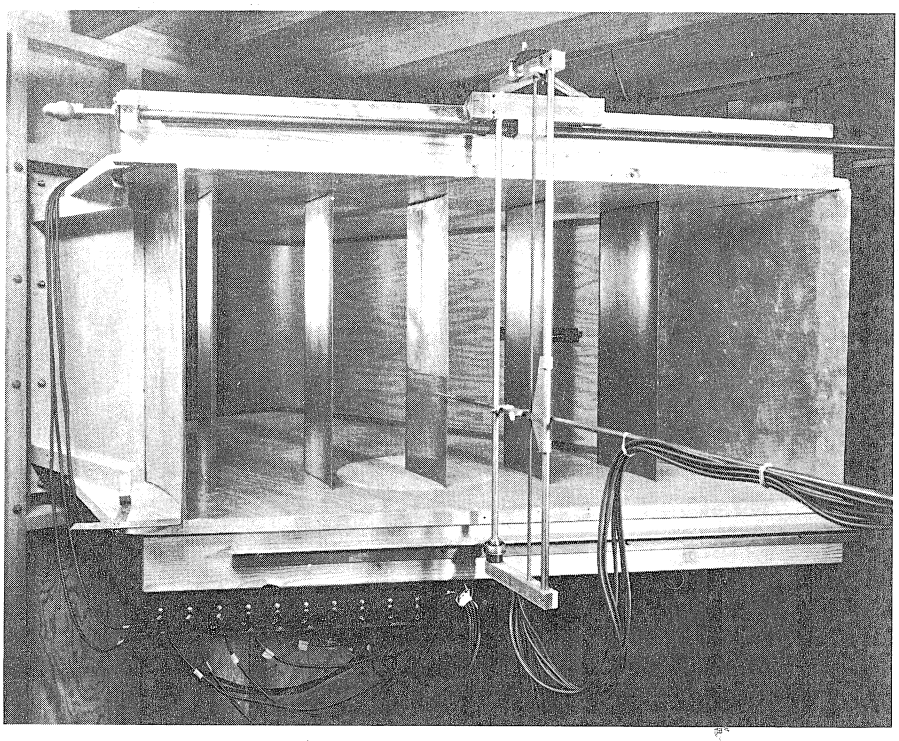

TEST SECTION VIEWED FROM DOWNSTREAM

FIGURE 5

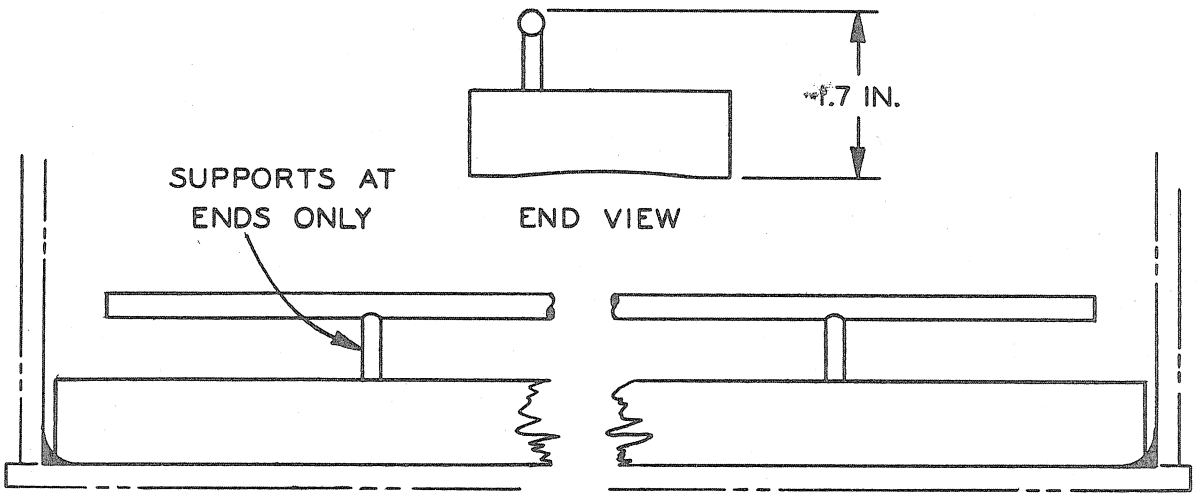

BOUNDARY LAYER FENCE

FIGURE 6

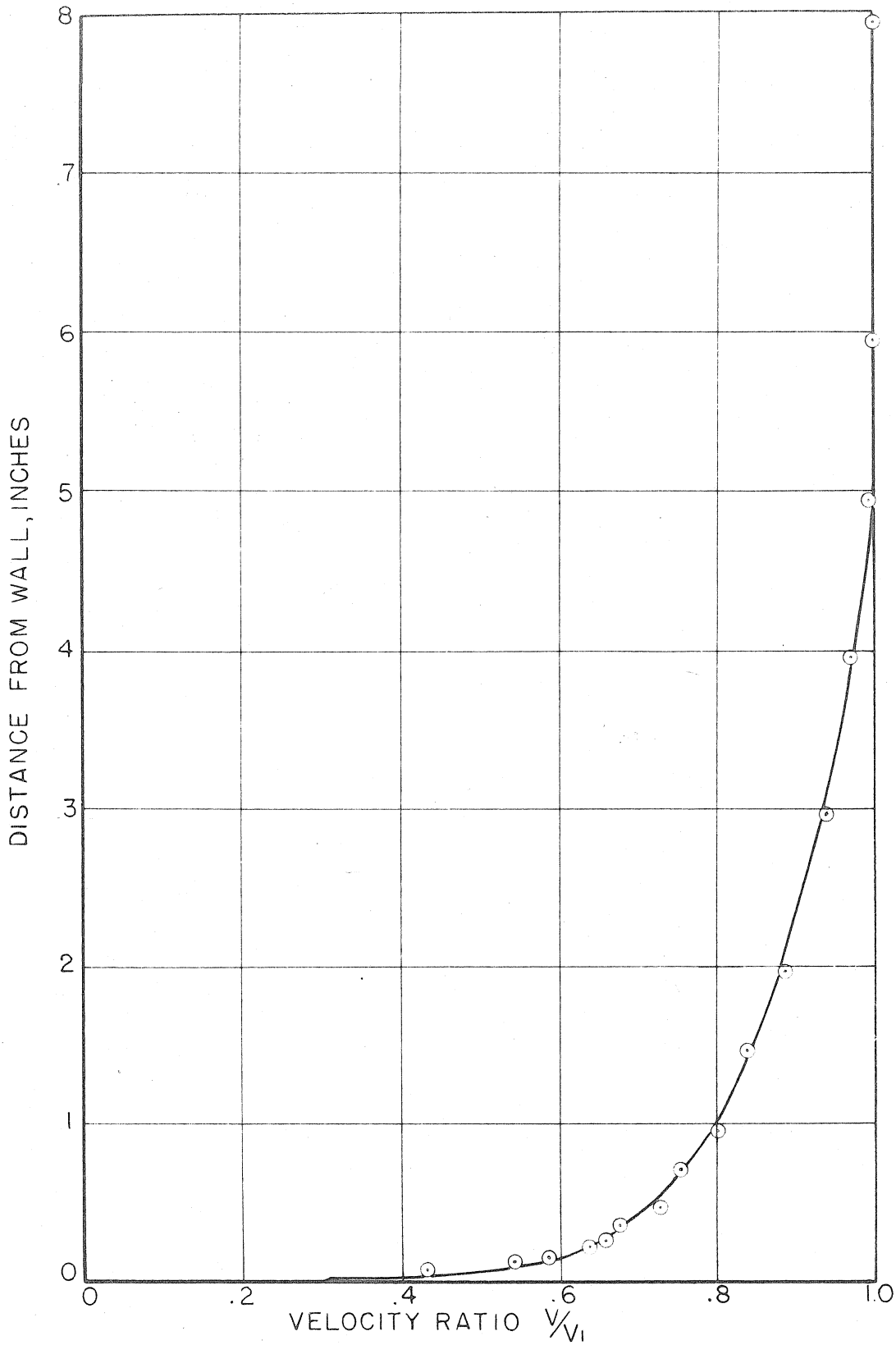

COMPARISON OF INLET WALL BOUNDARY LAYER VELOCITY PROFILE WITH 1/7 POWER LAW; BLADES REMOVED; SURVEY AT OC PLANE

FIGURE 7

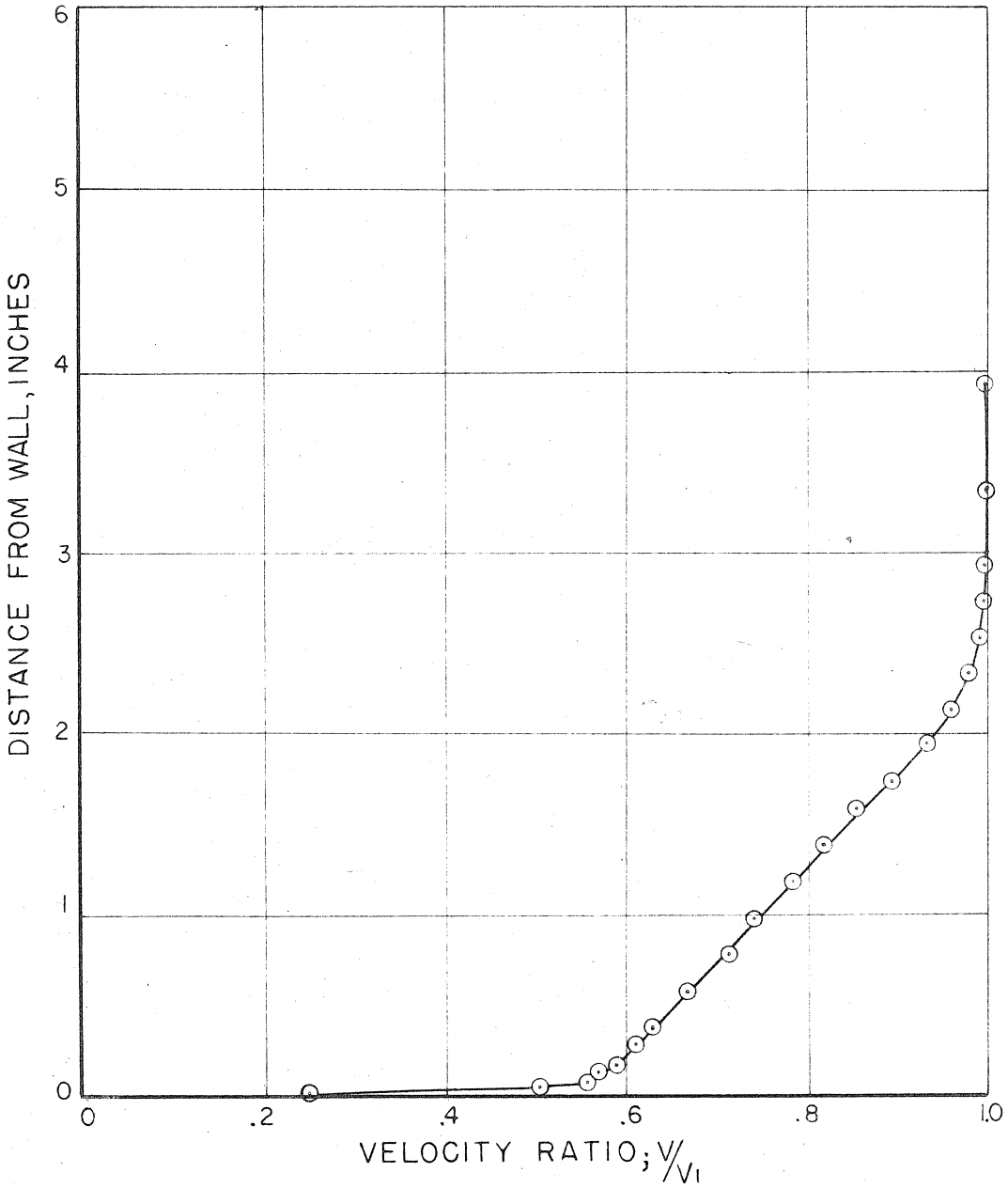

INLET WALL BOUNDARY LAYER VELOCITY PROFILE

BLADES INSTALLED, SURVEY I CHORD AHEAD

FIGURE 8

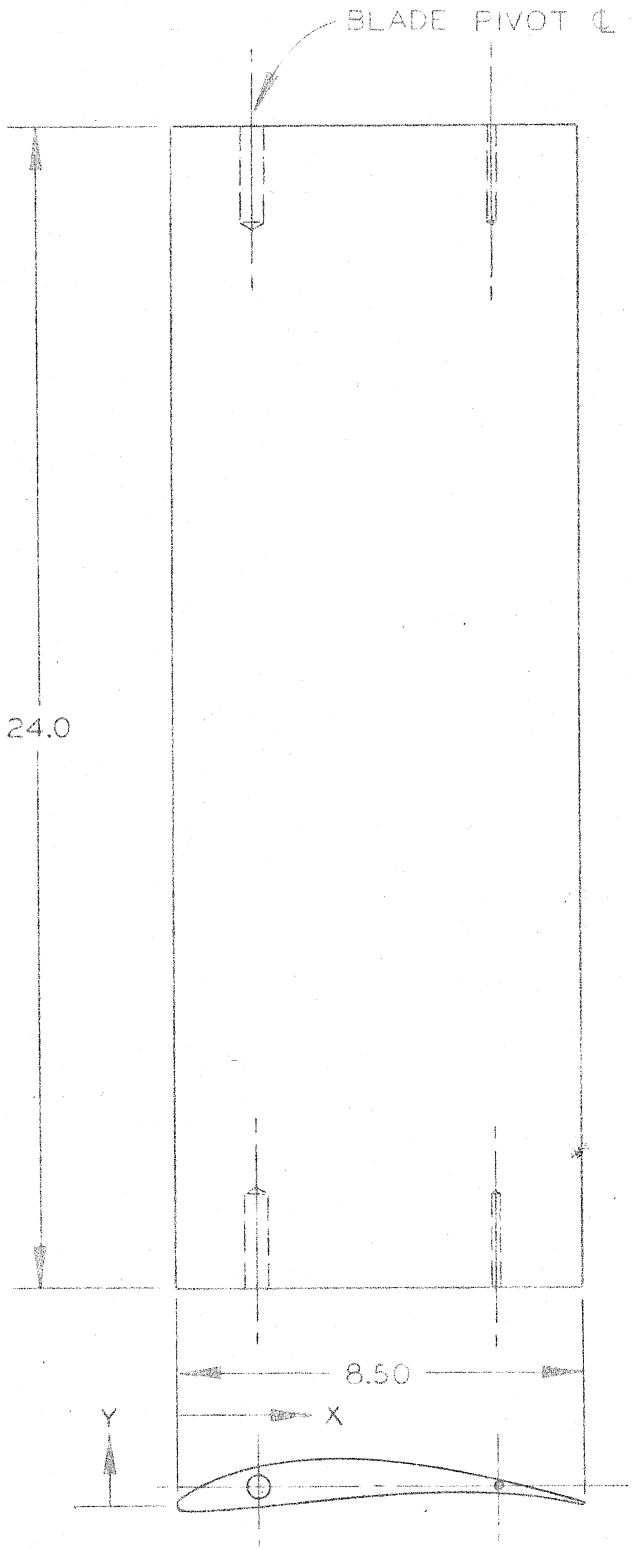

COORDINATES GIVEN IN TABLE 1

CASCADE BLADE

FIGURE 9

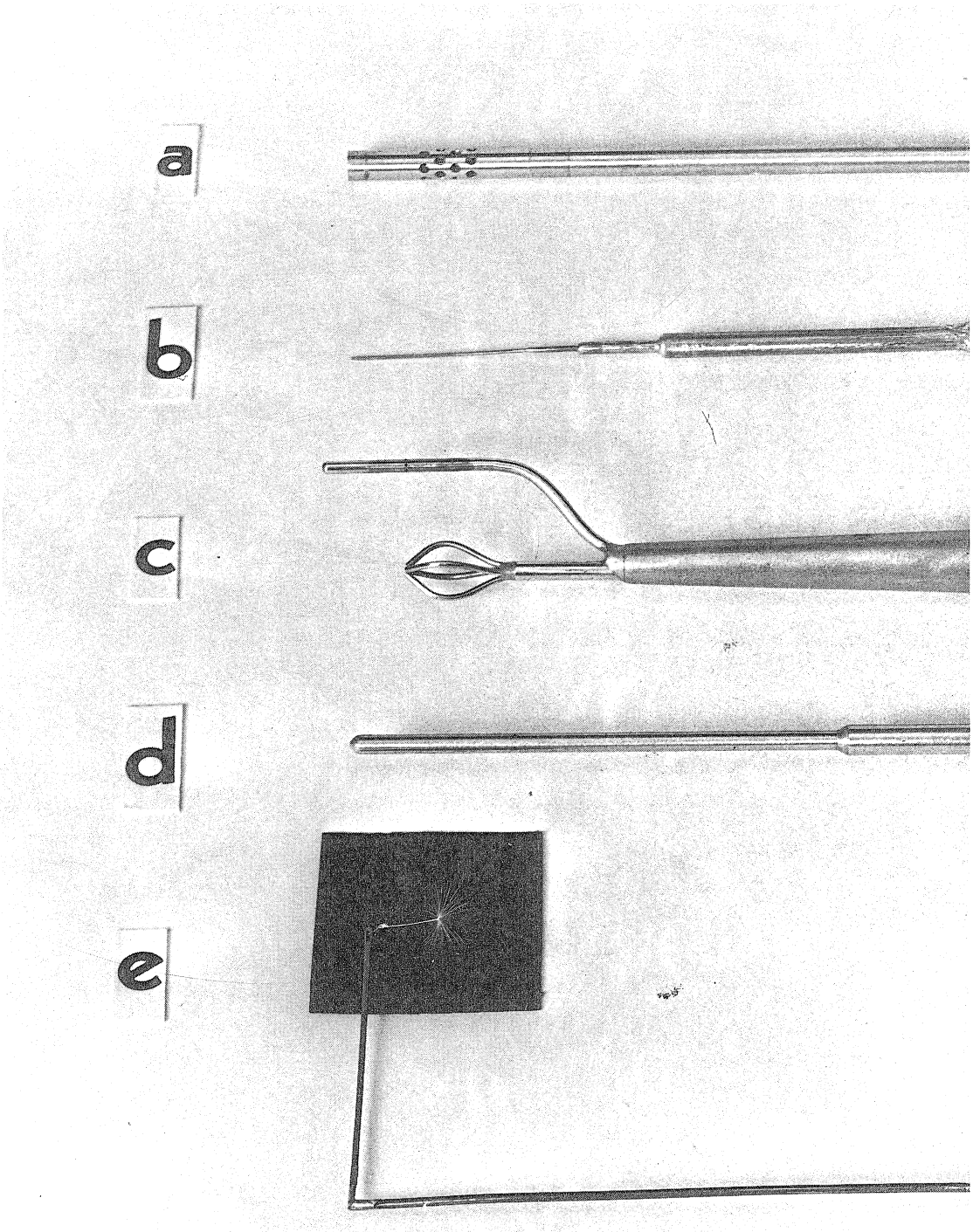

SURVEY PROBES USED IN EXPERIMENTAL STUDY

FIGURE 10

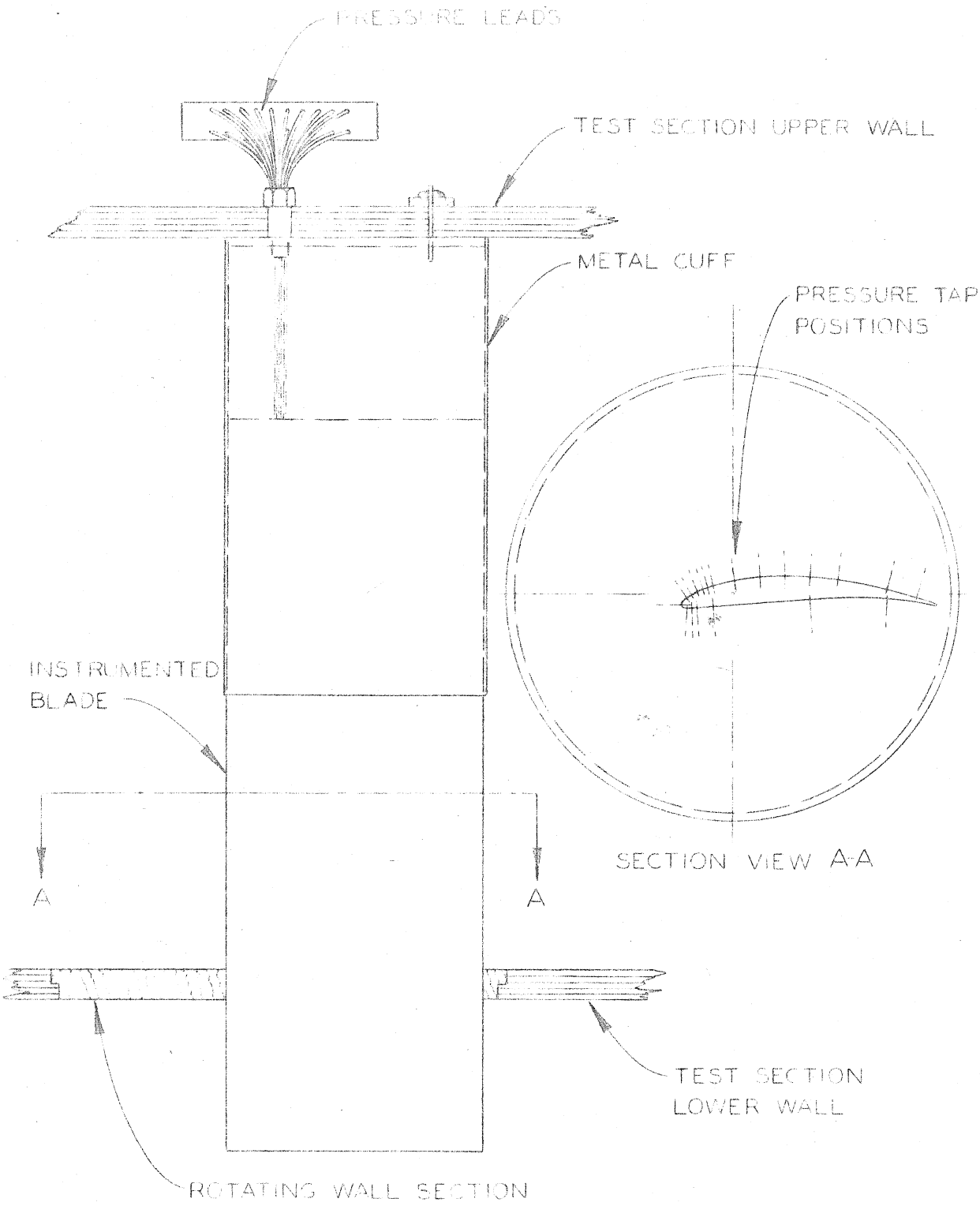

INSTRUMENTED BLADE & CUFF ARRANGEMENT

FIGURE 11

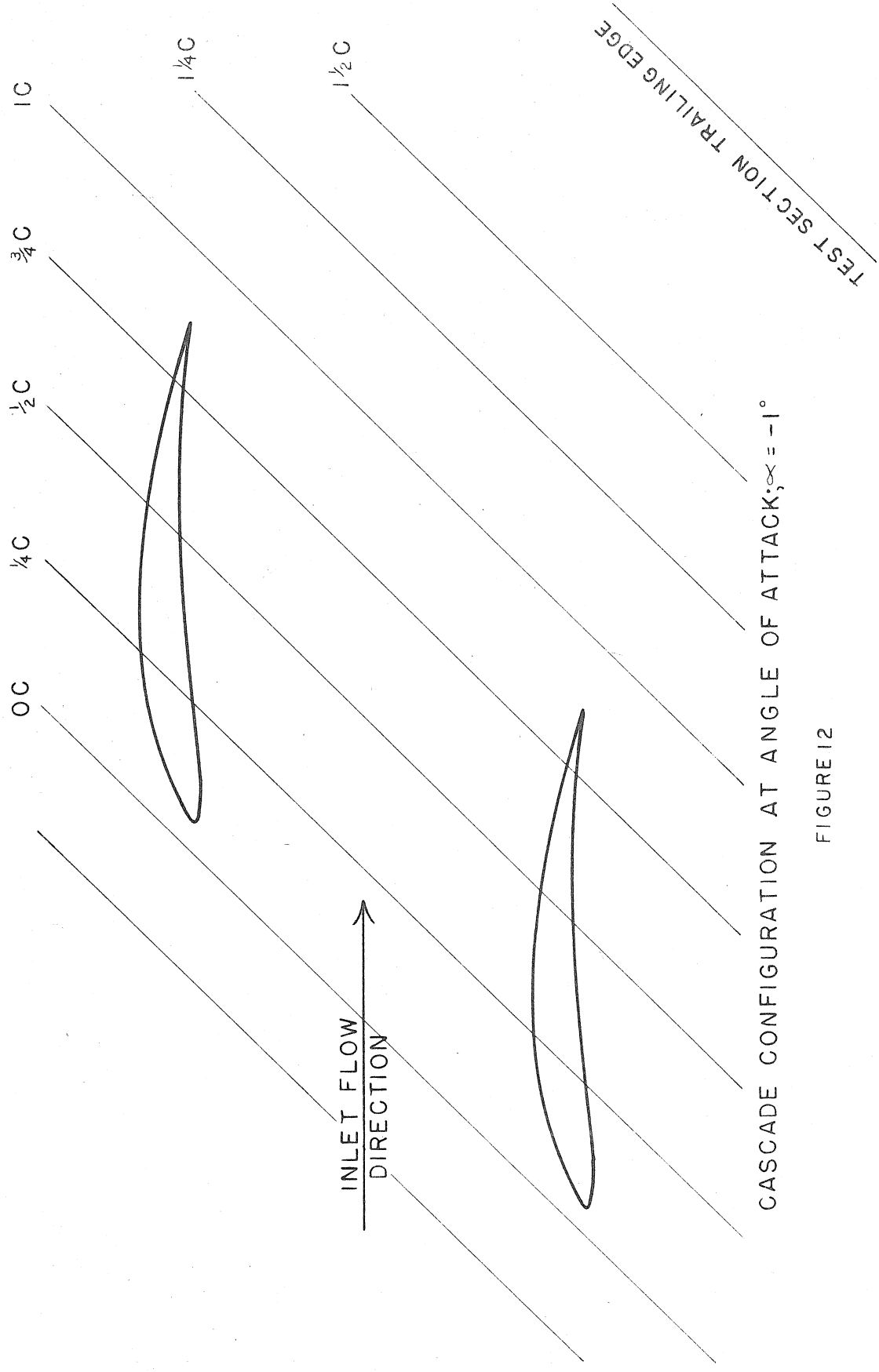

CASCADE CONFIGURATION AT ANGLE OF ATTACK; $\alpha = -1°$

FIGURE 12

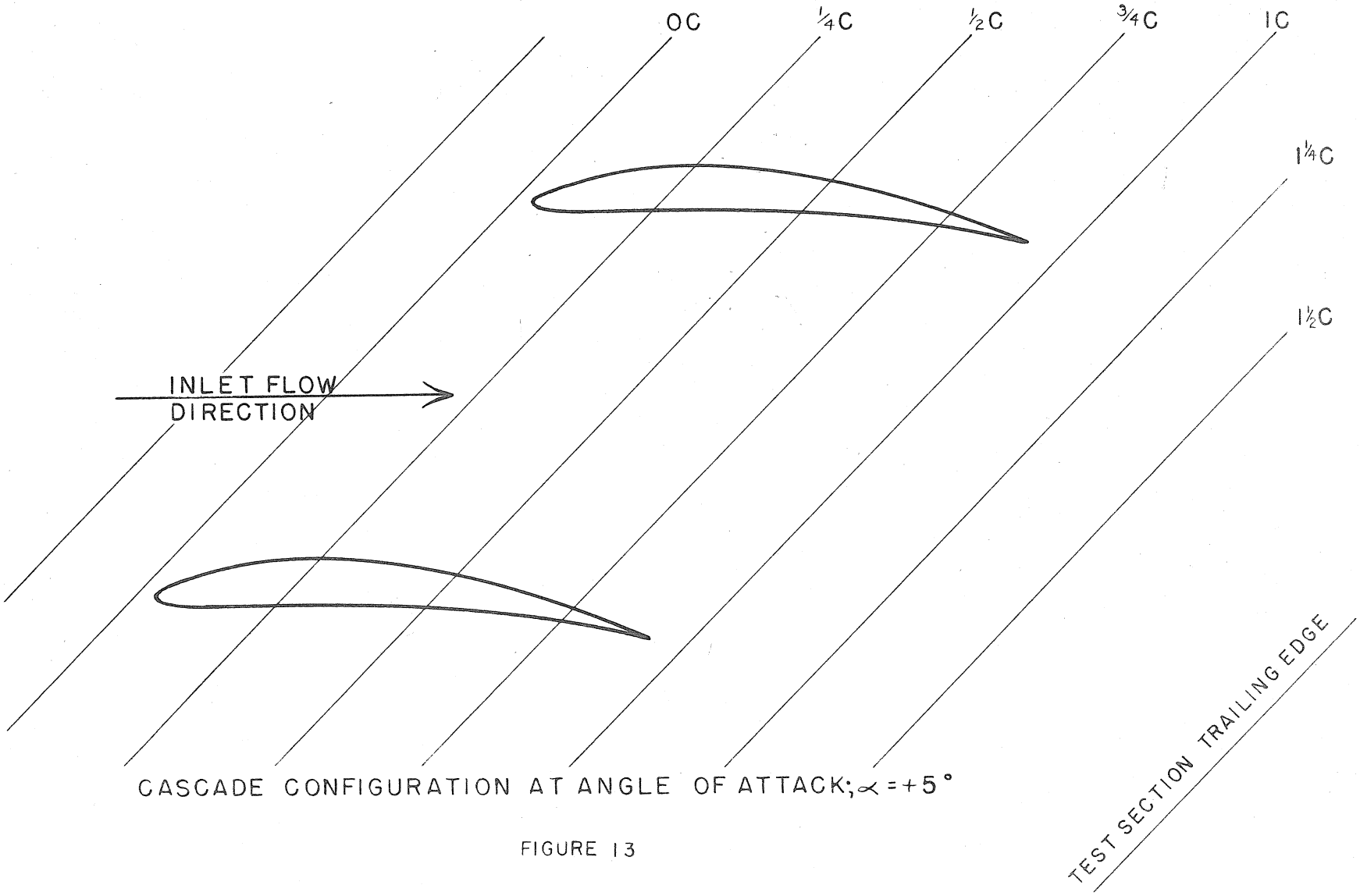

CASCADE CONFIGURATION AT ANGLE OF ATTACK; $\alpha = +5°$

FIGURE 13

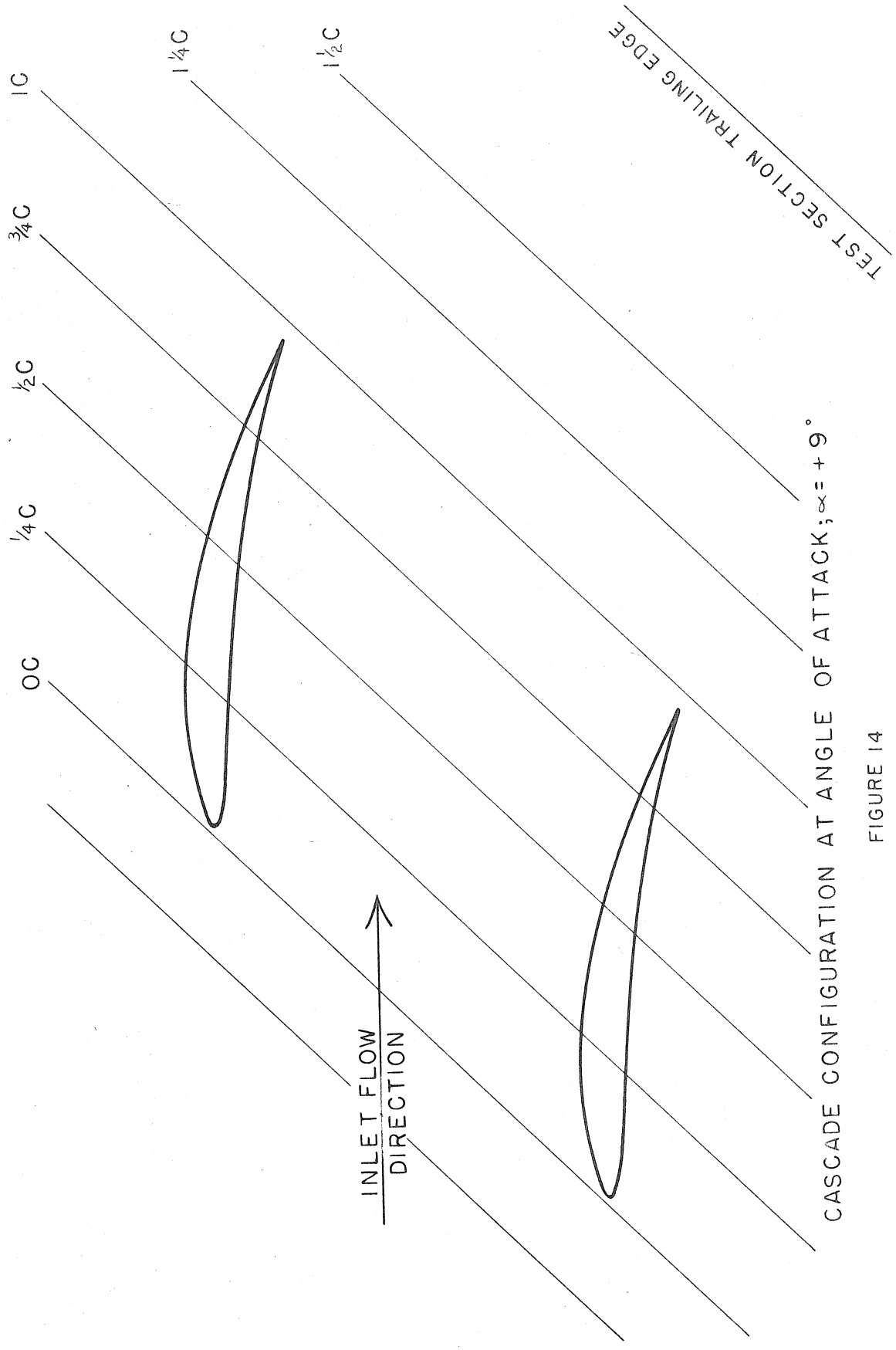

CASCADE CONFIGURATION AT ANGLE OF ATTACK; $\alpha = +9^{\circ}$

FIGURE 14

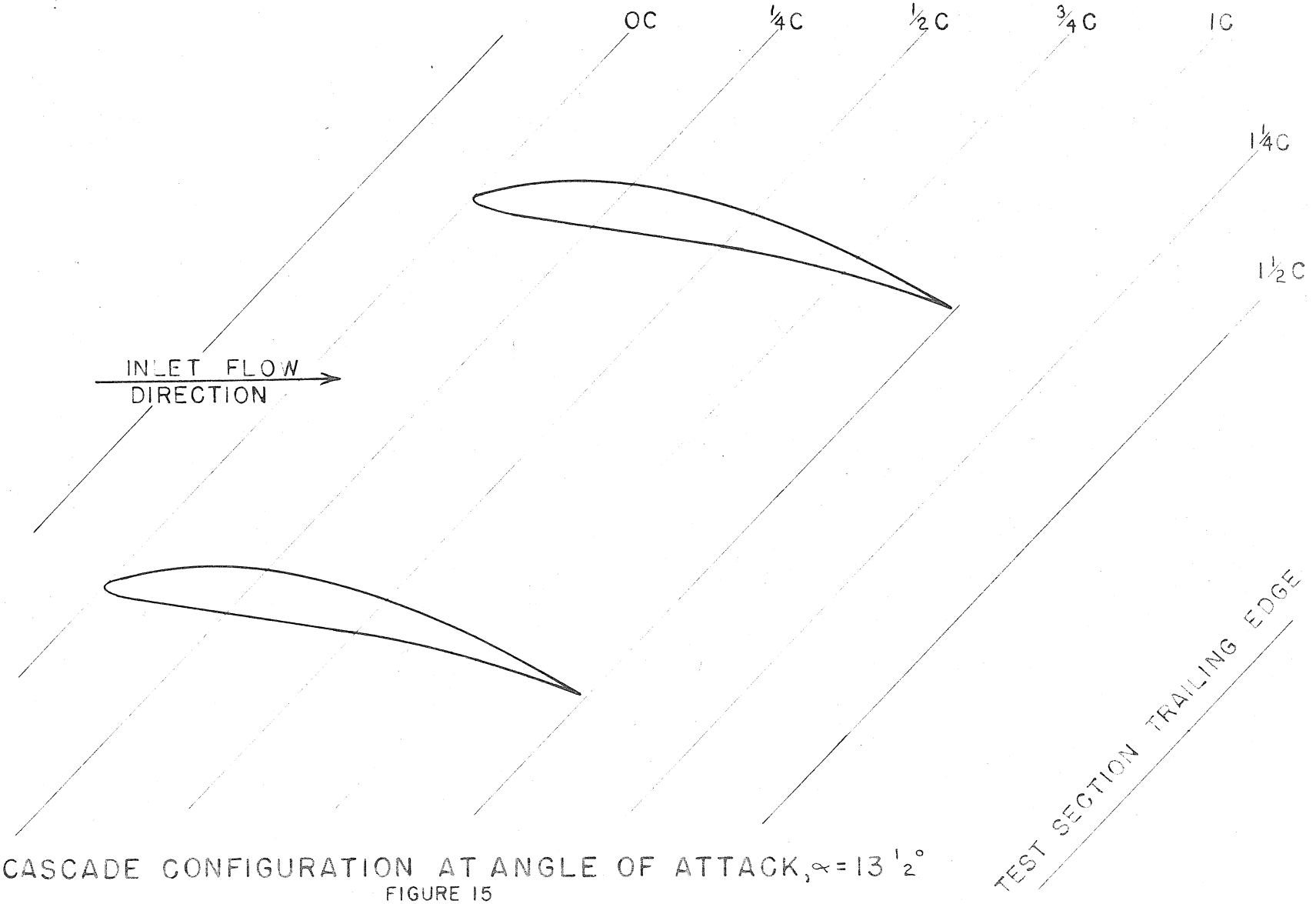

CASCADE CONFIGURATION AT ANGLE OF ATTACK, $\alpha = 13\frac{1}{2}°$

FIGURE 15

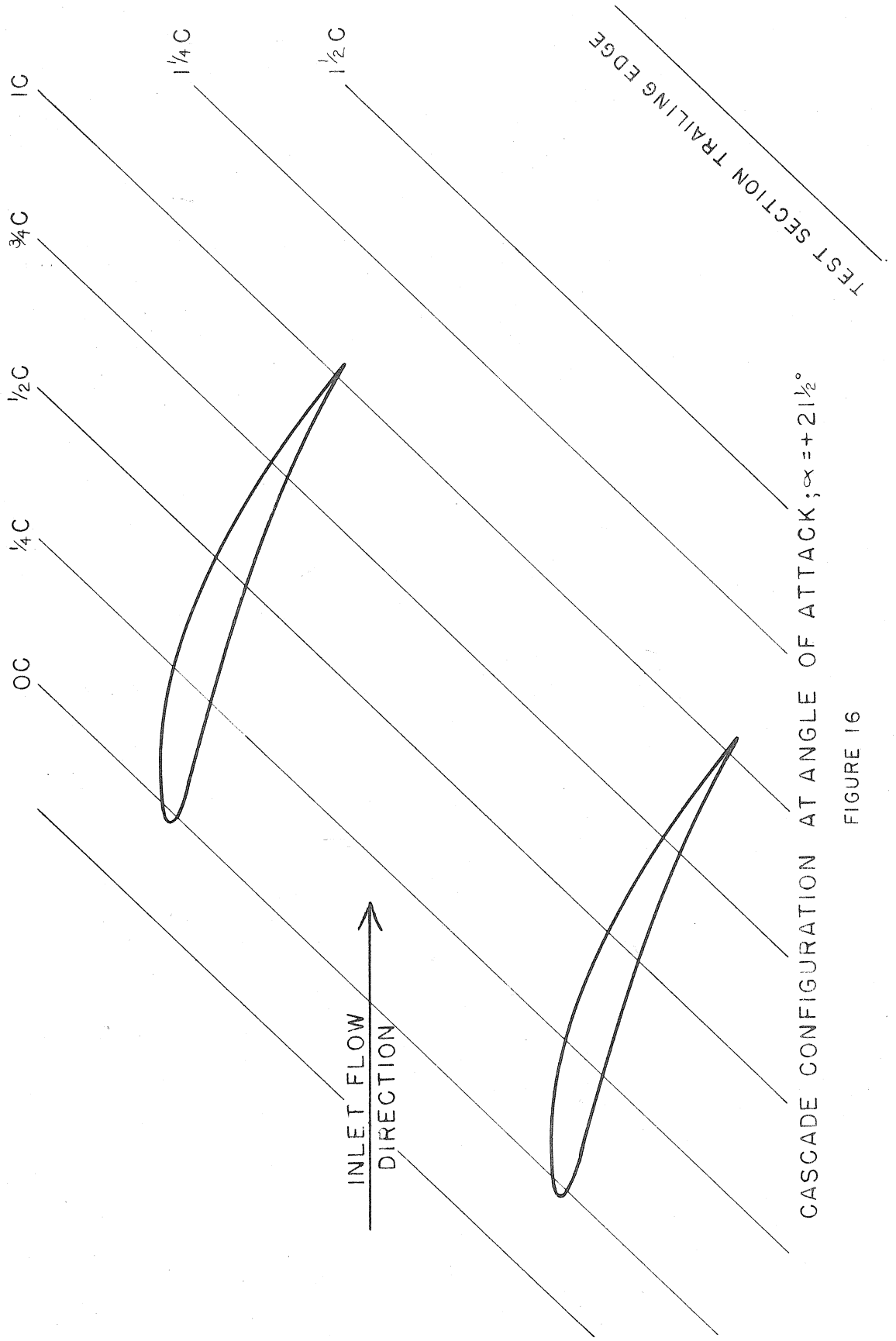

CASCADE CONFIGURATION AT ANGLE OF ATTACK; $\alpha = +21\frac{1}{2}°$

FIGURE 16

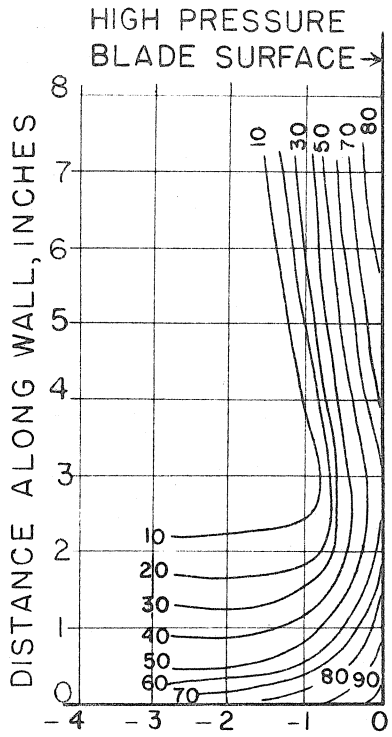

TOTAL PRESSURE PROFILE MAP; ½C; ∝ = -1°

FIGURE 17

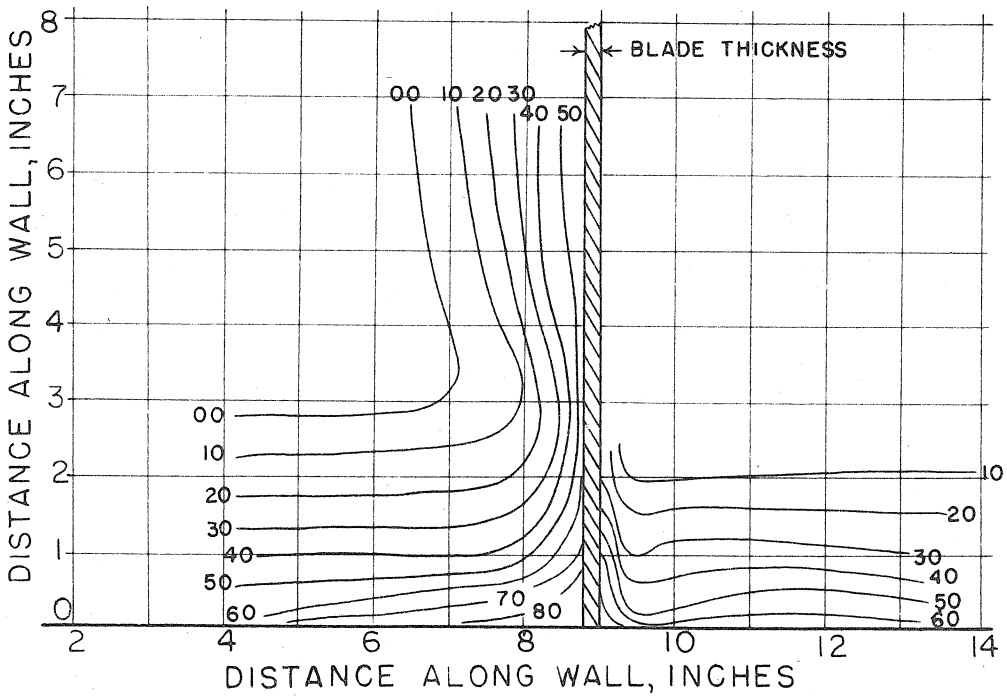

TOTAL PRESSURE PROFILE MAP; ¾C; ∝ = -1°

FIGURE 18

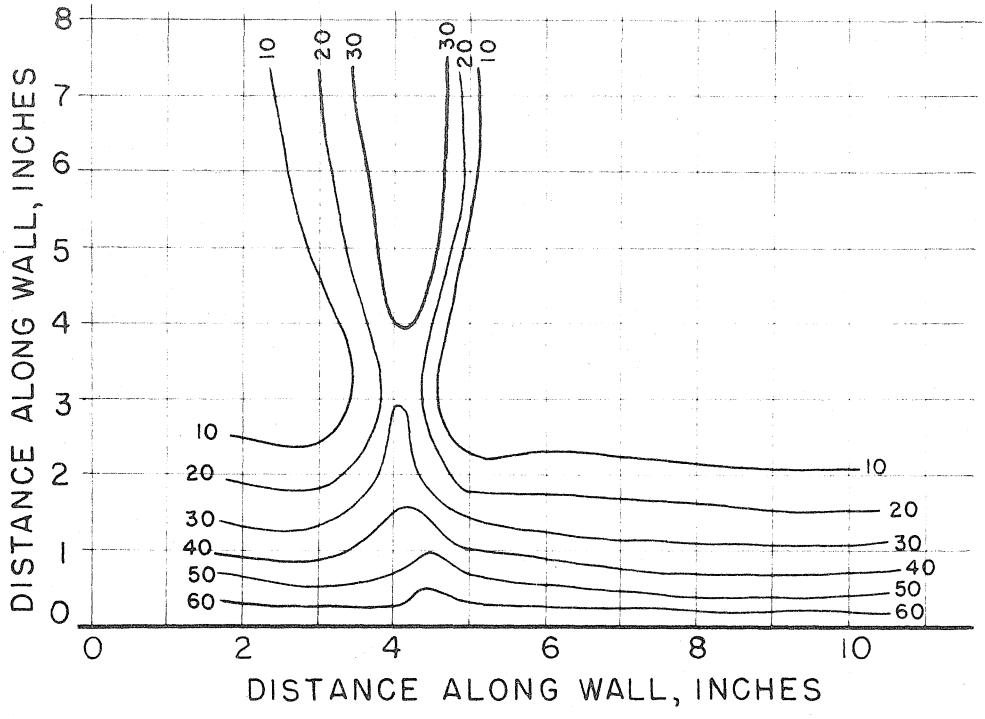

TOTAL PRESSURE PROFILE MAP; 1¼C; $\alpha = -1°$

FIGURE 19

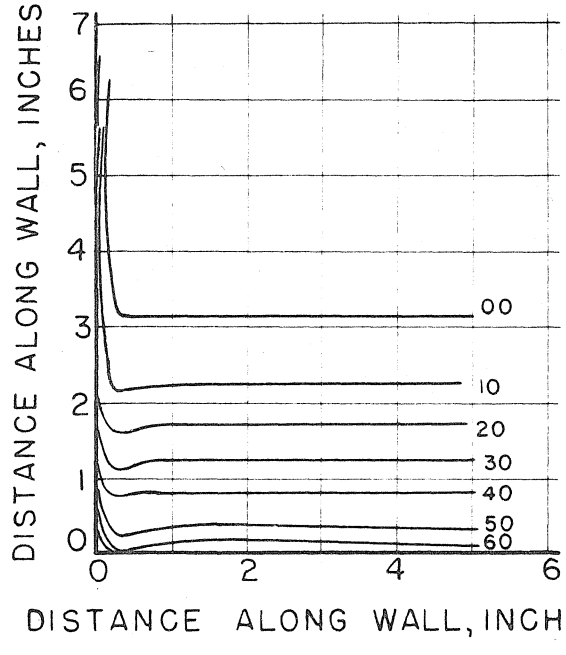

TOTAL PRESSURE PROFILE MAP; ½C; $\alpha = 5°$

FIGURE 20

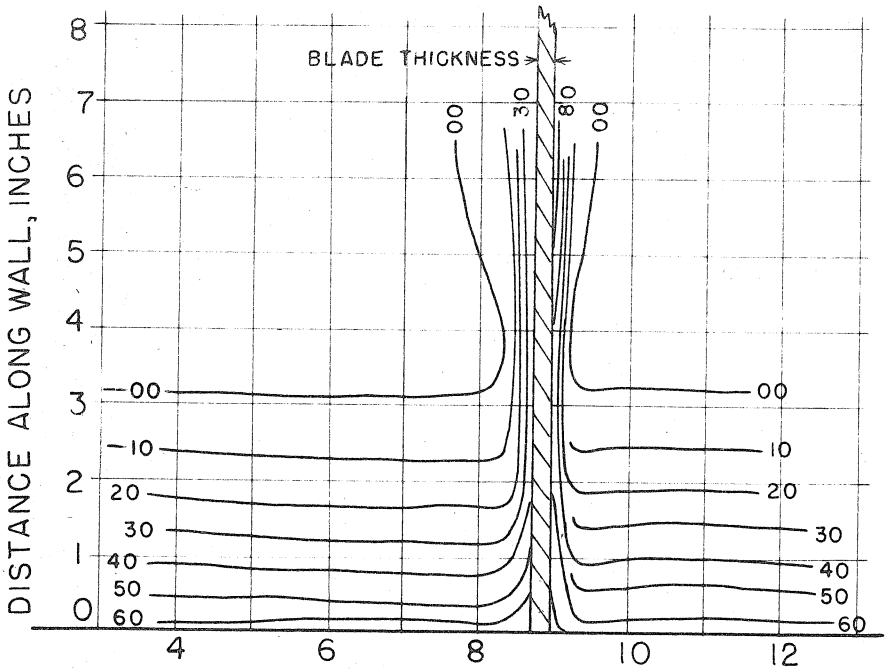

TOTAL PRESSURE PROFILE MAP; ¾ C; $\alpha = 5°$

FIGURE 21

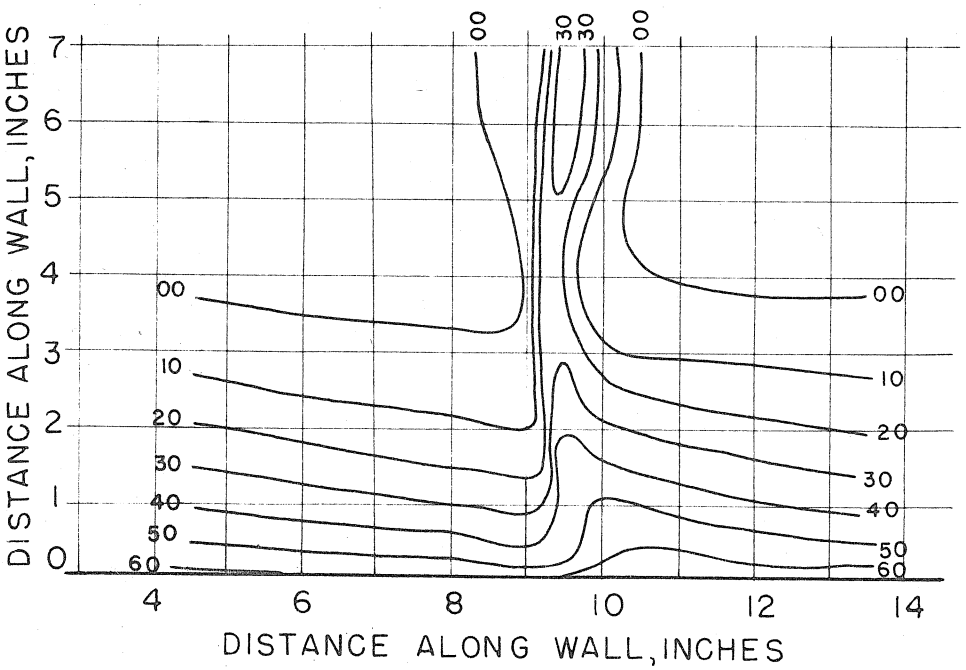

TOTAL PRESSURE PROFILE MAP; 1¼C; $\alpha = 5°$

FIGURE 22

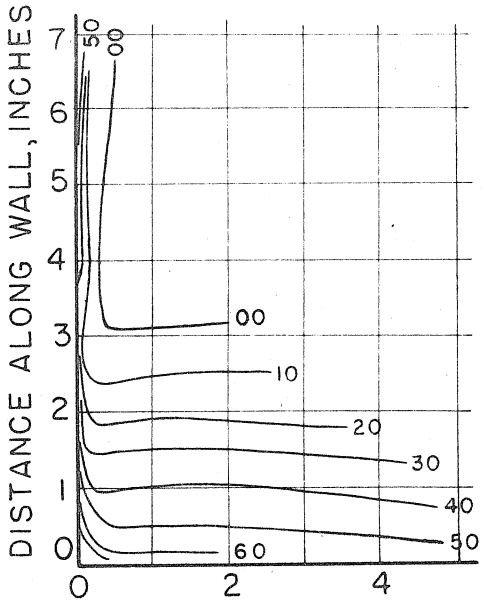

TOTAL PRESSURE PROFILE MAP; ½C; $\alpha = 9°$

FIGURE 23

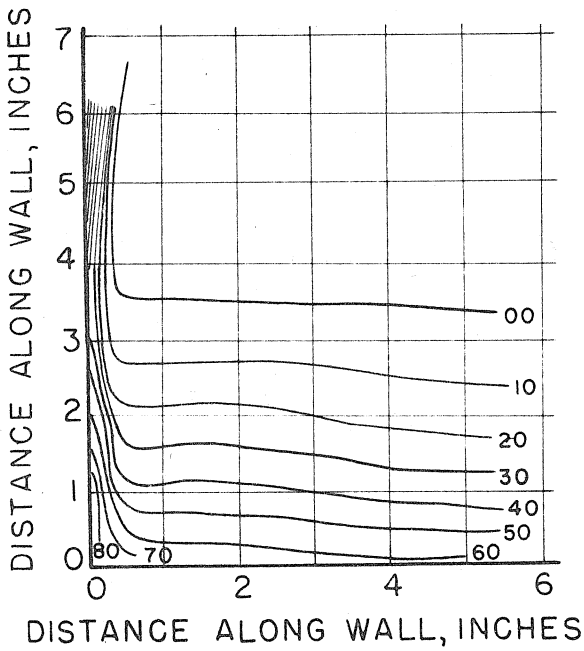

TOTAL PRESSURE PROFILE MAP; ¾C; $\alpha = 9°$

FIGURE 24

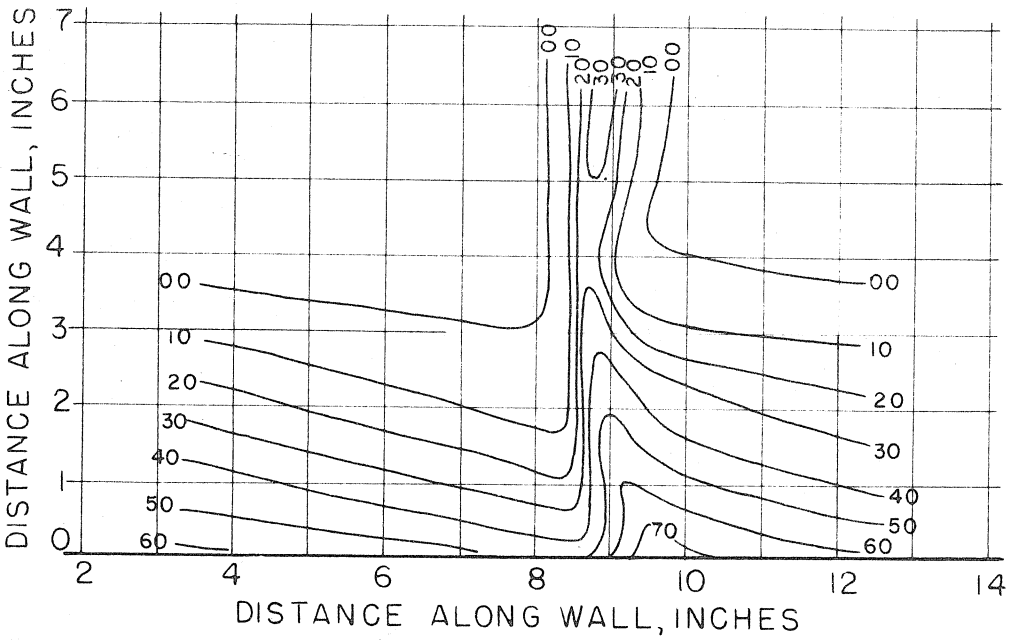

TOTAL PRESSURE PROFILE MAP; 1¼C; α=9°

FIGURE 25

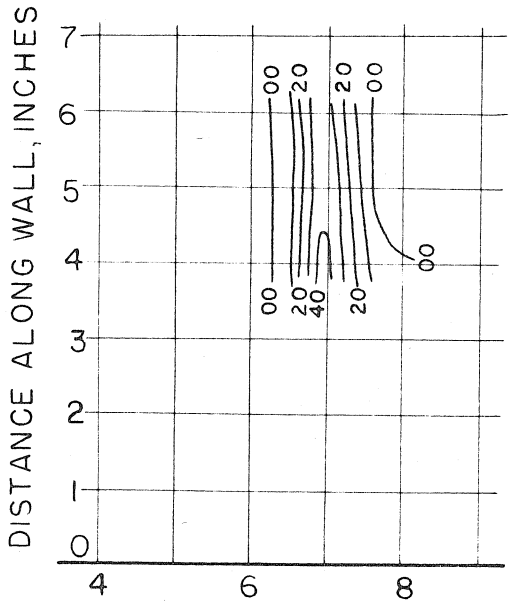

TOTAL PRESSURE PROFILE MAP WITH TURBULATOR WIRE ADDED; 1¼ C; α = 9°

FIGURE 26

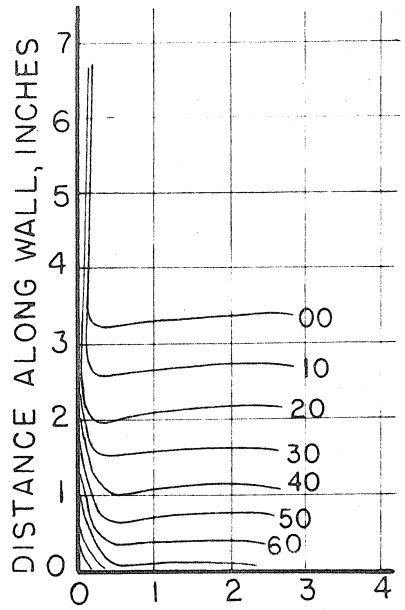

TOTAL PRESSURE PROFILE MAP; ½ C; $\alpha = 13\frac{1}{2}^\circ$

FIGURE 27

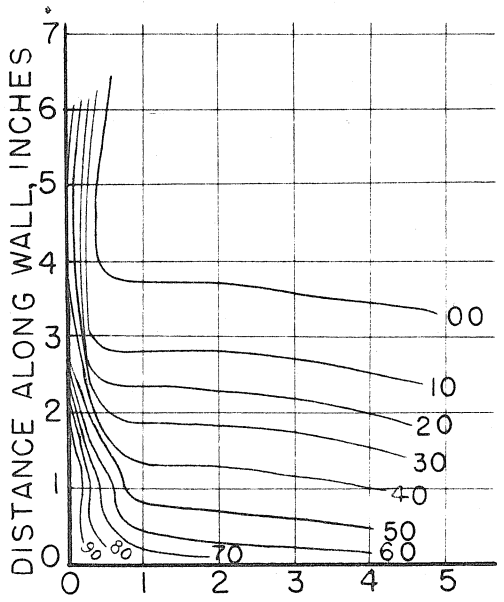

TOTAL PRESSURE PROFILE MAP; ¾ C; $\alpha = 13\frac{1}{2}^\circ$

FIGURE 28

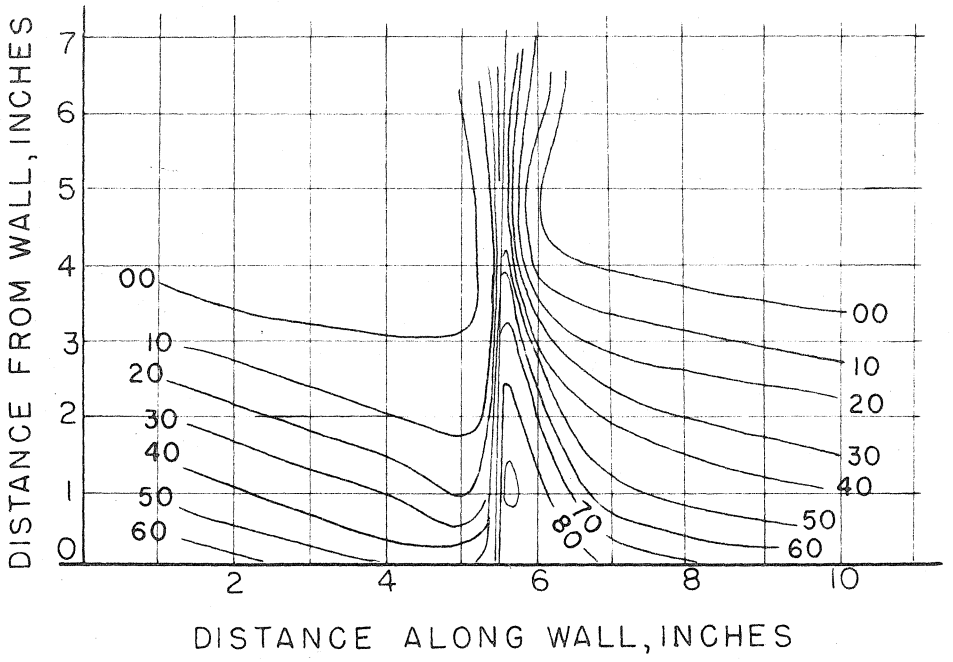

TOTAL PRESSURE PROFILE MAP; 1C; $\alpha = 13\frac{1}{2}°$

FIGURE 29

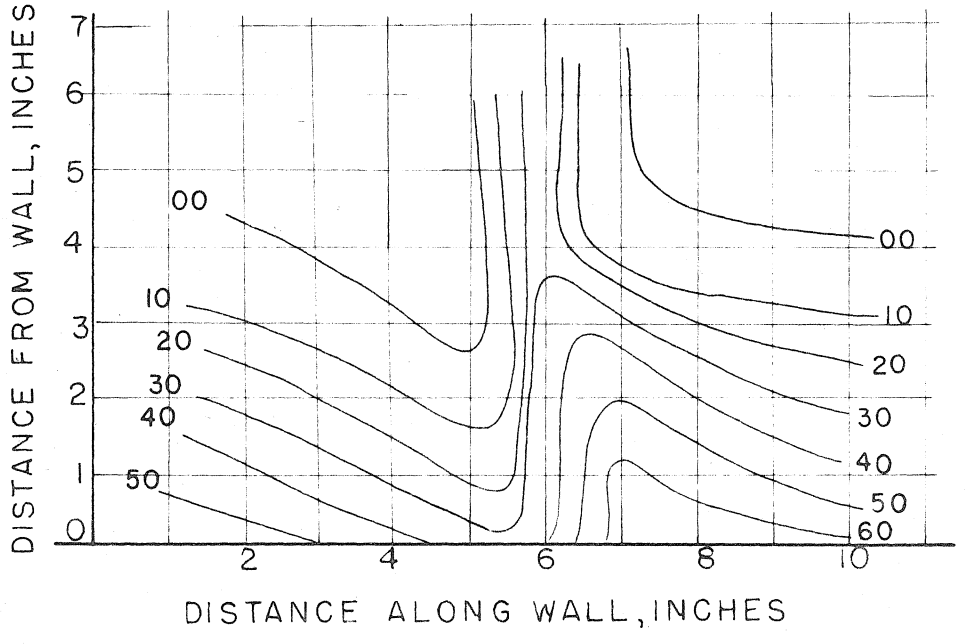

TOTAL PRESSURE PROFILE MAP; $1\frac{1}{2}$C; $\alpha = 13\frac{1}{2}°$

FIGURE 30

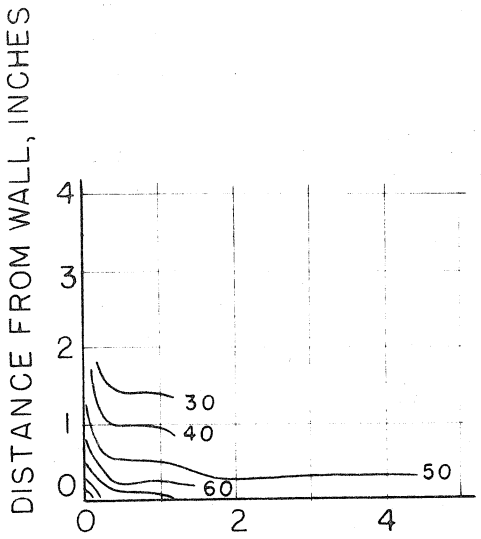

TOTAL PRESSURE PROFILE MAP; ¼ C; $\alpha = 21\frac{1}{2}°$

FIGURE 31

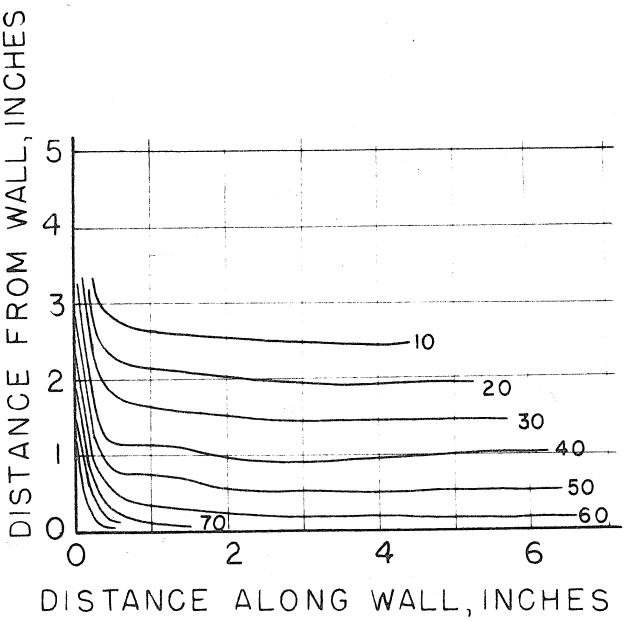

TOTAL PRESSURE PROFILE MAP; ½ C; $\alpha = 21\frac{1}{2}°$

FIGURE 32

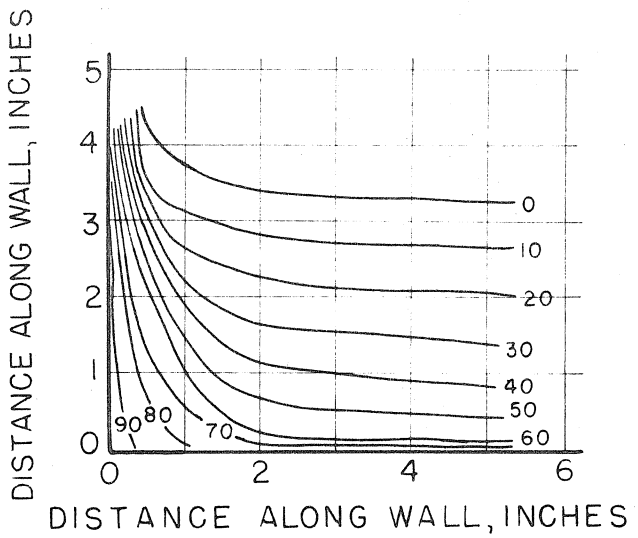

TOTAL PRESSURE PROFILE MAP; $\frac{3}{4}$ C; $\alpha = 21\frac{1}{2}^\circ$

FIGURE 33

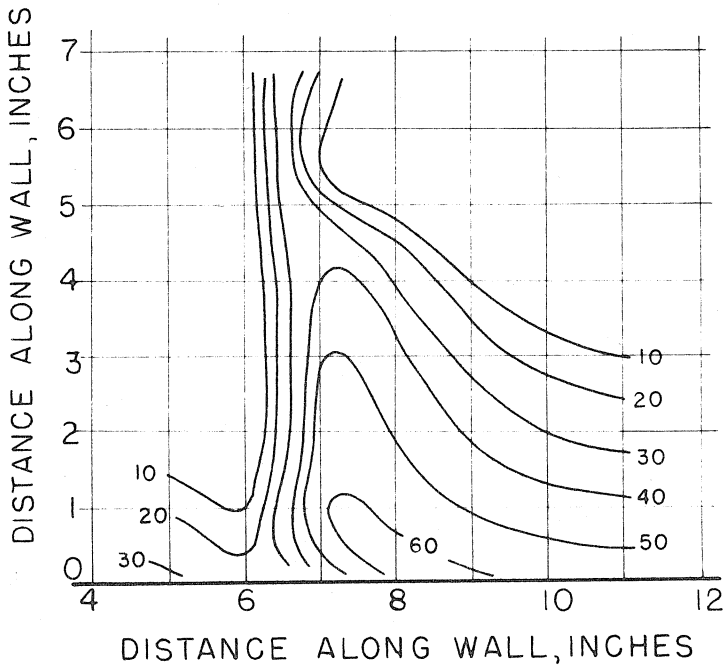

TOTAL PRESSURE PROFILE MAP; $1\frac{1}{2}$ C; $\alpha = 21\frac{1}{2}^\circ$

FIGURE 34

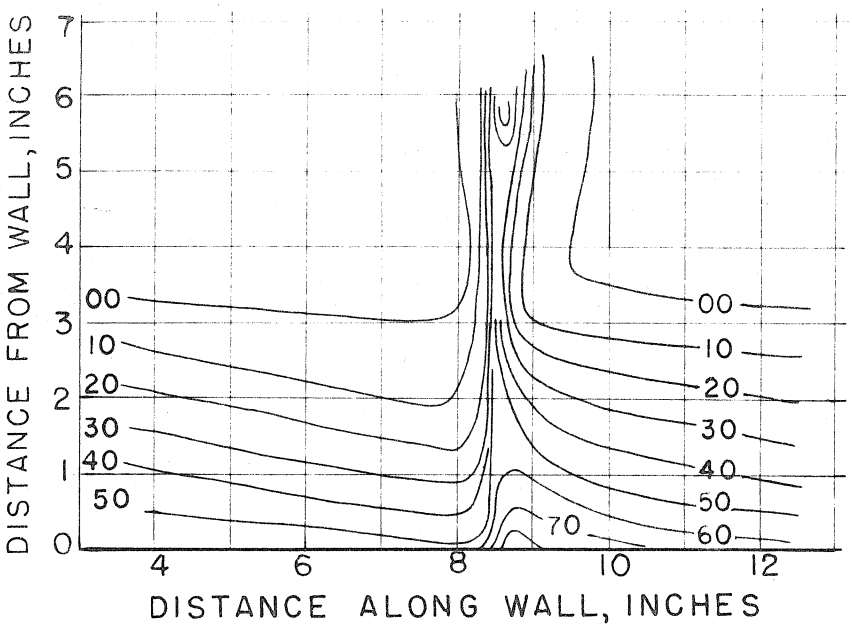

TOTAL PRESSURE PROFILE MAP; IC; $\alpha = 9^\circ$

FIGURE 35

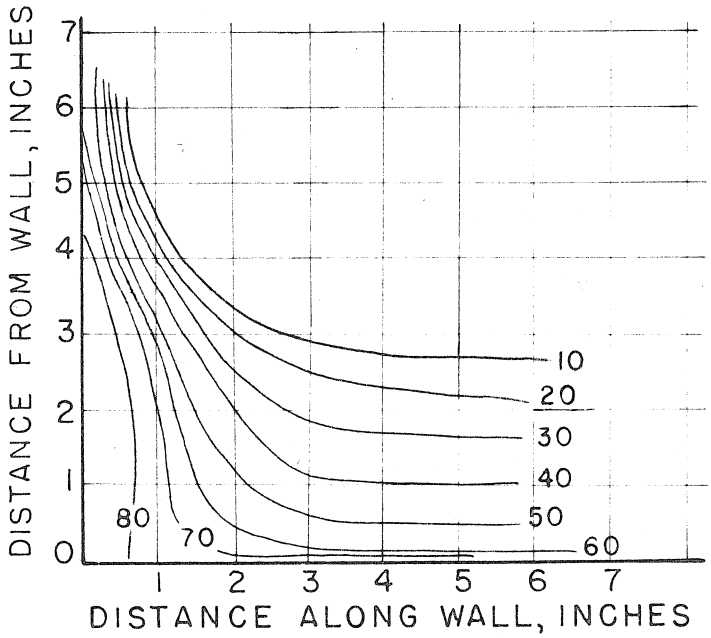

TOTAL PRESSURE PROFILE MAP; IC; $\alpha = 21\frac{1}{2}^\circ$

FIGURE 36

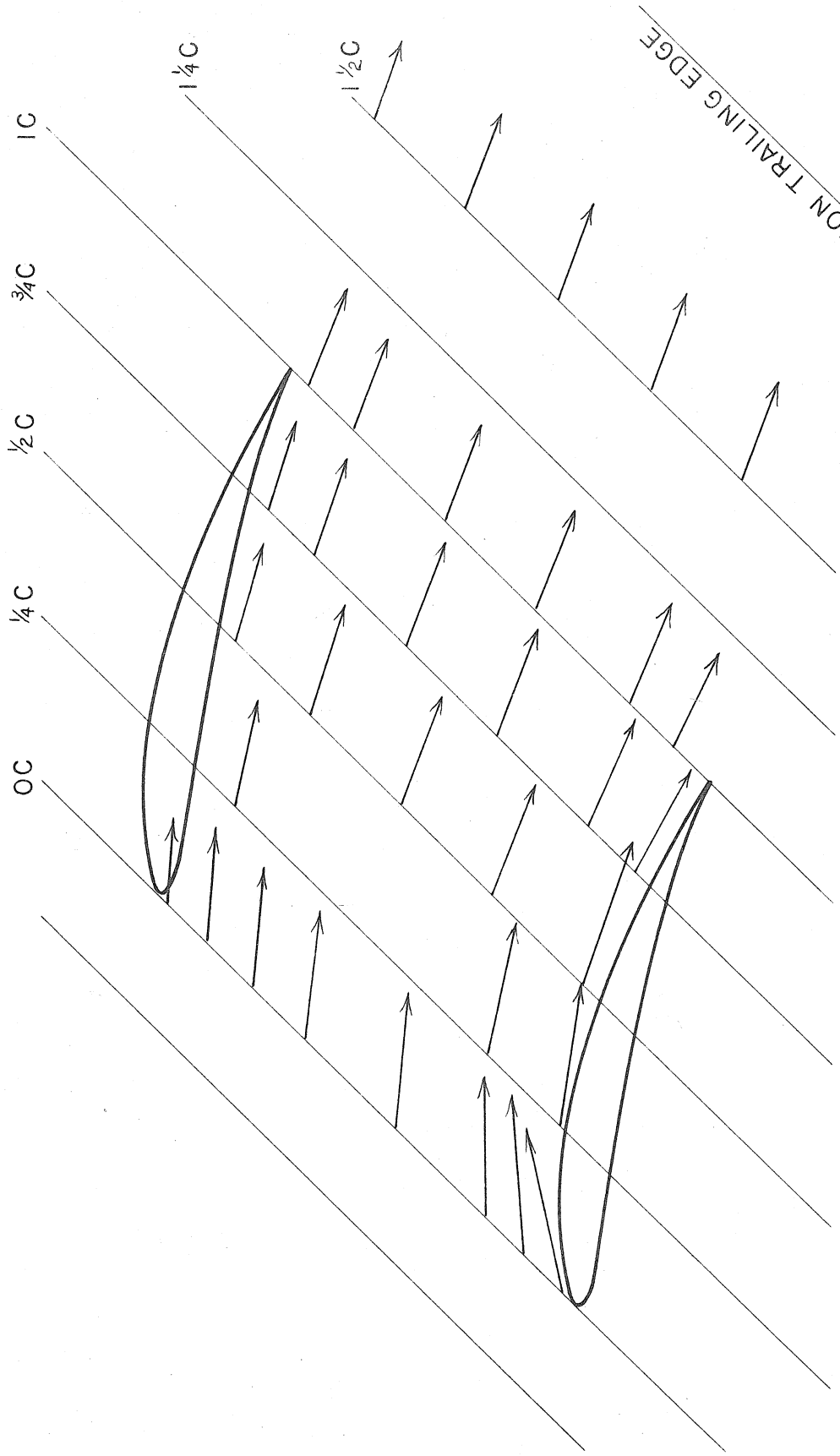

FLOW DIRECTION PLOT

DISTANCE FROM WALL 12 INCHES; $\alpha = 13\frac{1}{2}^{\circ}$

FIGURE 37

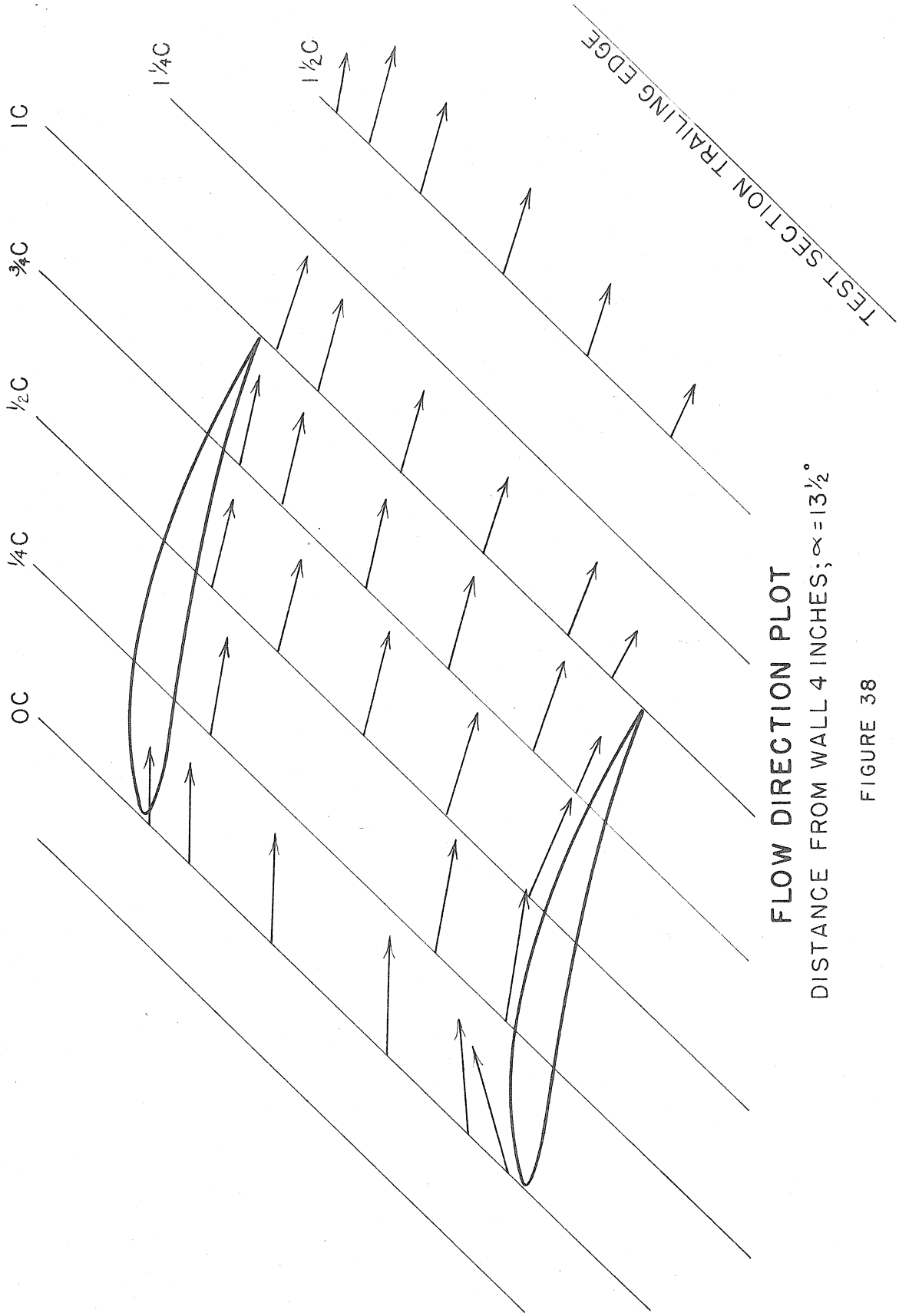

FLOW DIRECTION PLOT

DISTANCE FROM WALL 4 INCHES; $\alpha = 13\frac{1}{2}^{\circ}$

FIGURE 38

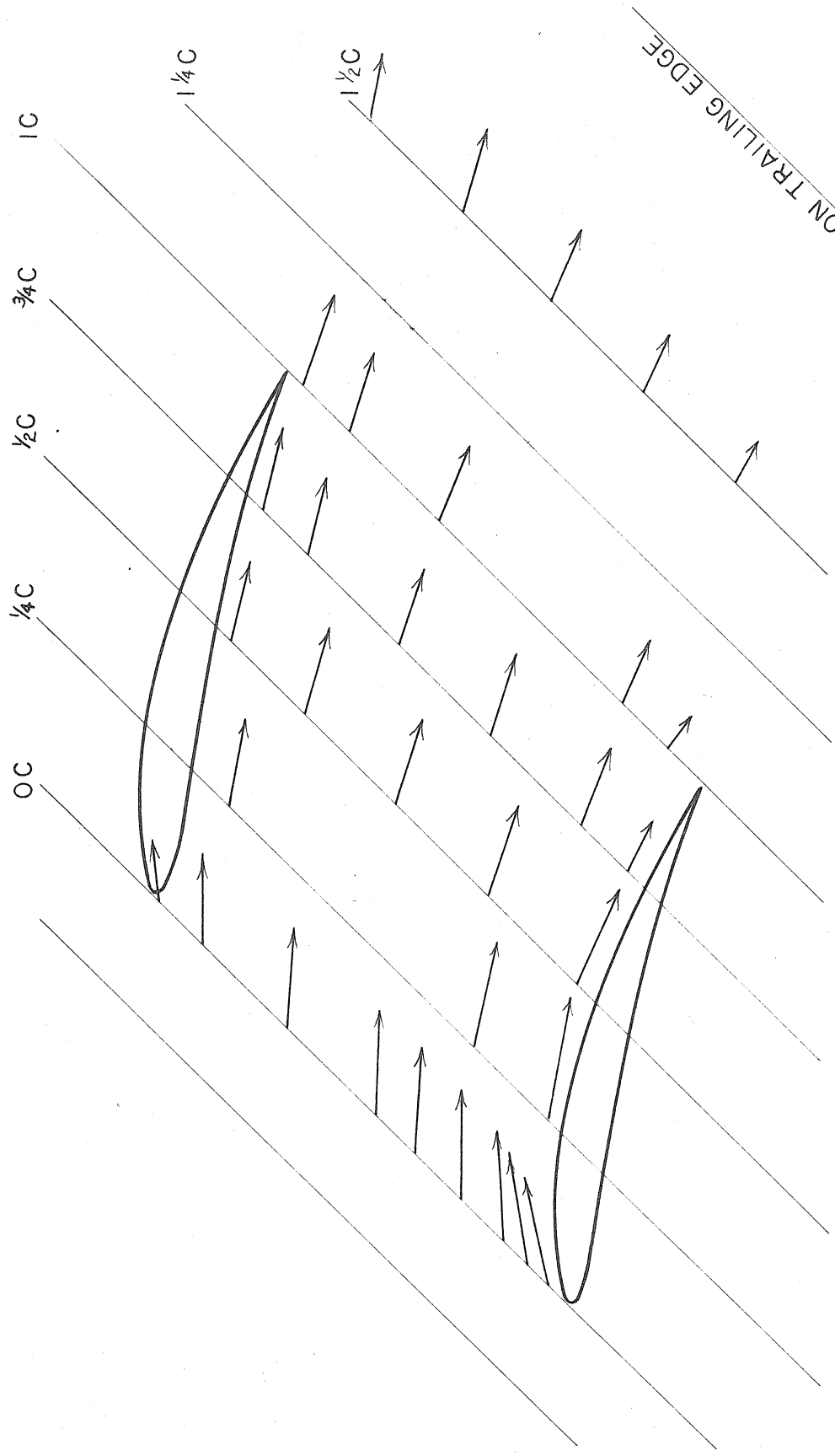

FLOW DIRECTION PLOT

DISTANCE FROM WALL 1.2 INCHES; $\alpha = 13\frac{1}{2}^{\circ}$

FIGURE 39

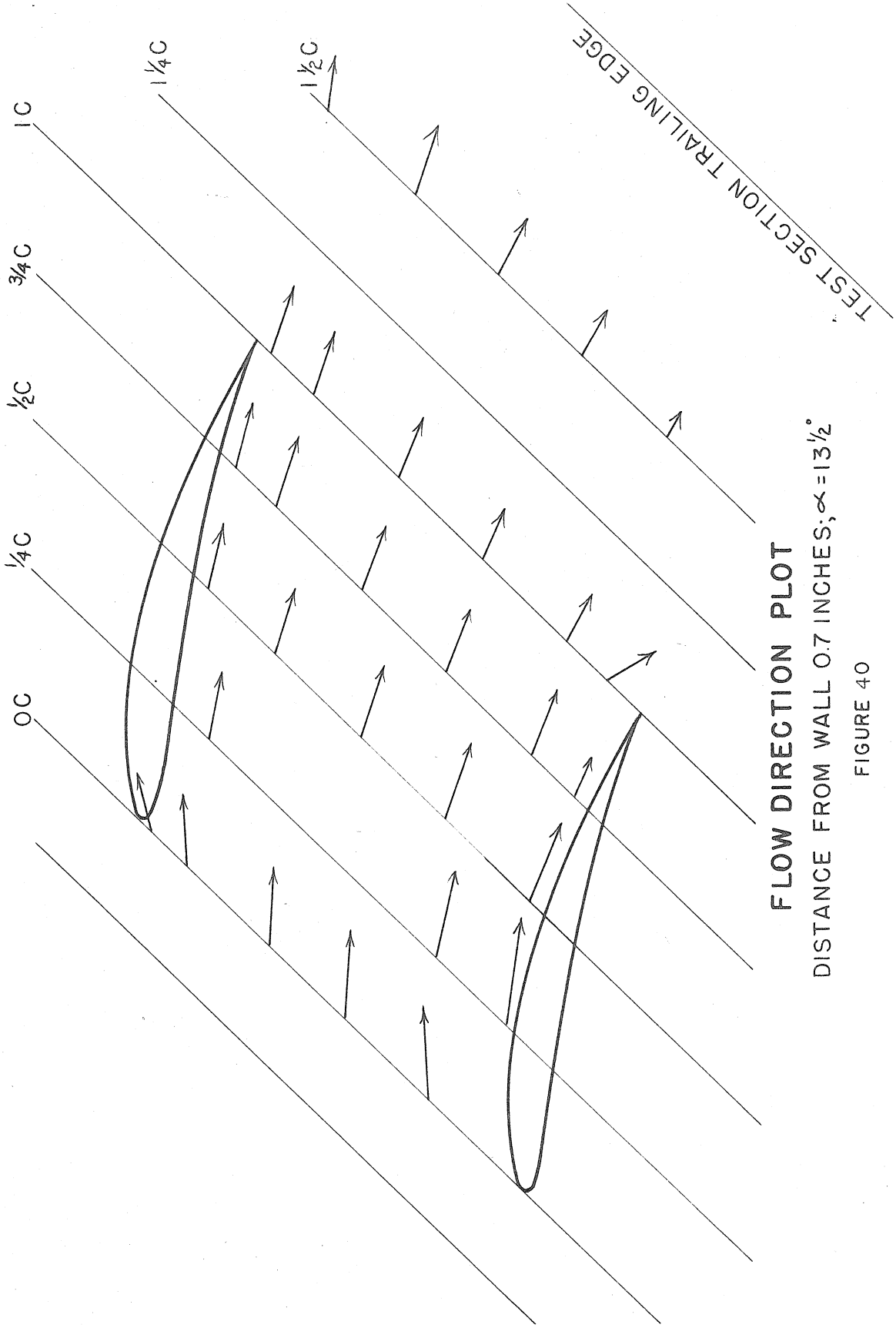

FLOW DIRECTION PLOT

DISTANCE FROM WALL 0.7 INCHES; $\alpha = 13\frac{1}{2}^{\circ}$

FIGURE 40

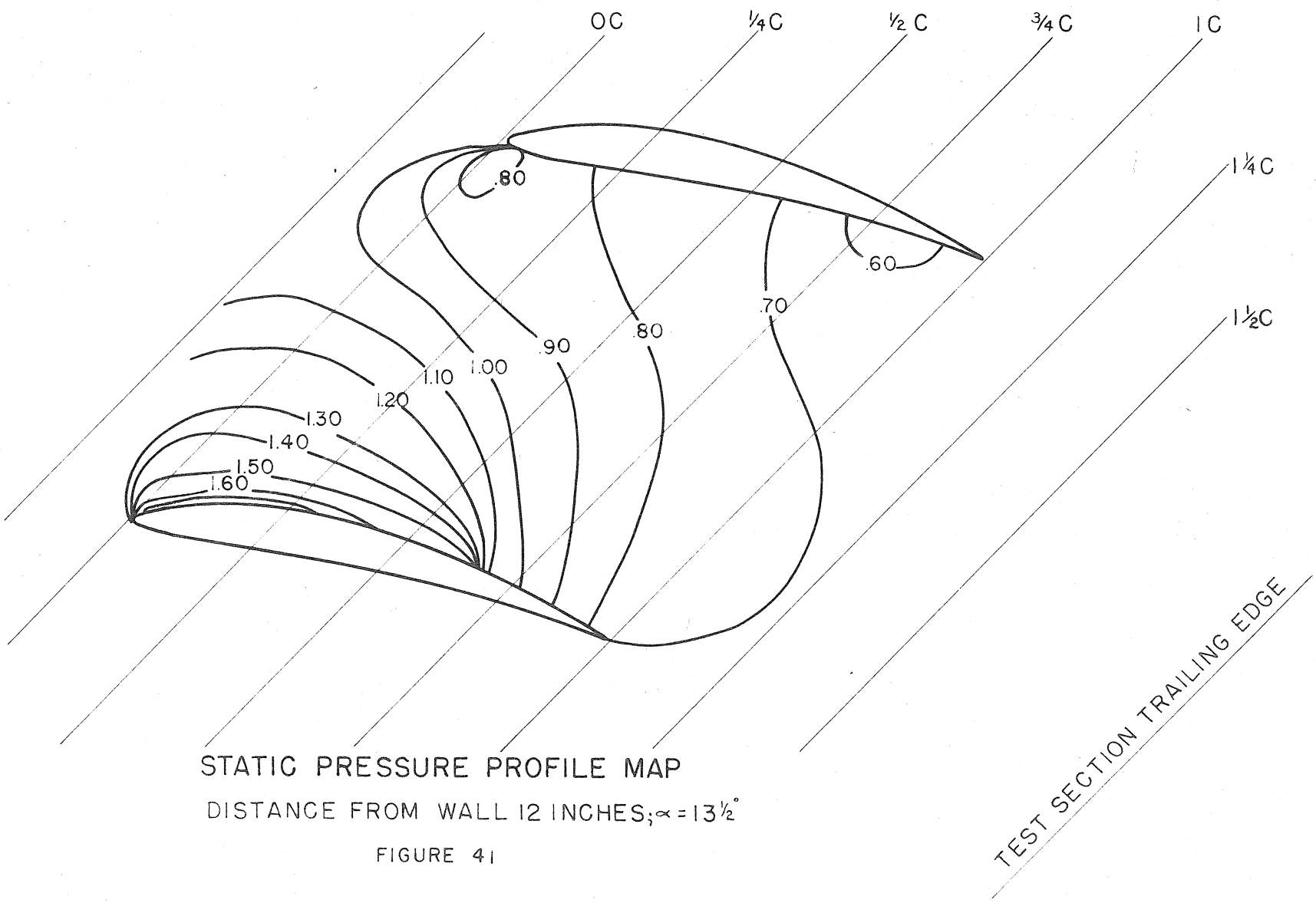

STATIC PRESSURE PROFILE MAP

DISTANCE FROM WALL 12 INCHES; $\alpha = 13\frac{1}{2}^{\circ}$

FIGURE 41

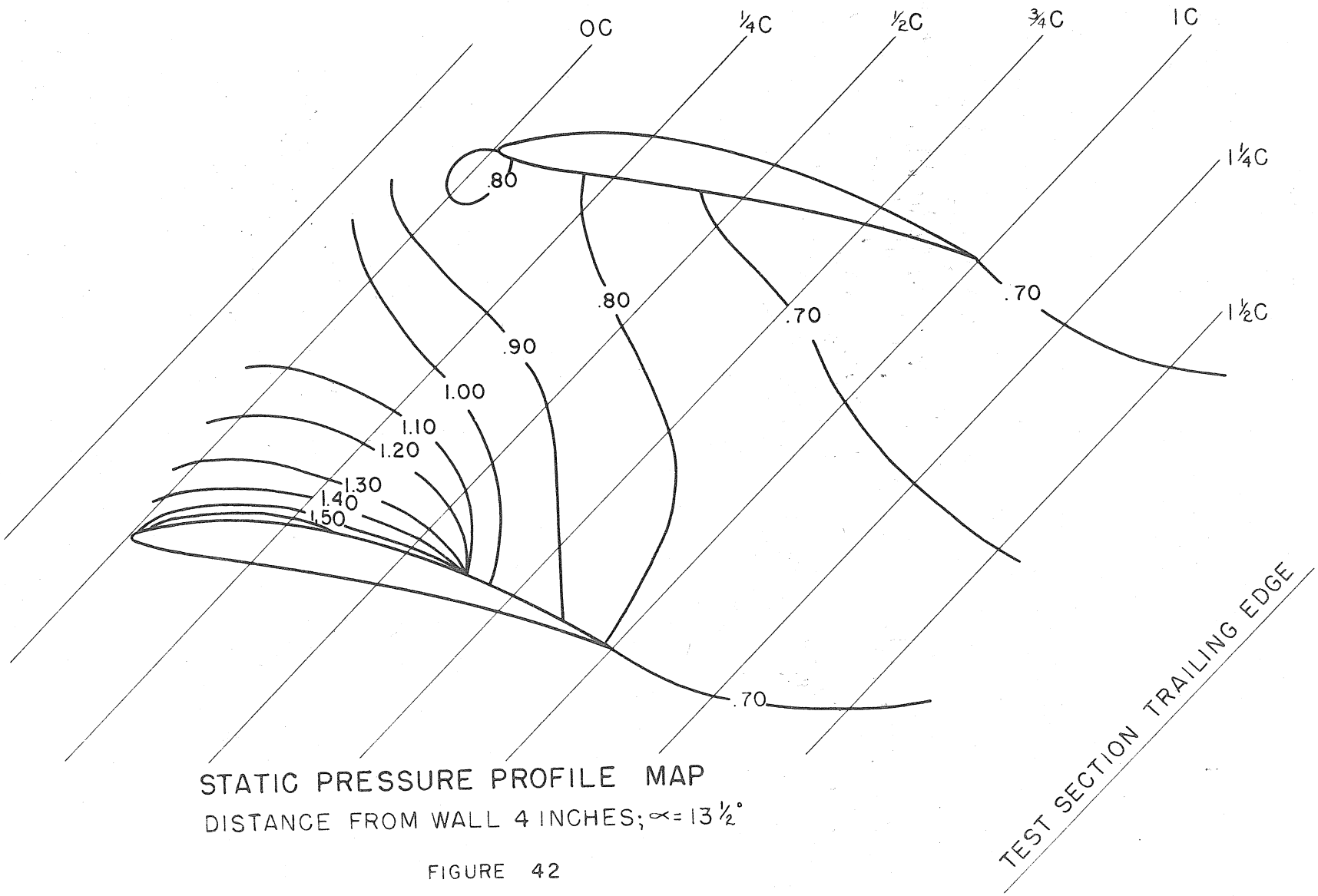

STATIC PRESSURE PROFILE MAP

DISTANCE FROM WALL 4 INCHES; $\alpha = 13\frac{1}{2}^{\circ}$

FIGURE 42

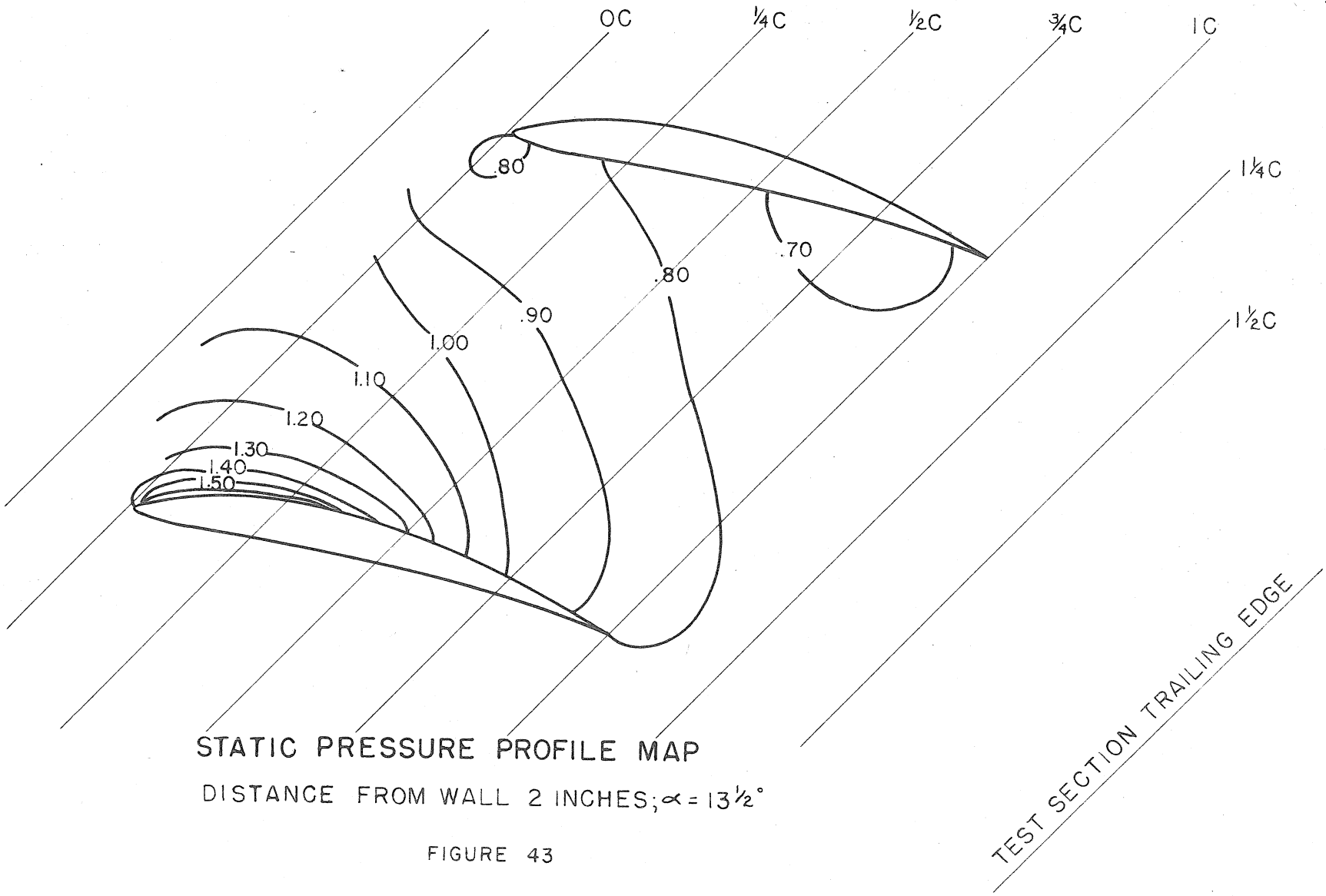

STATIC PRESSURE PROFILE MAP

DISTANCE FROM WALL 2 INCHES; $\alpha = 13\frac{1}{2}^{\circ}$

FIGURE 43

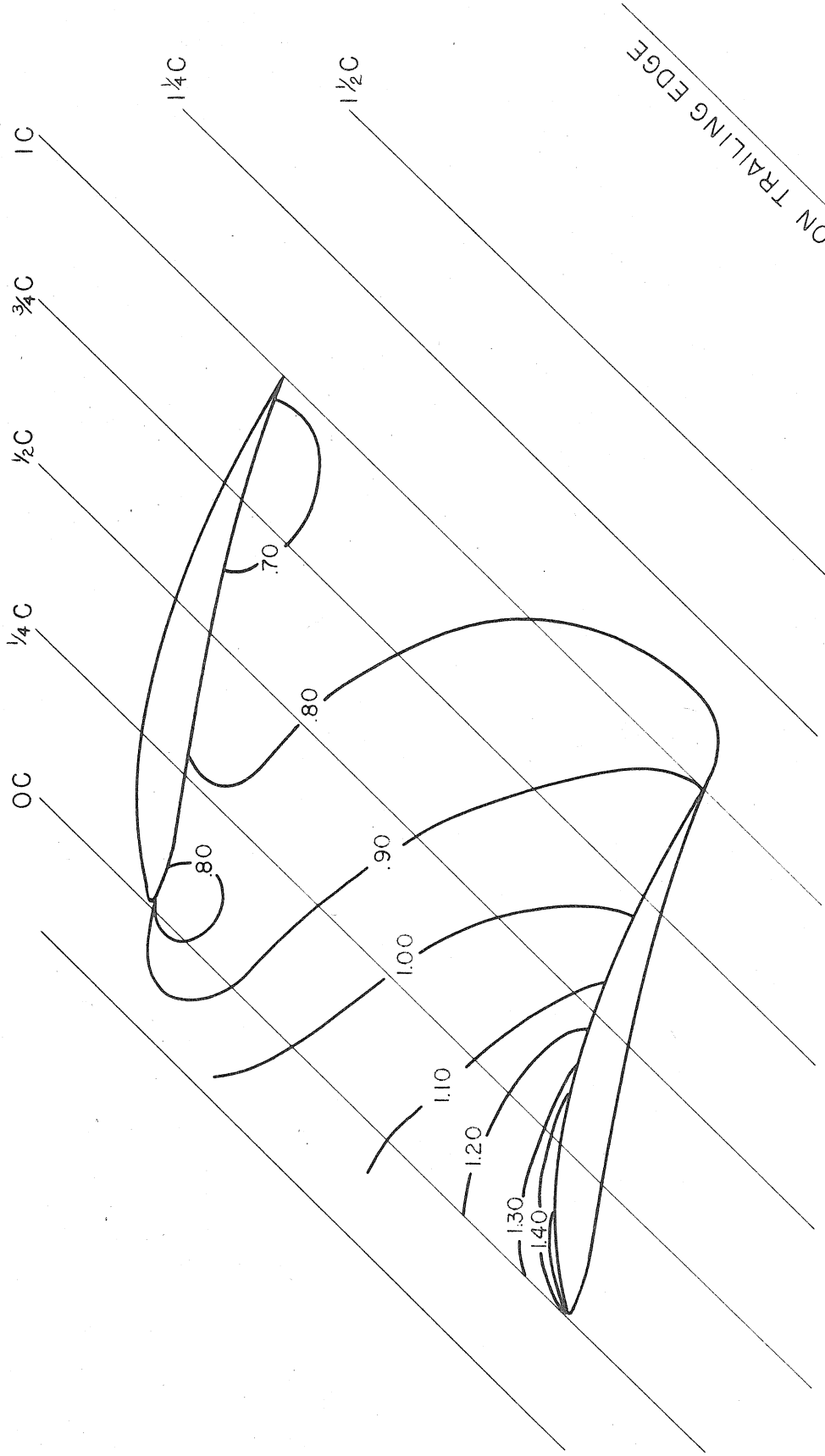

STATIC PRESSURE PROFILE MAP

DISTANCE FROM WALL 1.2 INCHES; $\alpha = 13\frac{1}{2}^{\circ}$

FIGURE 44

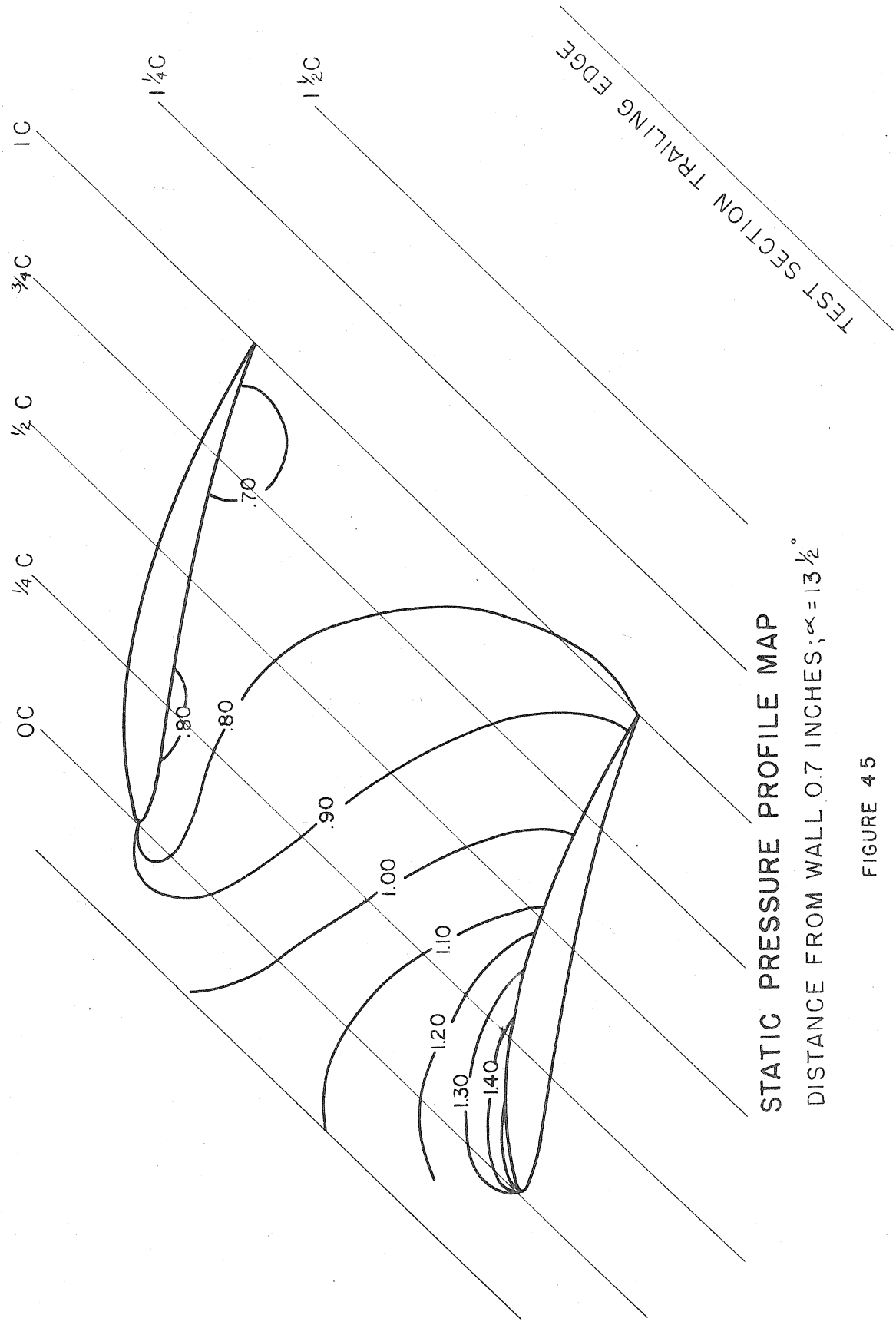

STATIC PRESSURE PROFILE MAP

DISTANCE FROM WALL 0.7 INCHES; $\alpha = 13\frac{1}{2}^{\circ}$

FIGURE 45

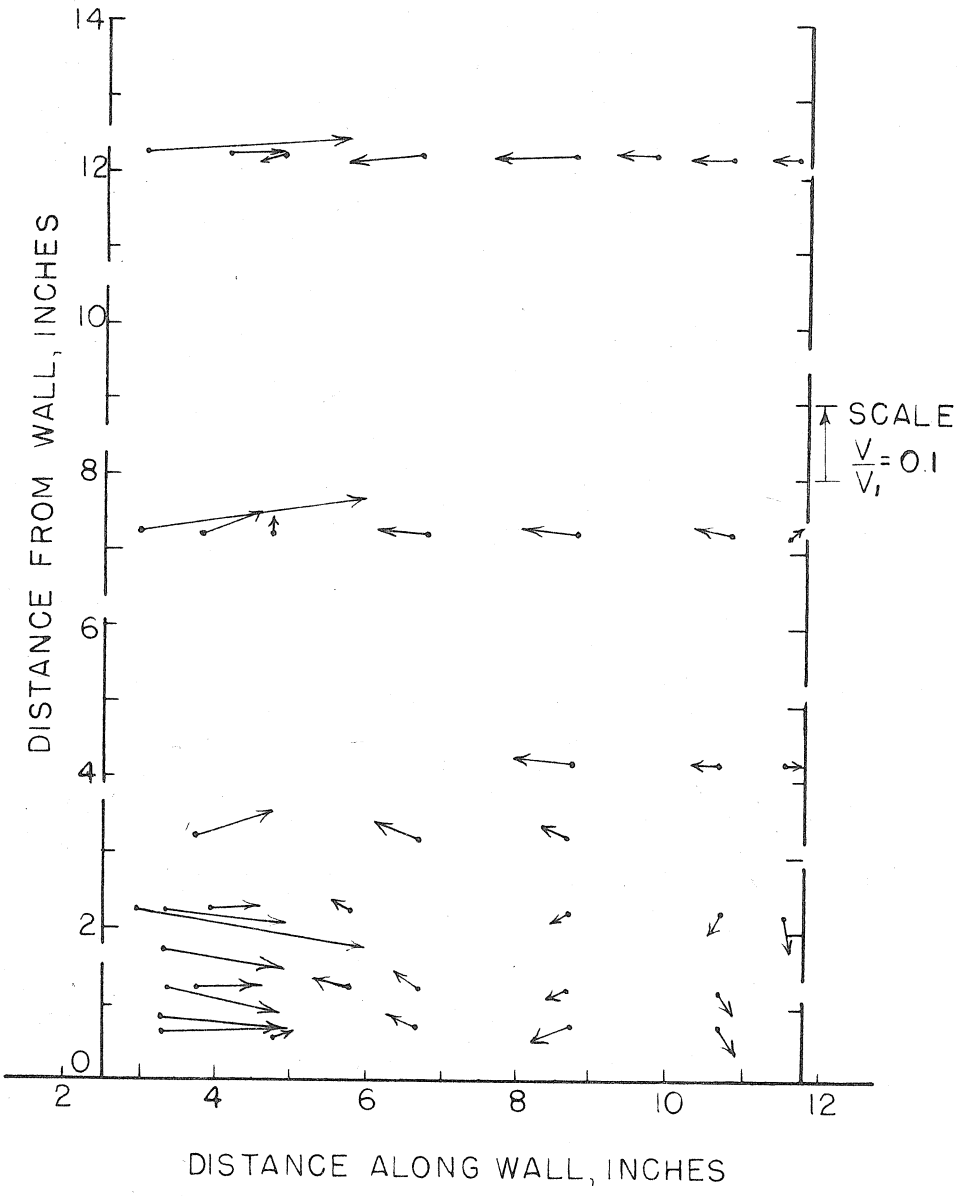

SECONDARY VELOCITY DIAGRAM; OC; $\alpha = 13\frac{1}{2}^{\circ}$

FIGURE 46

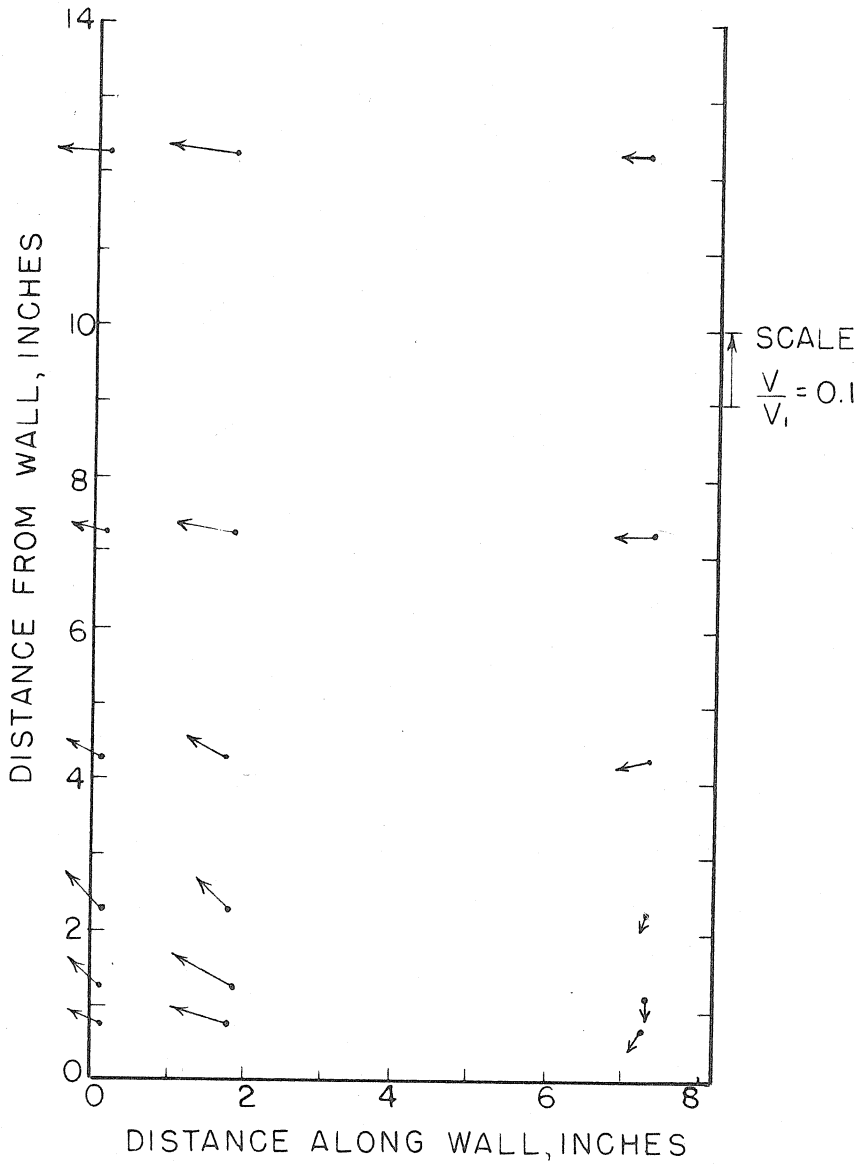

SECONDARY VELOCITY DIAGRAM ; ¼C ; $\alpha = 13\frac{1}{2}^{\circ}$

FIGURE 47

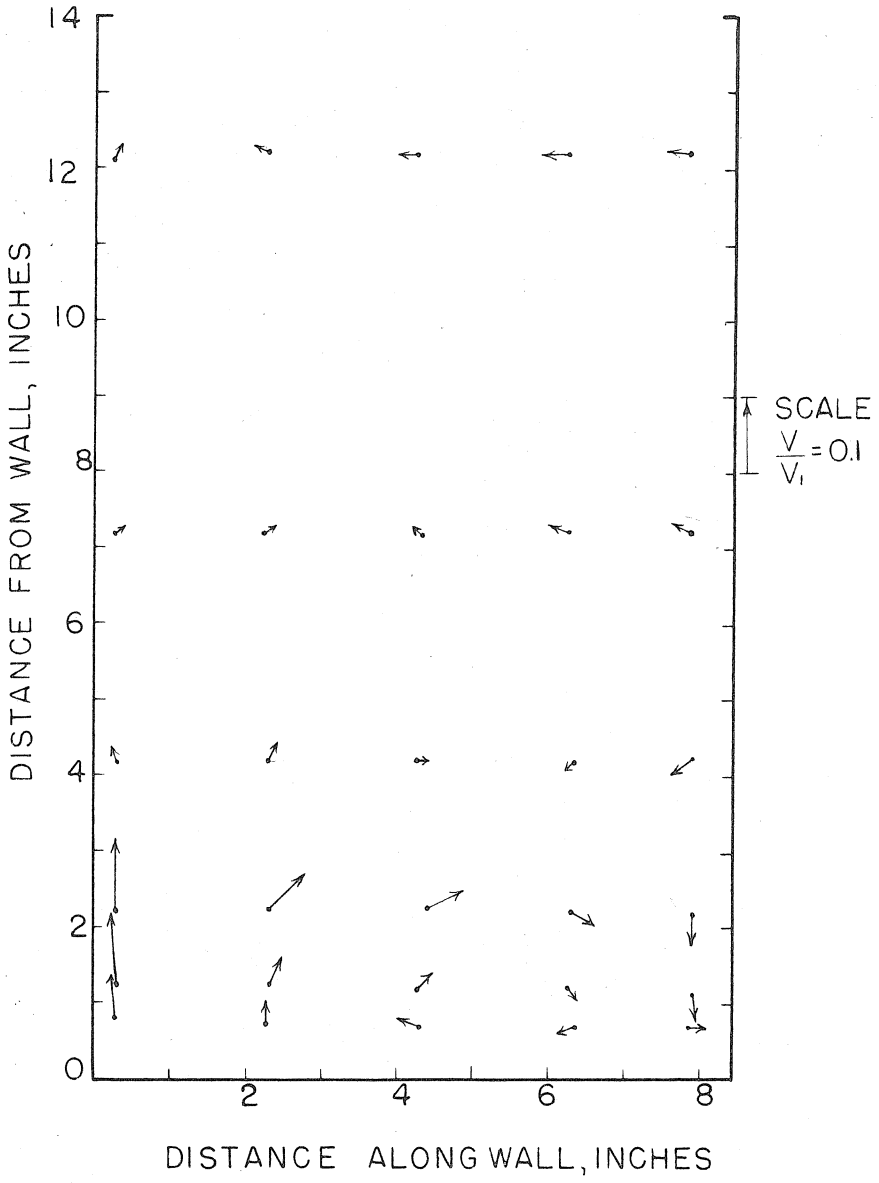

SECONDARY VELOCITY DIAGRAM; ½C; $\alpha = 13\frac{1}{2}^{\circ}$

FIGURE 48

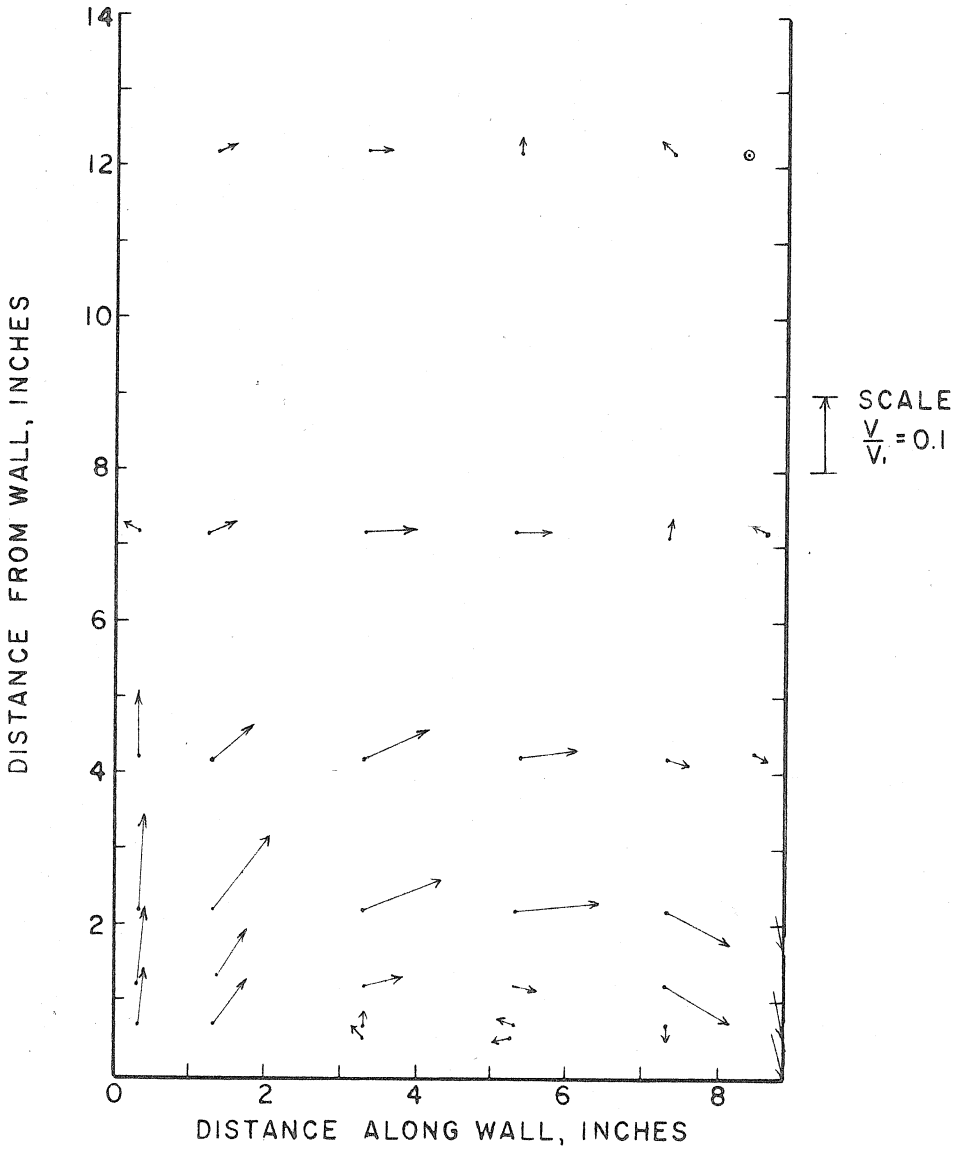

SECONDARY VELOCITY DIAGRAM; $\frac{3}{4}C$; $\alpha = 13\frac{1}{2}^{\circ}$

FIGURE 49

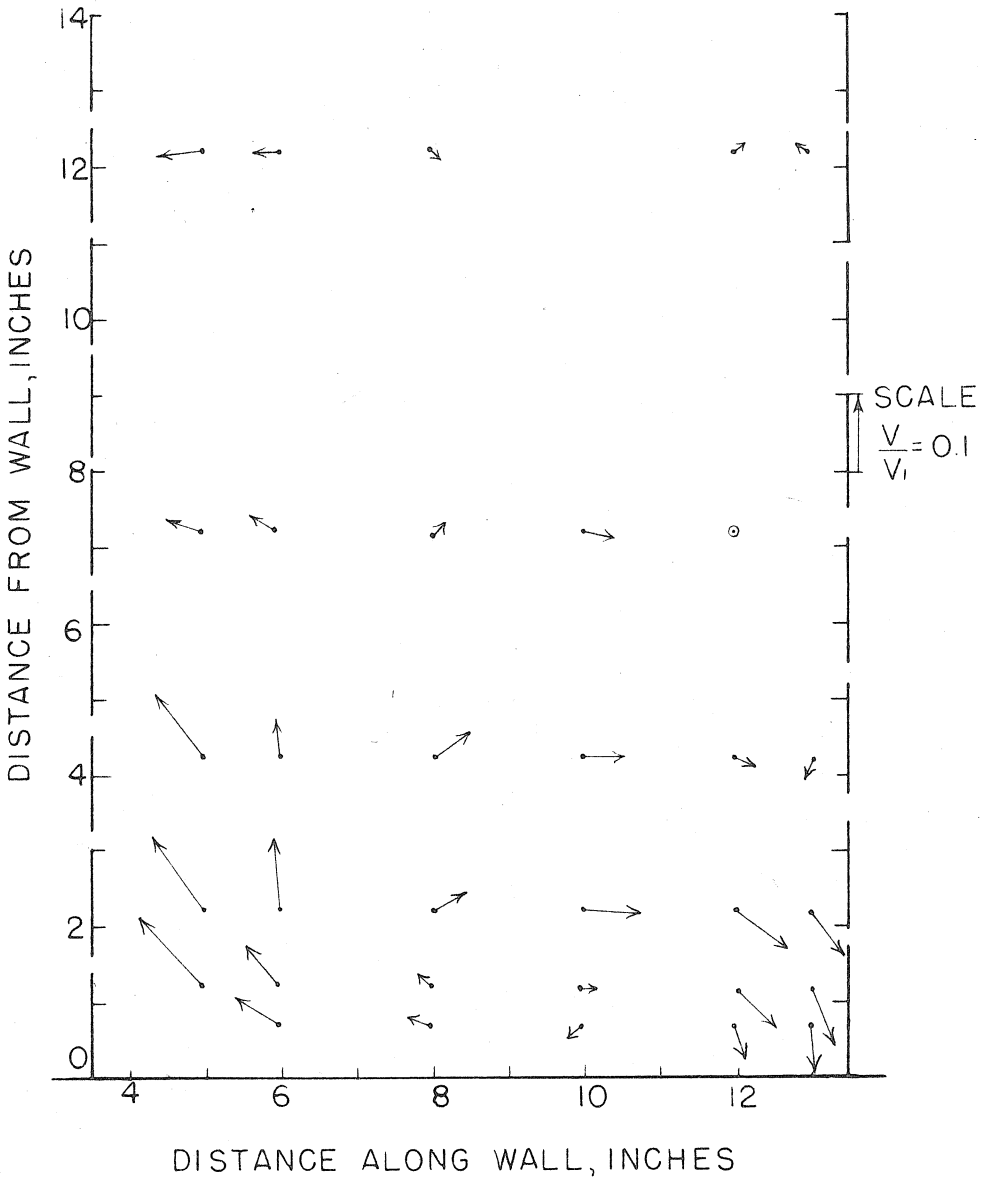

SECONDARY VELOCITY DIAGRAM; 1C; $\alpha = 13\frac{1}{2}^{\circ}$

FIGURE 50

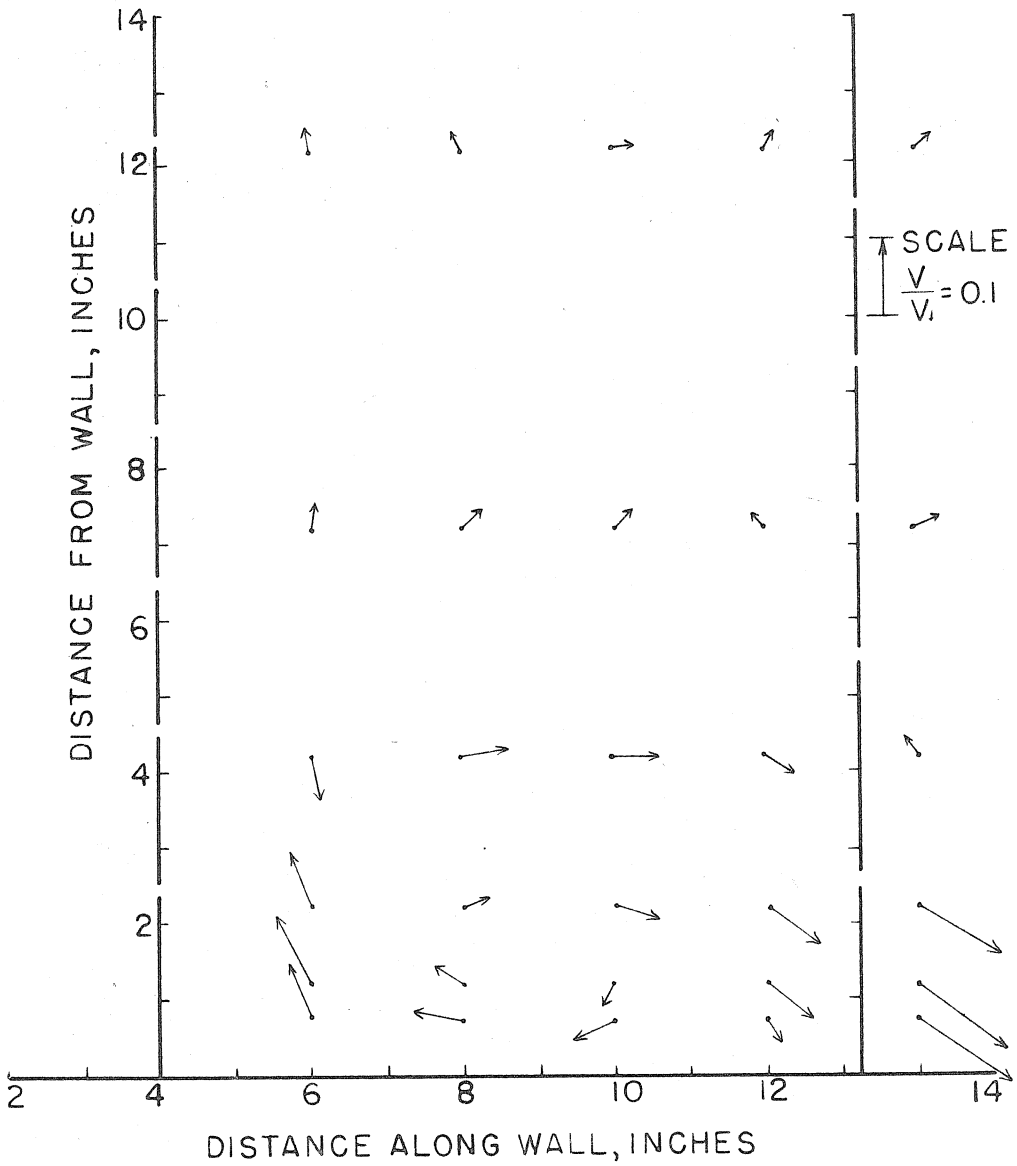

SECONDARY VELOCITY DIAGRAM, $1\frac{1}{2}$ C; $\alpha = 13\frac{1}{2}°$

FIGURE 51

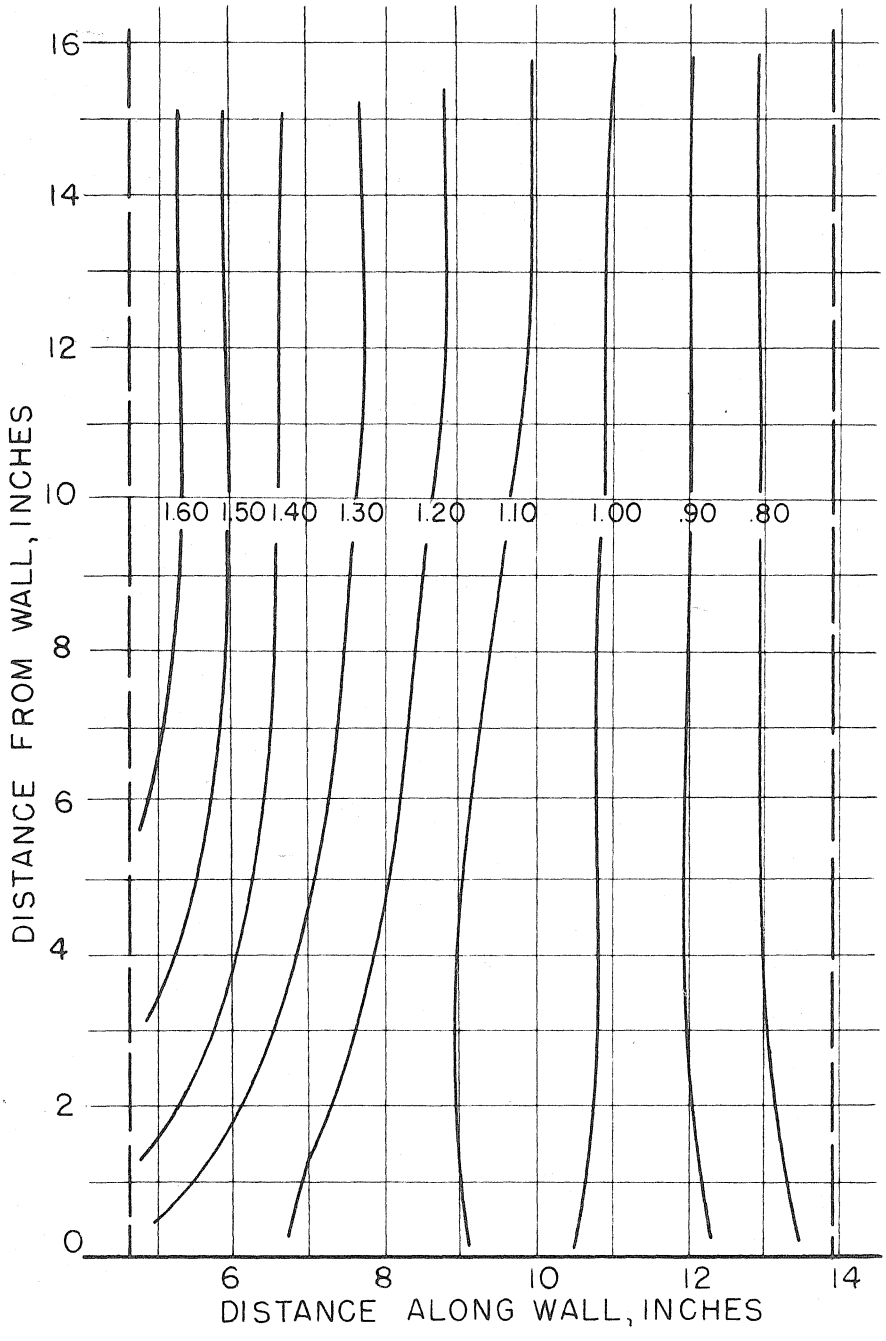

PROFILE MAP OF STATIC PRESSURE DISTRIBUTION; $\frac{P_{T_1} - P_S}{Q_1}$

OC SURVEY PLANE; $\alpha = 13\frac{1}{2}^{\circ}$

FIGURE 52

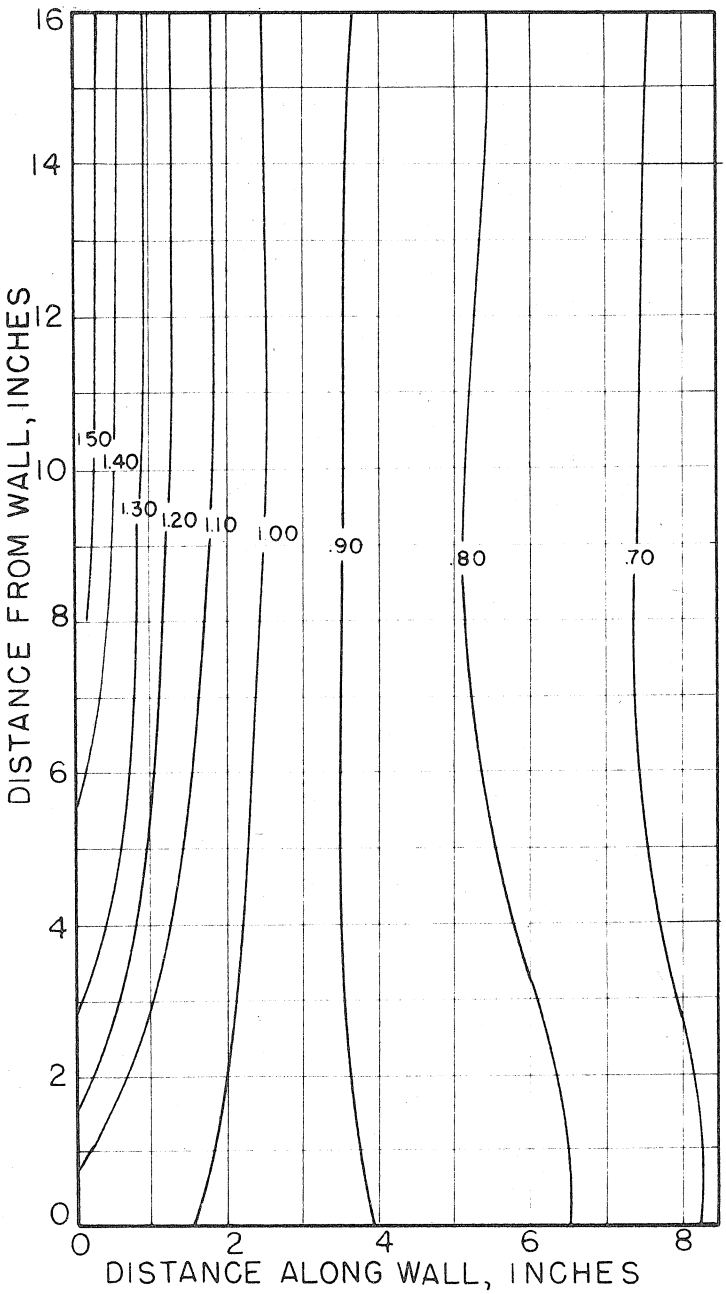

PROFILE MAP OF STATIC PRESSURE DISTRIBUTION; $\frac{P_T - P_S}{Q_1}$

½C SURVEY PLANE; $\alpha = 13\frac{1}{2}^\circ$

FIGURE 53

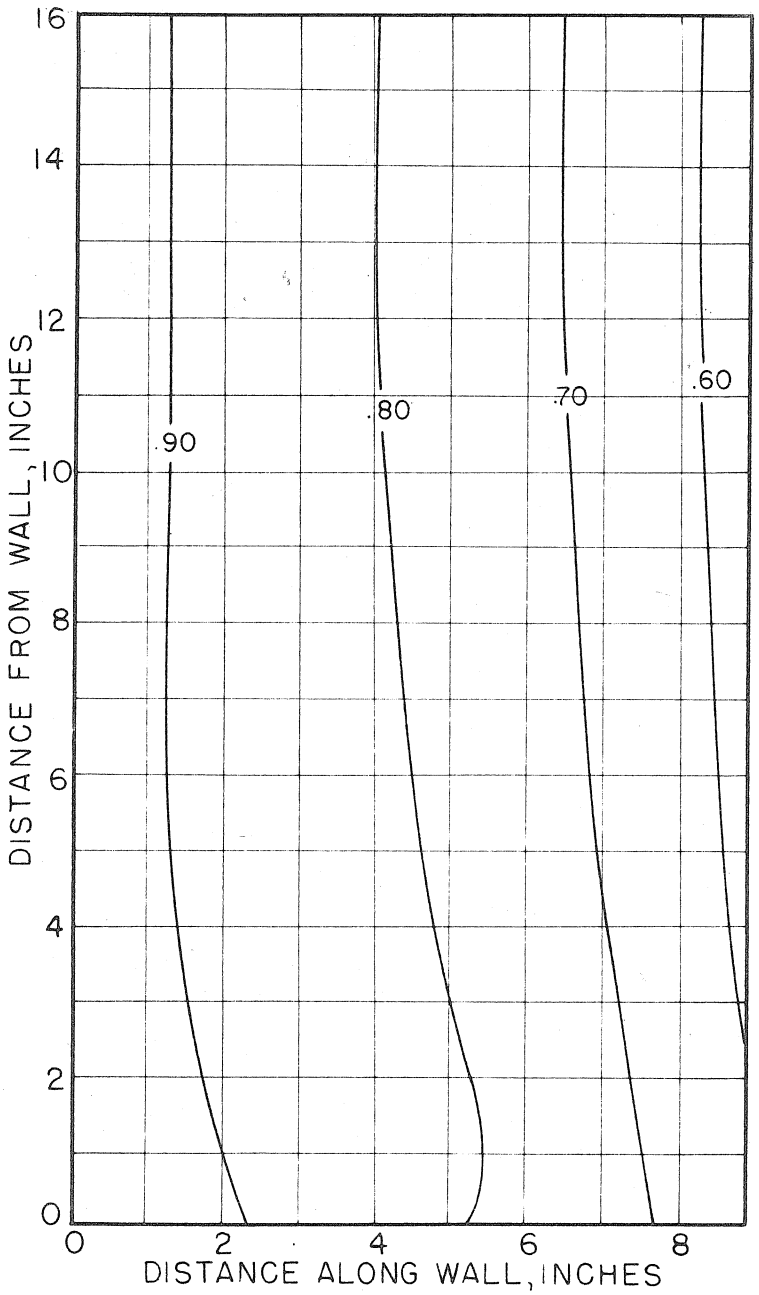

PROFILE MAP OF STATIC PRESSURE DISTRIBUTION; $\frac{P_{T_1}-P_S}{Q_1}$

¾C SURVEY PLANE; $\alpha = 13\frac{1}{2}°$

FIGURE 54

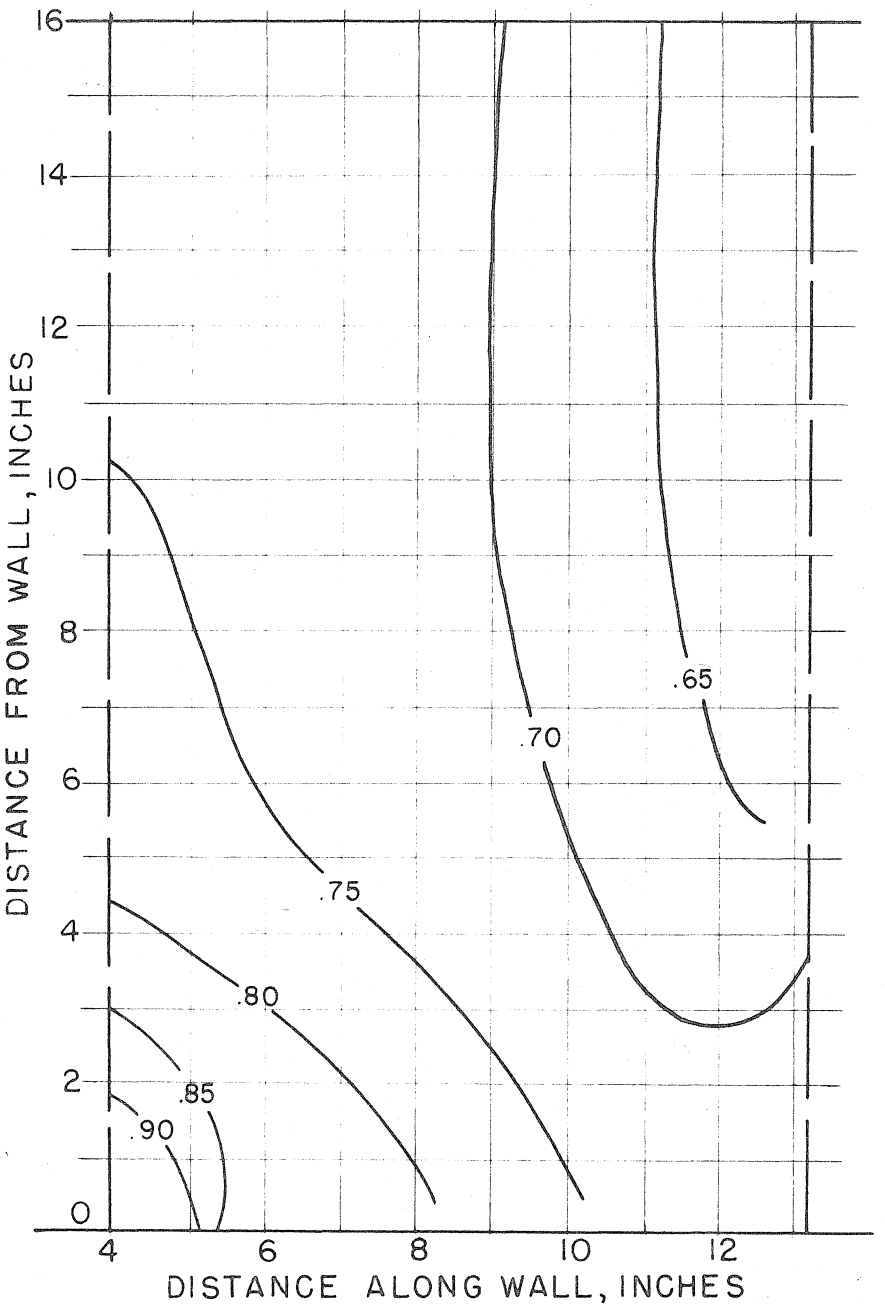

PROFILE MAP OF STATIC PRESSURE DISTRIBUTION; $\frac{P_t - P_s}{Q_1}$

IC SURVEY PLANE; 13½°

FIGURE 55

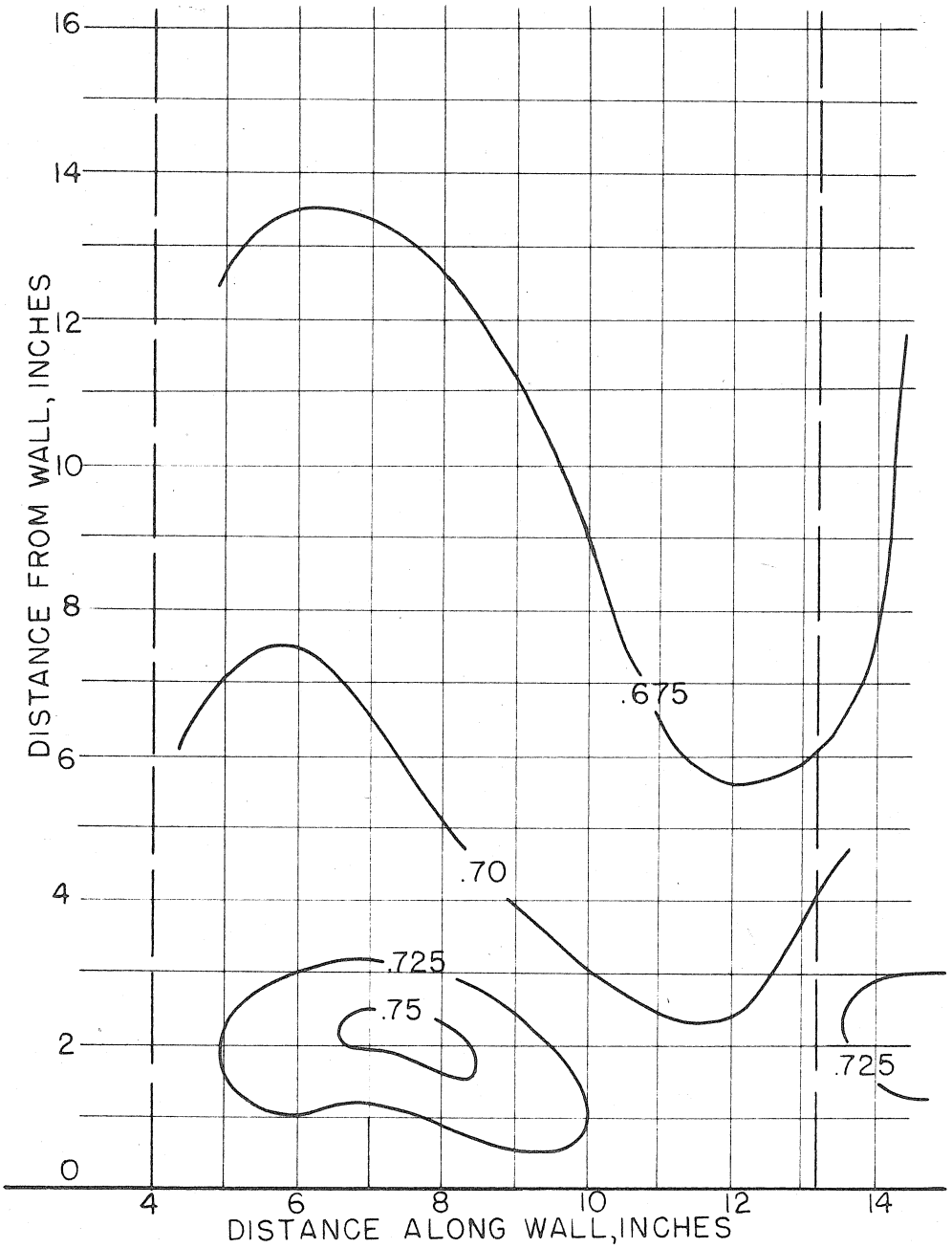

PROFILE MAP OF STATIC PRESSURE DISTRIBUTION; $\frac{P_{T_1} - P_s}{Q_1}$

1½C SURVEY PLANE, $\alpha = 13\frac{1}{2}^\circ$

FIGURE 56

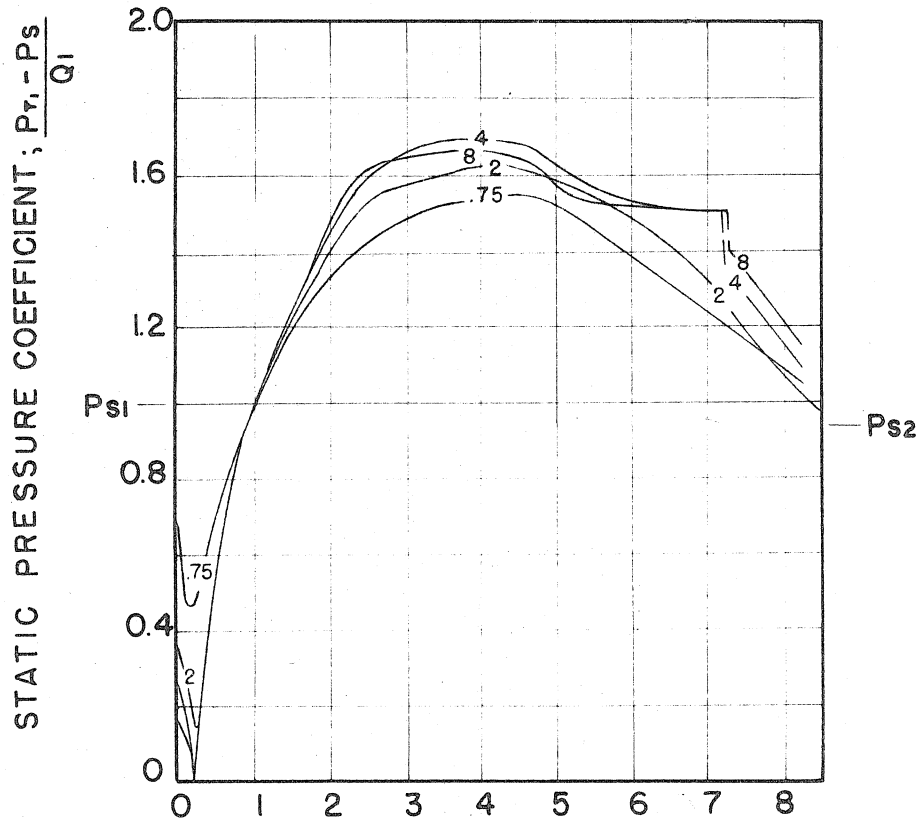

CHORDWISE STATIC PRESSURE DISTRIBUTIONS ON LOW PRESSURE SURFACE OF BLADE, AT VARIOUS DISTANCES FROM END WALL; $\alpha = -1°$

FIGURE 57

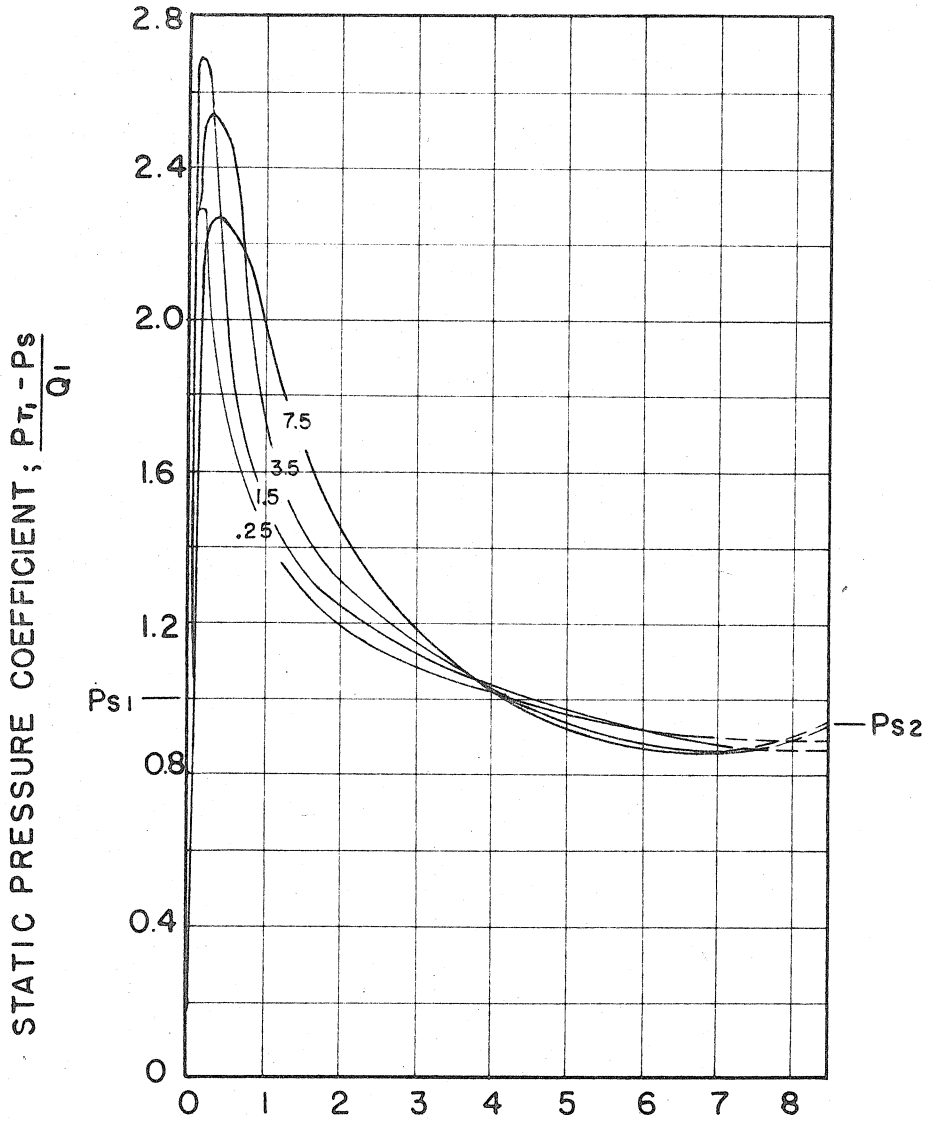

CHORDWISE STATIC PRESSURE DISTRIBUTIONS ON HIGH PRESSURE SURFACE OF BLADE, AT VARIOUS DISTANCES FROM END WALL; $\alpha = -1°$

FIGURE 58

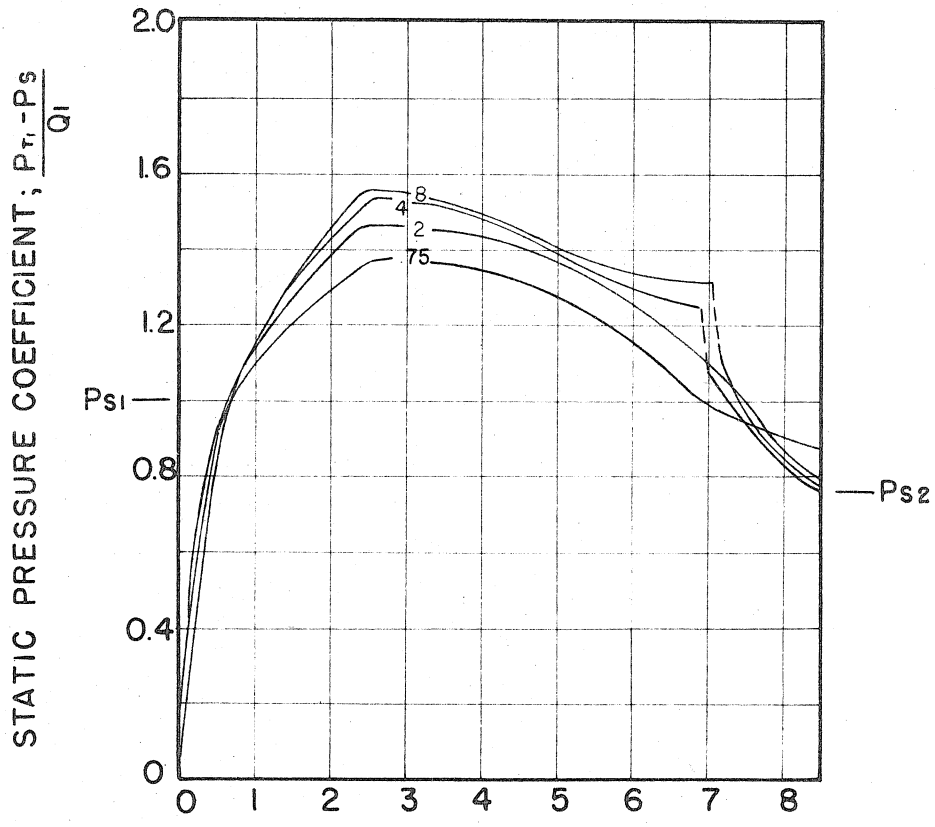

CHORDWISE STATIC PRESSURE DISTRIBUTIONS ON LOW PRESSURE SURFACE OF BLADE, AT VARIOUS DISTANCES FROM END WALL; $\alpha = 5°$

FIGURE 59

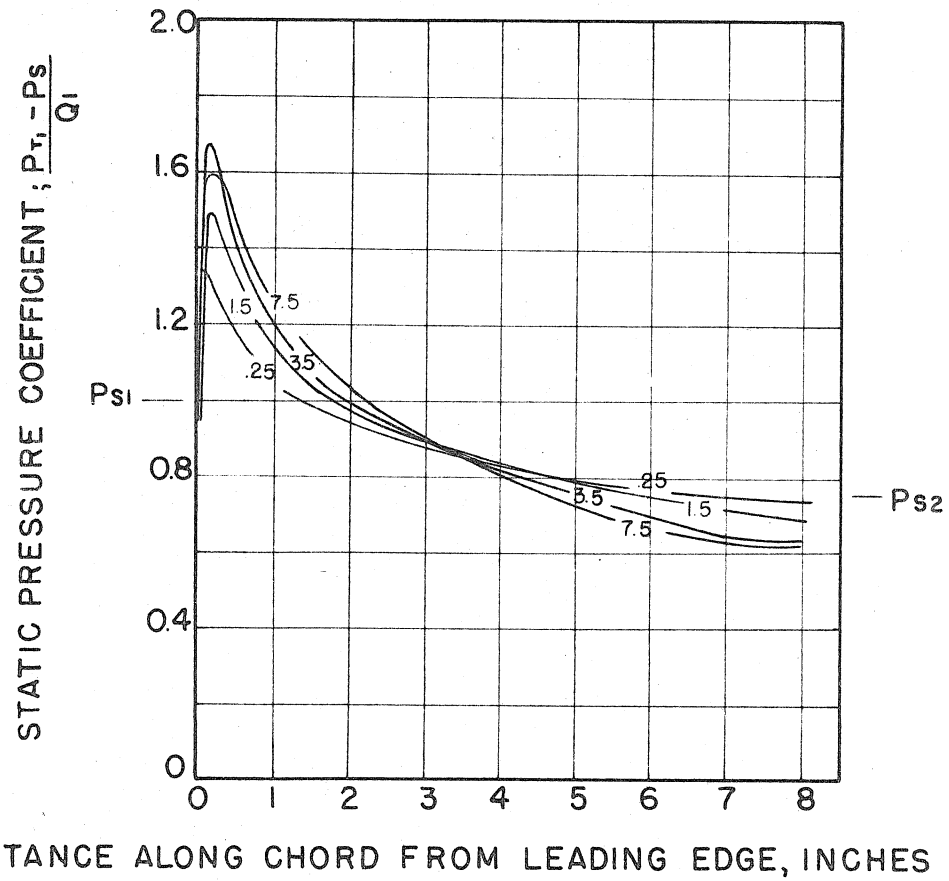

CHORDWISE STATIC PRESSURE DISTRIBUTIONS ON HIGH PRESSURE SURFACE OF BLADE, AT VARIOUS DISTANCES FROM END WALL; $\alpha = 5°$

FIGURE 60

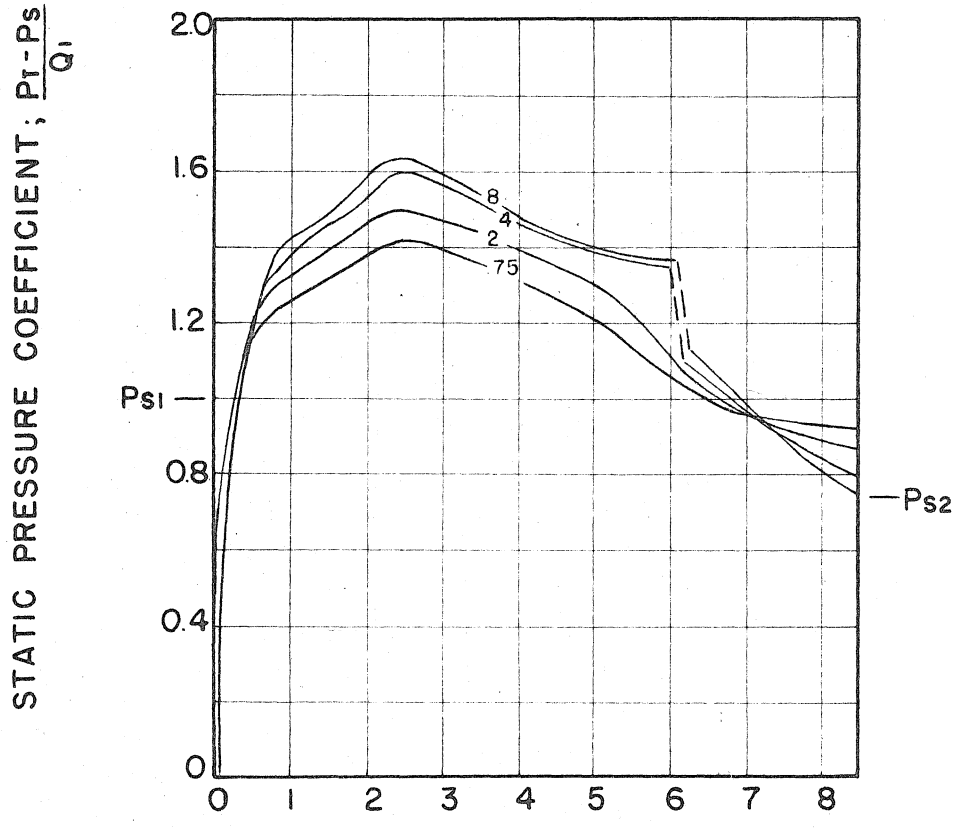

CHORDWISE STATIC PRESSURE DISTRIBUTIONS ON LOW PRESSURE SURFACE OF BLADE, AT VARIOUS DISTANCES FROM END WALL; $\alpha = 9°$

FIGURE 61

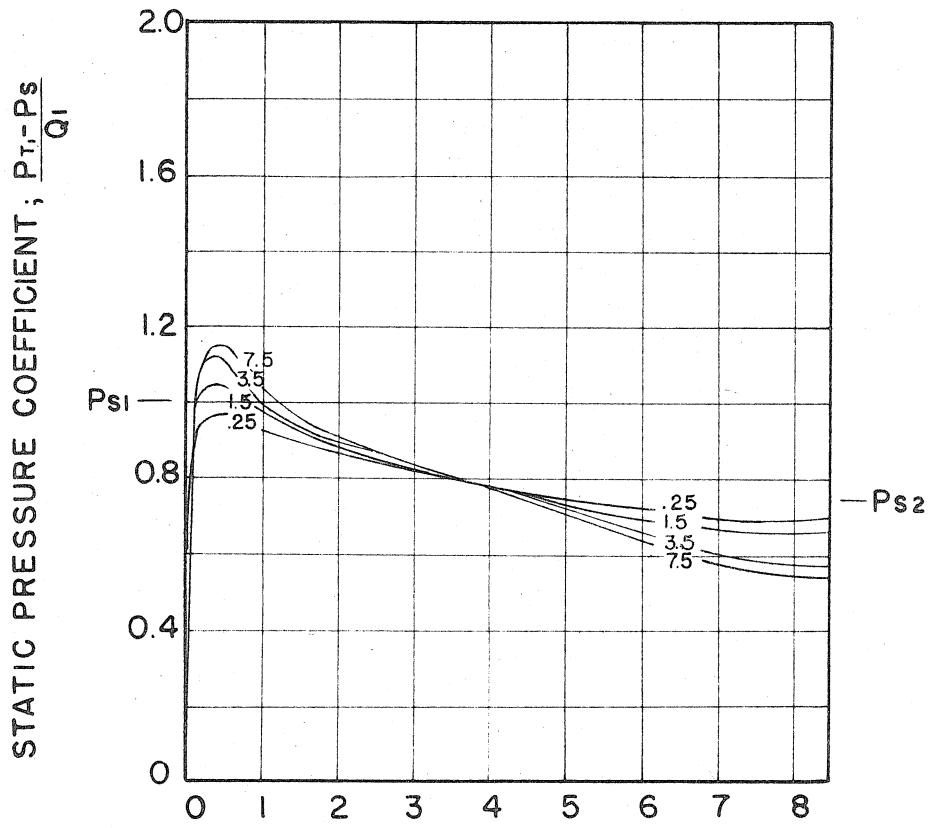

CHORDWISE STATIC PRESSURE DISTRIBUTIONS ON HIGH PRESSURE SURFACE OF BLADE, AT VARIOUS DISTANCES FROM END WALL; $\alpha = 9°$

FIGURE 62

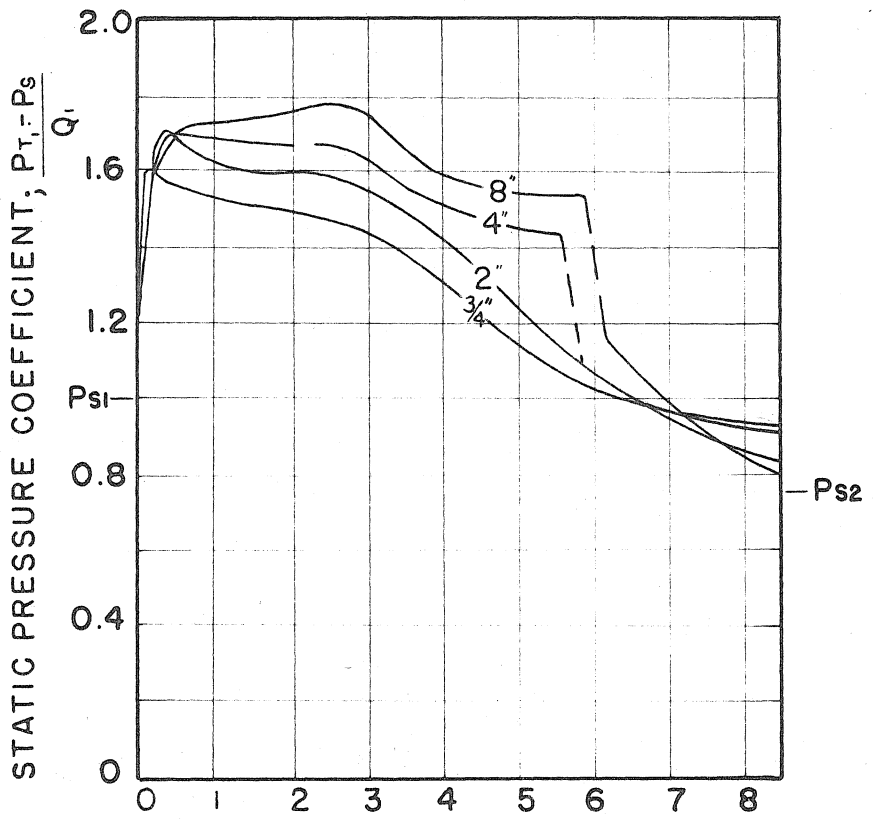

CHORDWISE STATIC PRESSURE DISTRIBUTIONS ON LOW PRESSURE SURFACE OF BLADE, AT VARIOUS DISTANCES FROM END WALL; $\alpha = 13\frac{1}{2}^\circ$

FIGURE 63

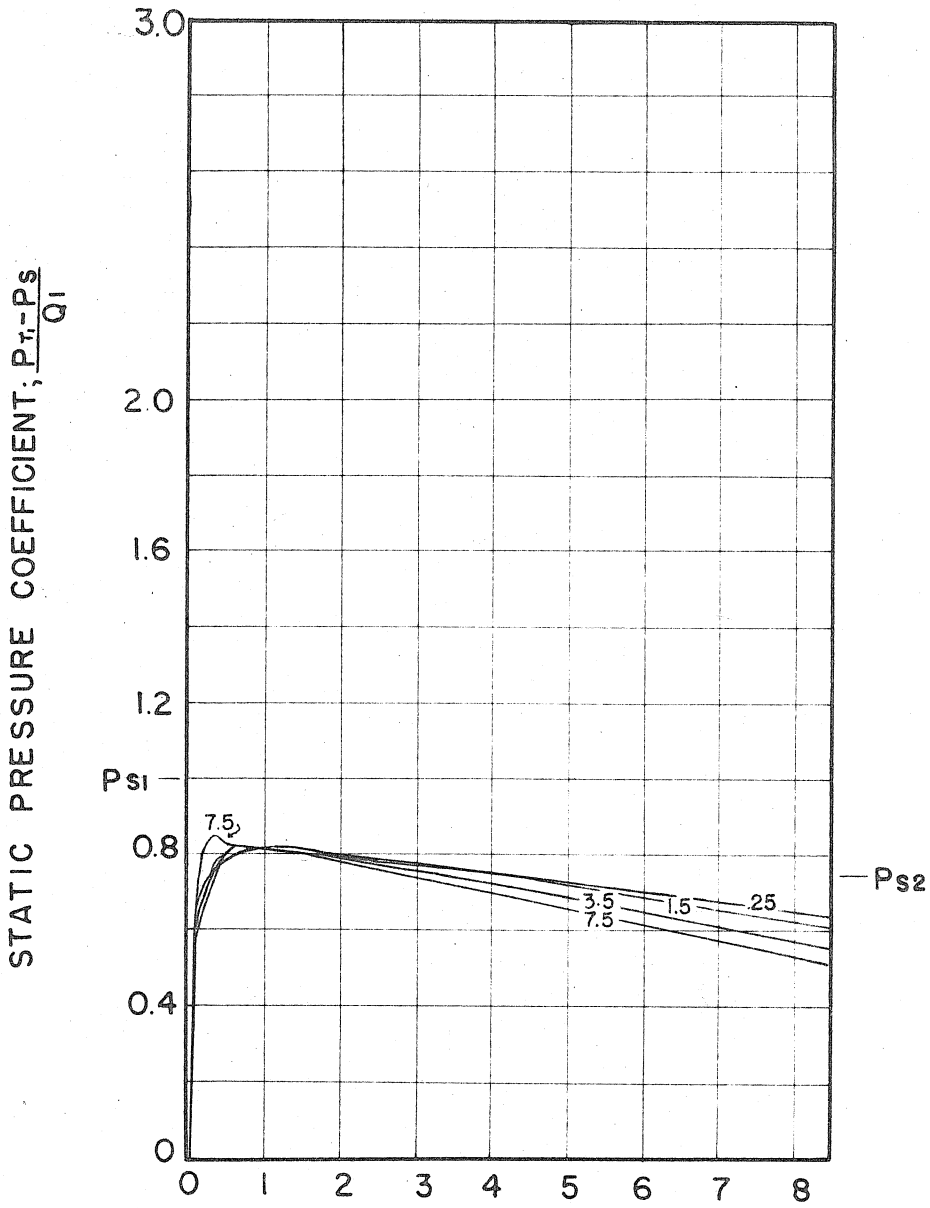

CHORDWISE STATIC PRESSURE DISTRIBUTIONS ON HIGH PRESSURE SURFACE OF BLADE, AT VARIOUS DISTANCES FROM END WALL; $\alpha = 13\frac{1}{2}°$

FIGURE 64

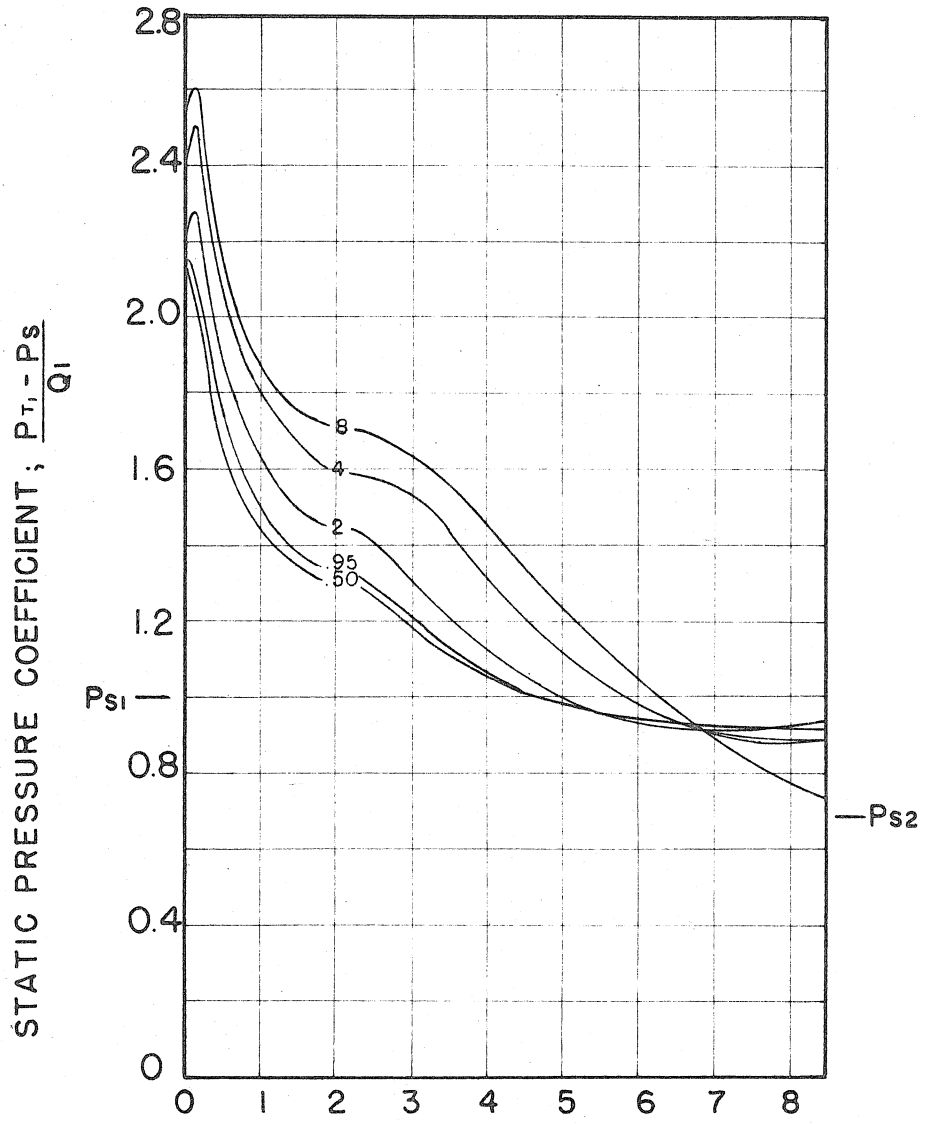

CHORDWISE STATIC PRESSURE DISTRIBUTIONS ON LOW PRESSURE SURFACE OF BLADE, AT VARIOUS DISTANCES FROM END WALL; $\alpha = 21\frac{1}{2}°$

FIGURE 65

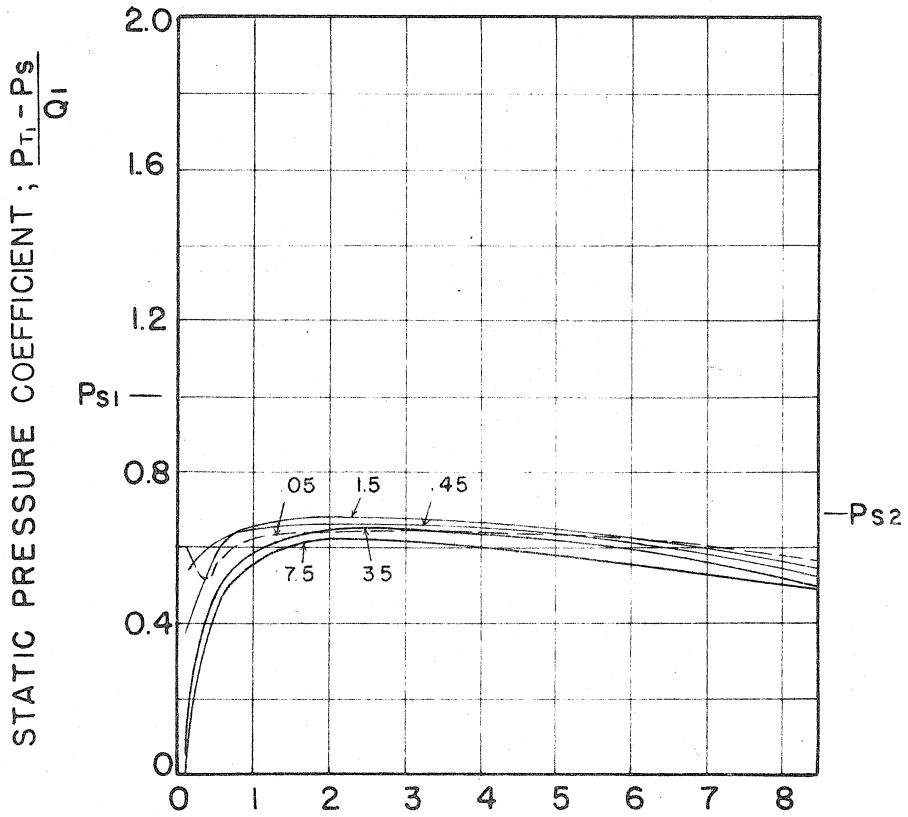

CHORDWISE STATIC PRESSURE DISTRIBUTIONS ON HIGH PRESSURE SURFACE OF BLADE, AT VARIOUS DISTANCES FROM END WALL, $\alpha = 21\frac{1}{2}^\circ$

FIGURE 66

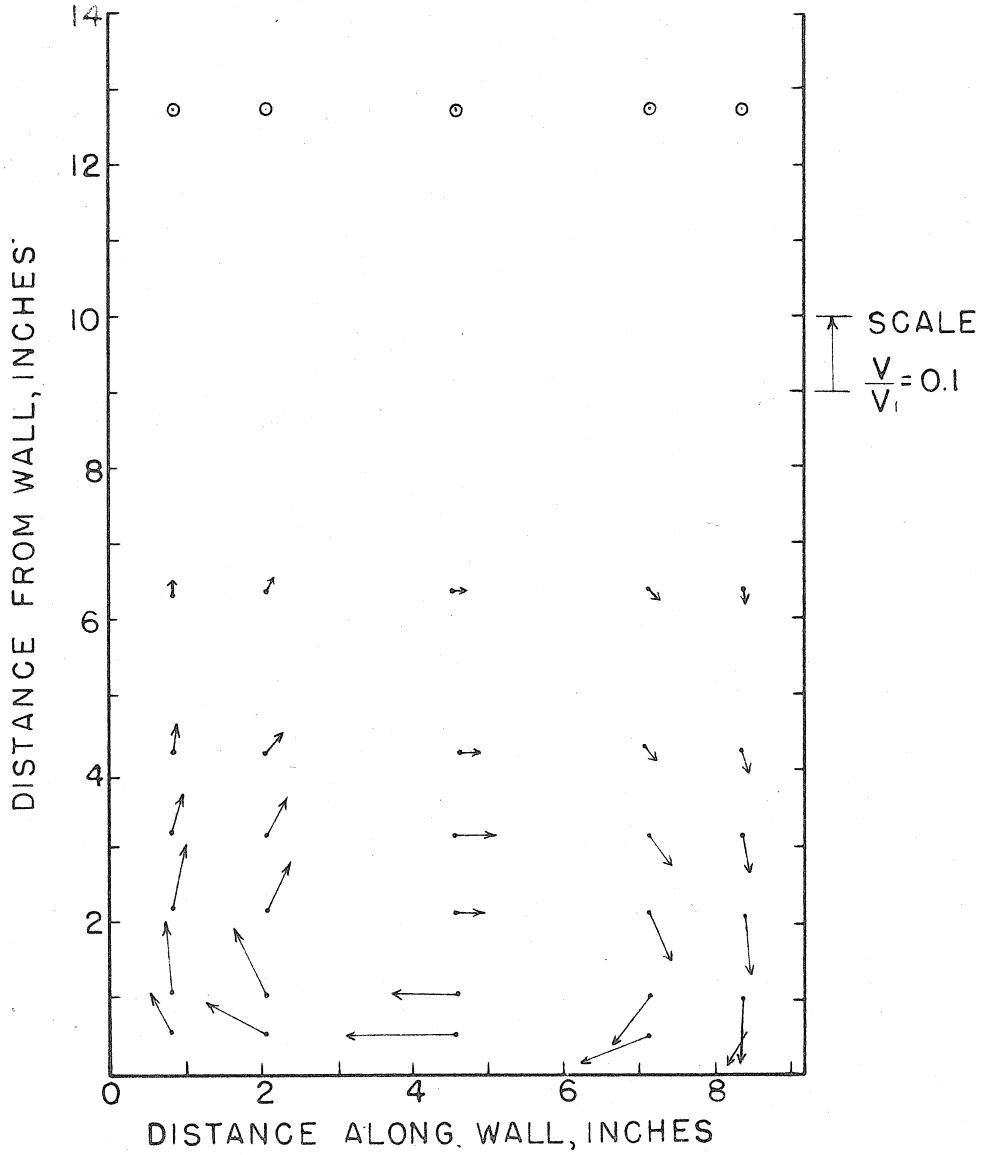

SECONDARY VELOCITIES FROM ANALYTICAL MODEL

FIGURE 67

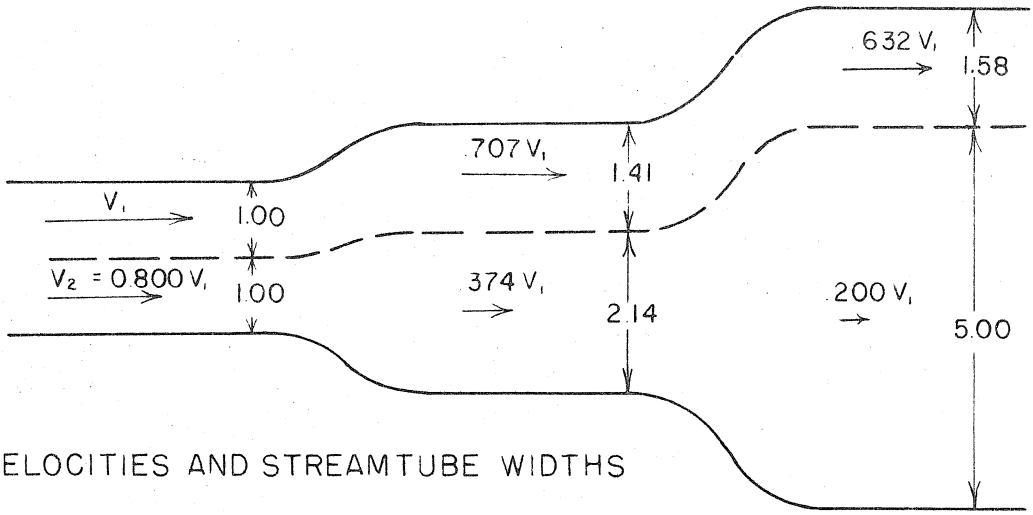

VELOCITIES AND STREAMTUBE WIDTHS

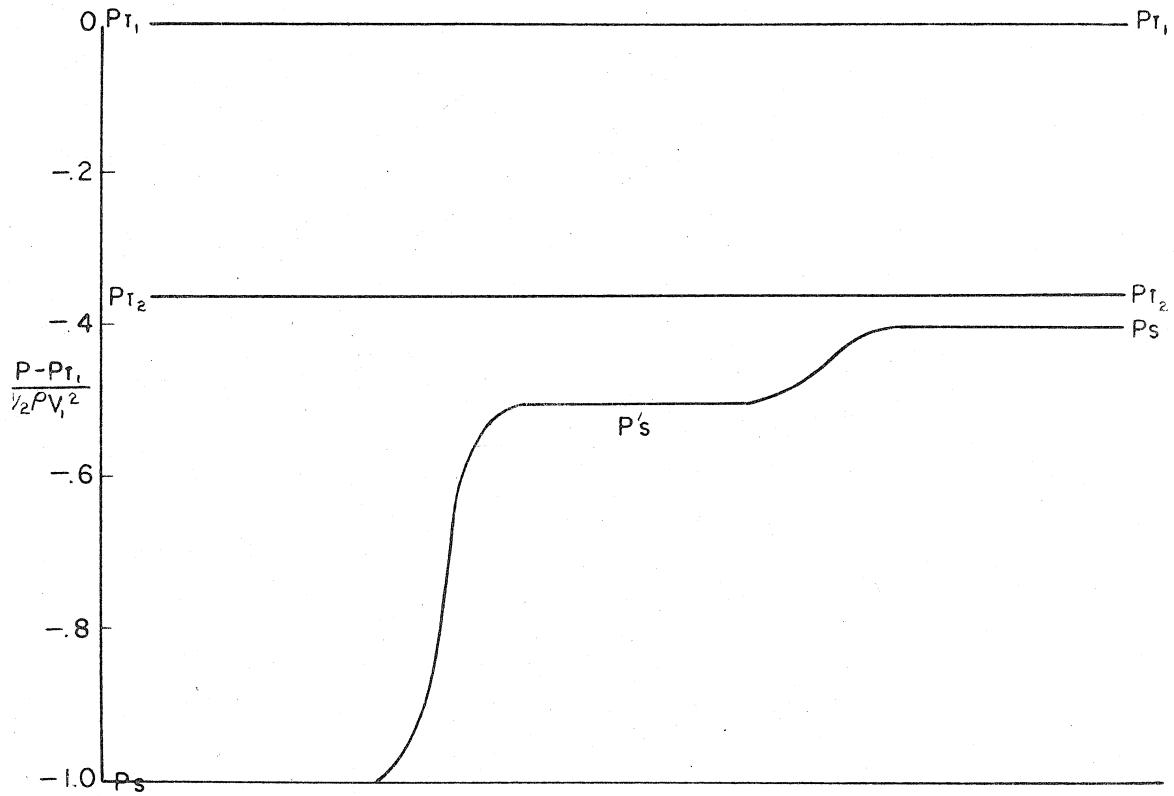

STATIC AND TOTAL PRESSURE

DIFFUSION OF AN INVISCID INCOMPRESSIBLE, QUASI-ONE-DIMENSIONAL FLOW

ILLUSTRATIVE EXAMPLE

FIGURE 68

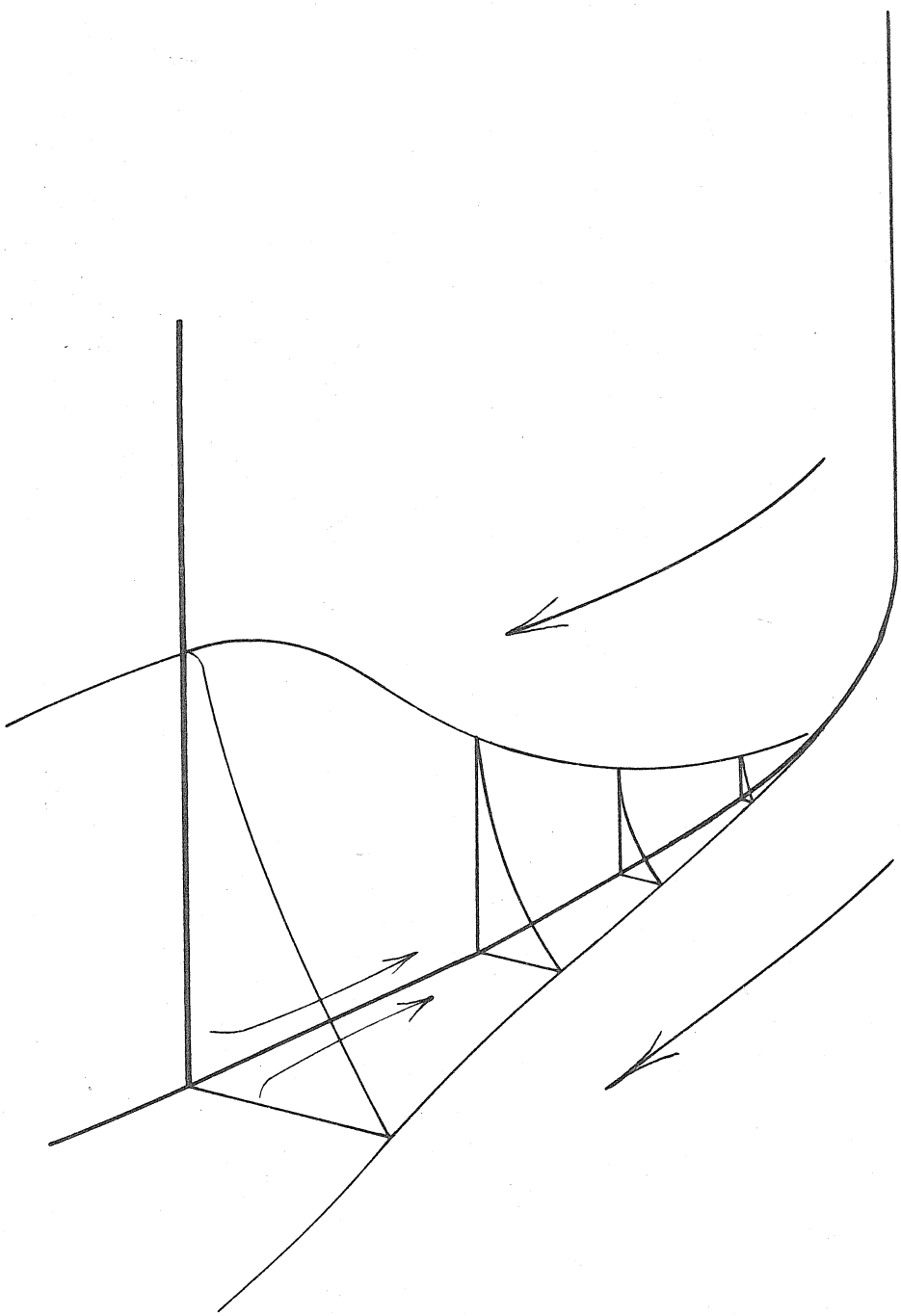

EXTENT OF MIXING REGION

FIGURE 69

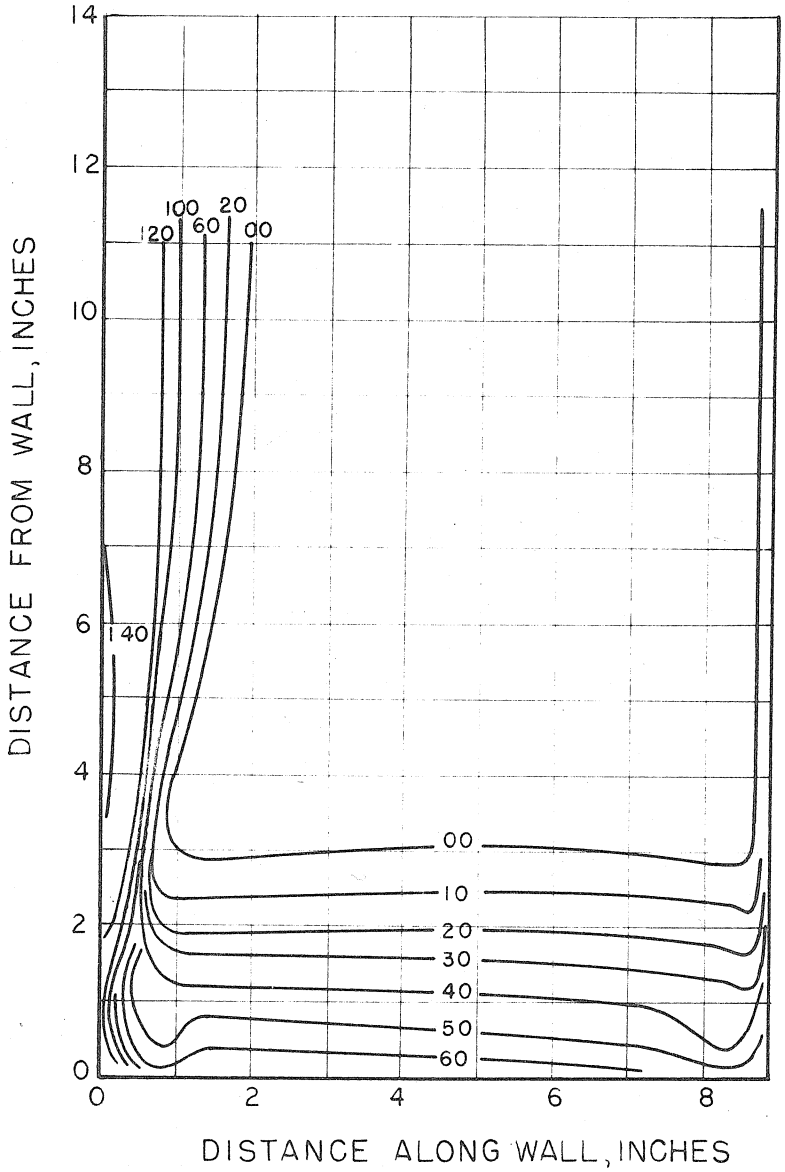

TOTAL PRESSURE PROFILE MAP AT SUBCRITICAL REYNOLDS NUMBER

LOW SPEED; Rn = 67,000; ¾C; $\alpha = 13\frac{1}{2}^{\circ}$

FIGURE 70

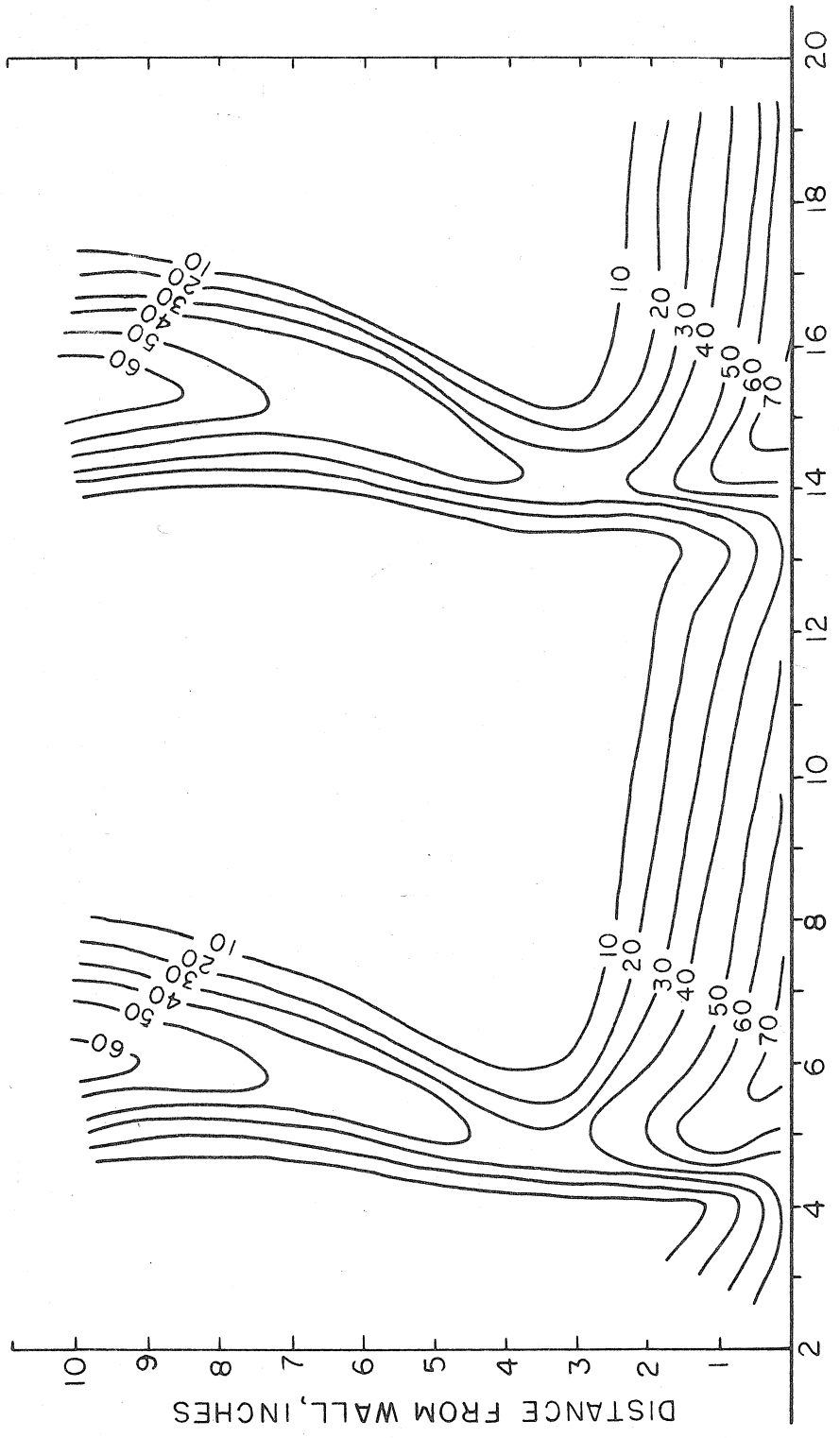

TOTAL PRESSURE PROFILE MAP AT SUBCRITICAL REYNOLDS NUMBER

LOW SPEED, Rn = 67,000, 1½C, $\alpha = 13\frac{1}{2}^{\circ}$

FIGURE 71

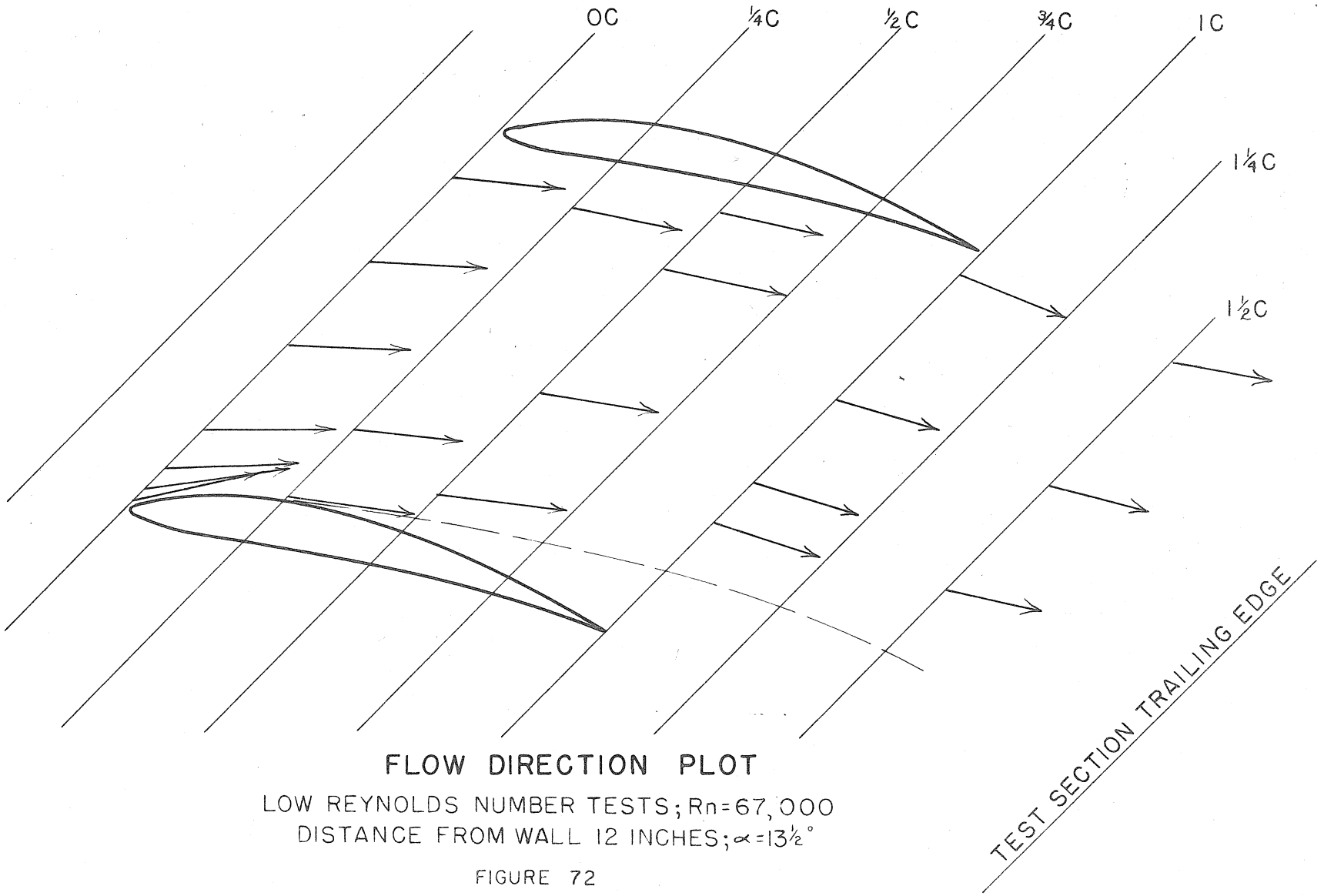

FLOW DIRECTION PLOT

LOW REYNOLDS NUMBER TESTS; Rn=67,000
DISTANCE FROM WALL 12 INCHES; $\alpha = 13\frac{1}{2}^\circ$

FIGURE 72

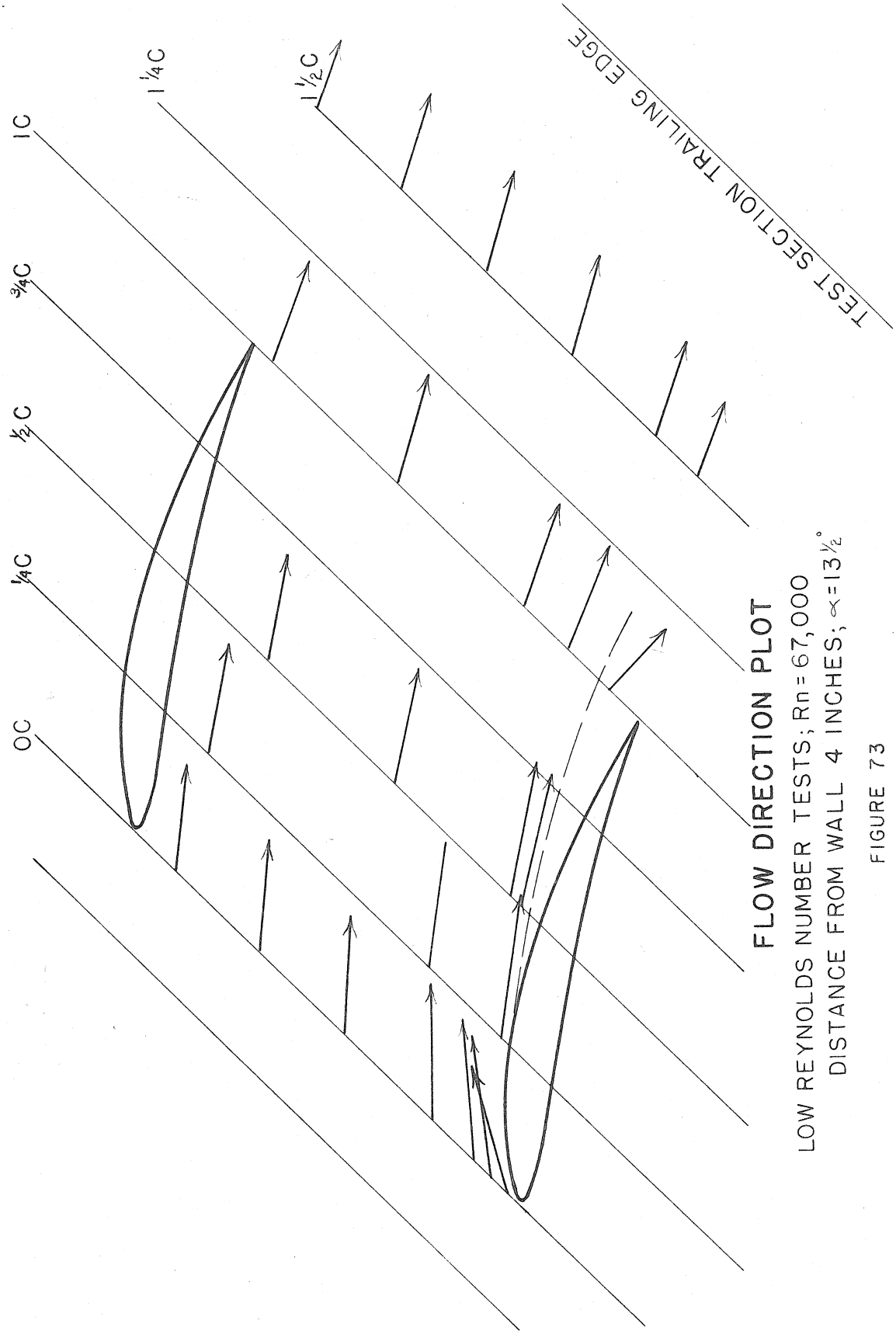

FLOW DIRECTION PLOT

LOW REYNOLDS NUMBER TESTS; Rn = 67,000

DISTANCE FROM WALL 4 INCHES; $\alpha = 13\frac{1}{2}^{\circ}$

FIGURE 73

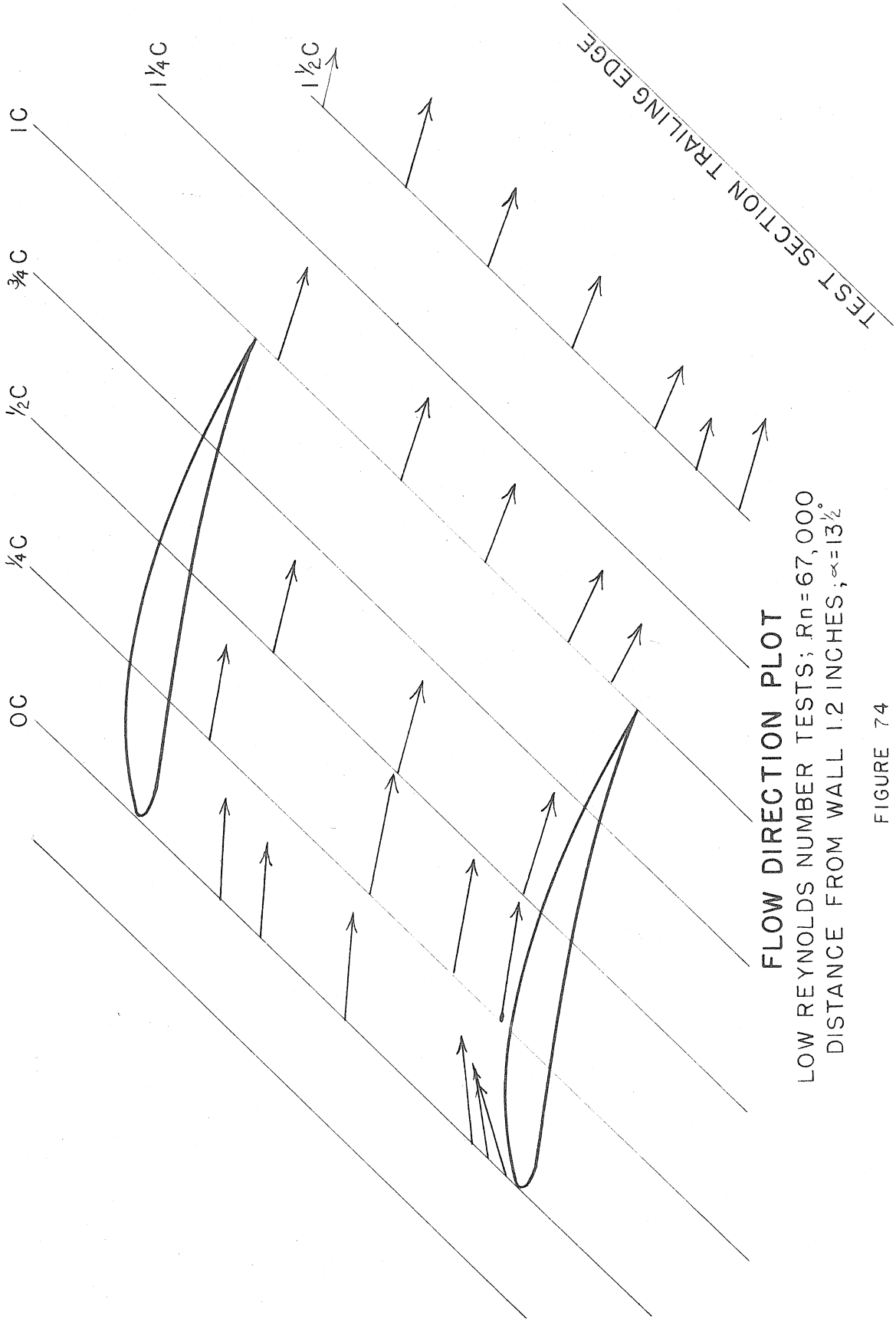

FLOW DIRECTION PLOT
LOW REYNOLDS NUMBER TESTS; Rn = 67,000
DISTANCE FROM WALL 1.2 INCHES; $\alpha = 13\frac{1}{2}^{\circ}$

FIGURE 74

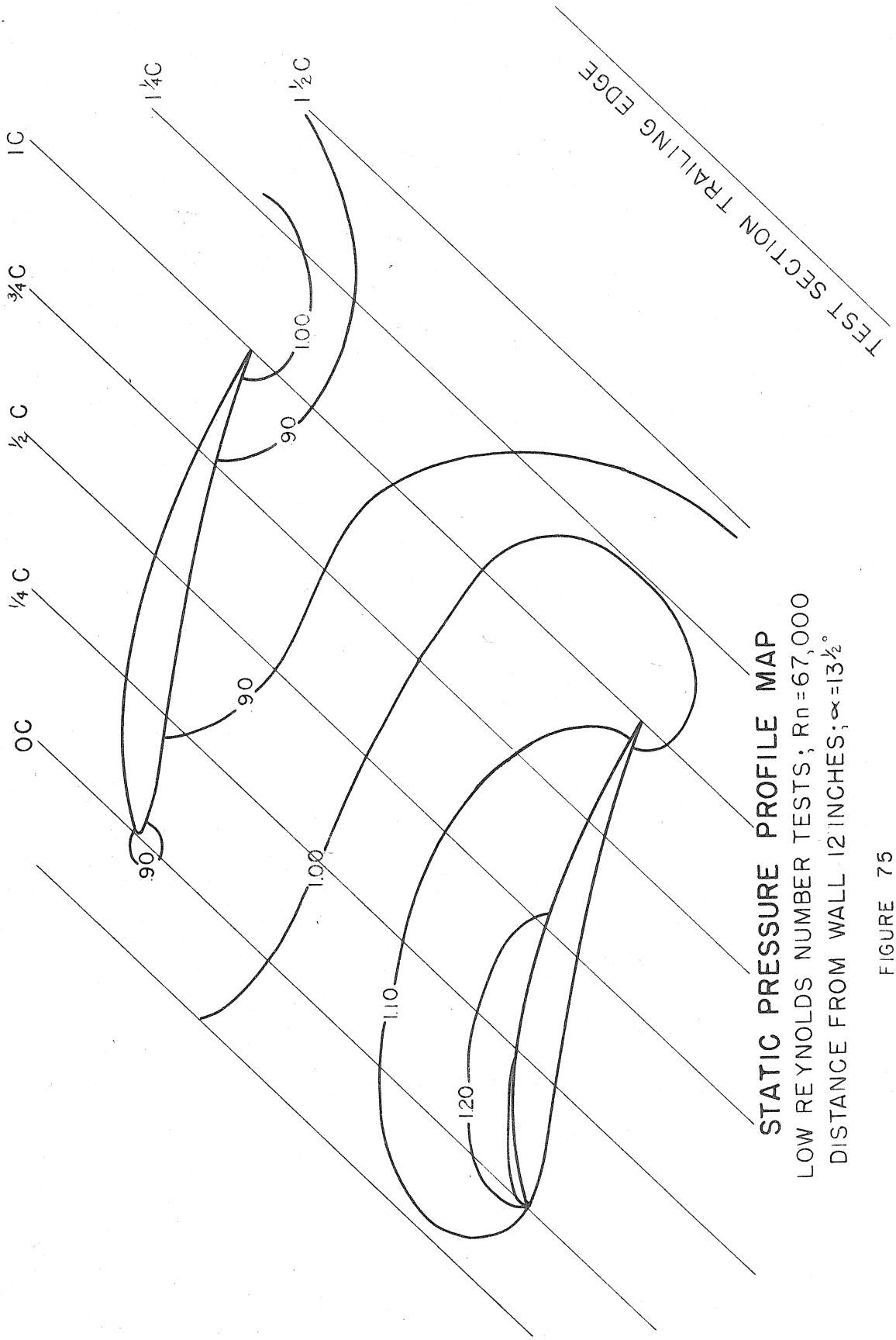

STATIC PRESSURE PROFILE MAP

LOW REYNOLDS NUMBER TESTS; Rn=67,000

DISTANCE FROM WALL 12 INCHES; $\alpha = 13\frac{1}{2}°$

FIGURE 75

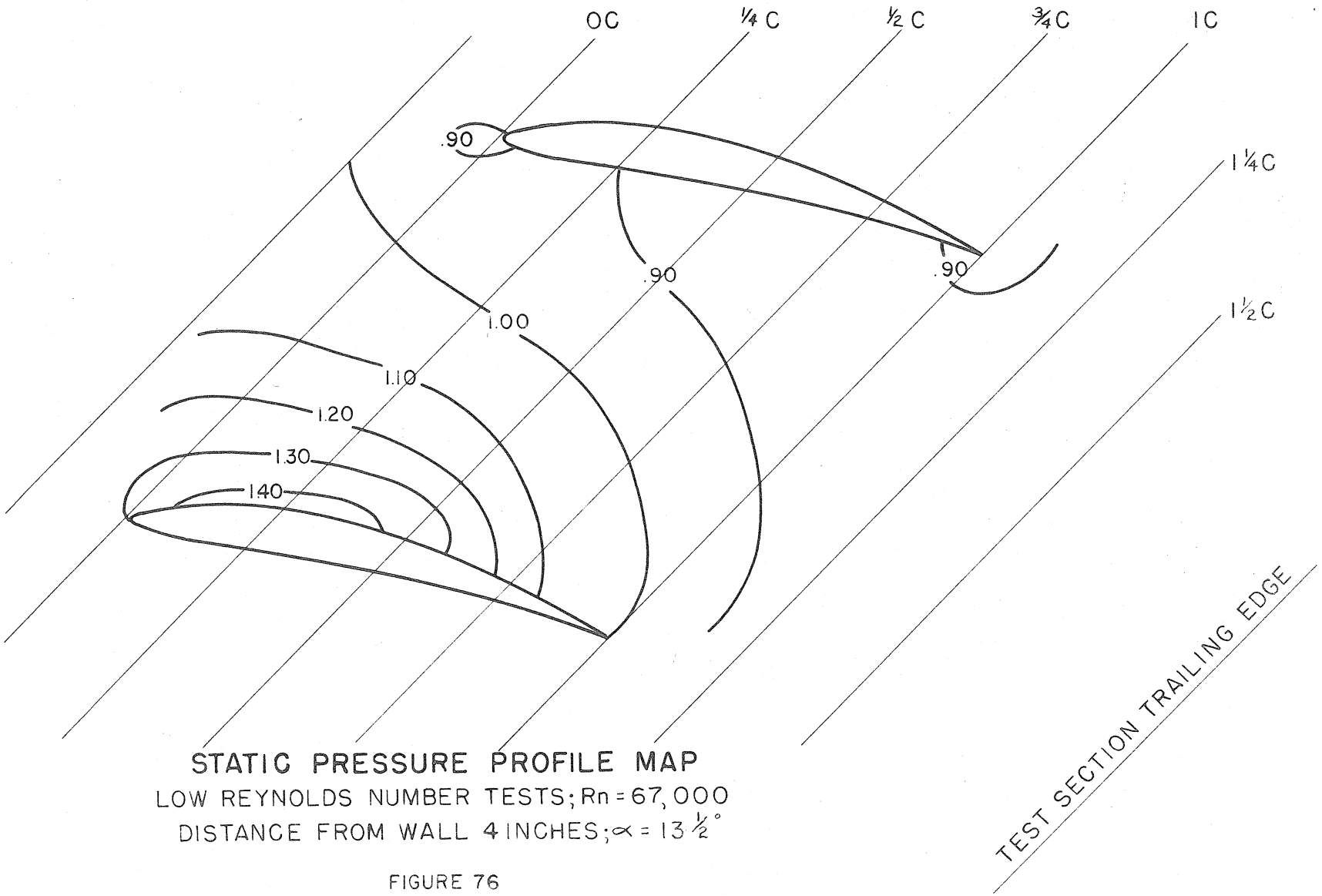

STATIC PRESSURE PROFILE MAP
LOW REYNOLDS NUMBER TESTS; Rn = 67,000
DISTANCE FROM WALL 4 INCHES; $\alpha = 13\frac{1}{2}^{\circ}$

FIGURE 76

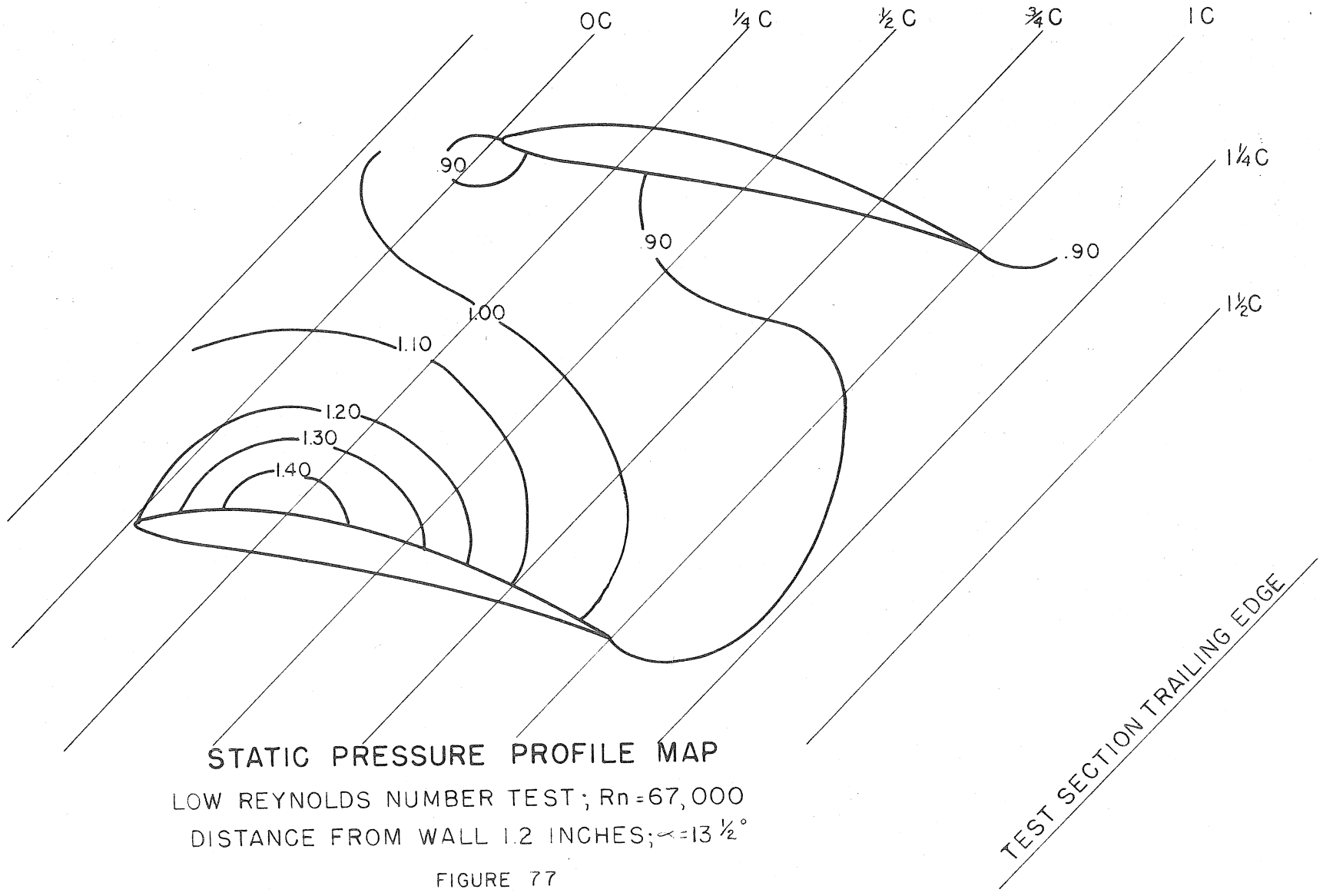

STATIC PRESSURE PROFILE MAP

LOW REYNOLDS NUMBER TEST; Rn = 67,000

DISTANCE FROM WALL 1.2 INCHES; $\alpha = 13\frac{1}{2}°$

FIGURE 77

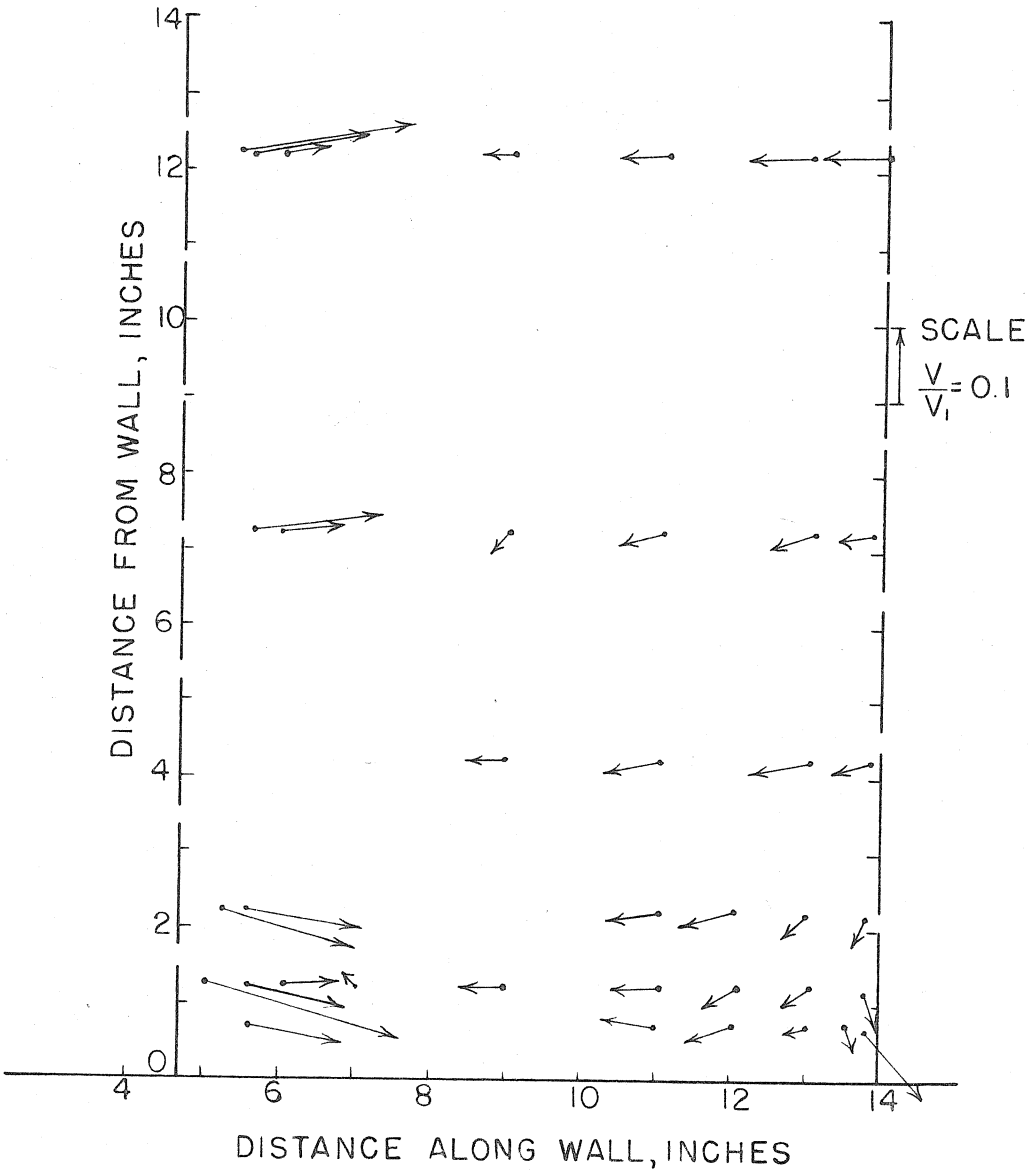

SECONDARY VELOCITY DIAGRAM; OC; $\alpha = 13\frac{1}{2}°$
LOW REYNOLDS NUMBER TESTS; Rn = 67,000

FIGURE 78

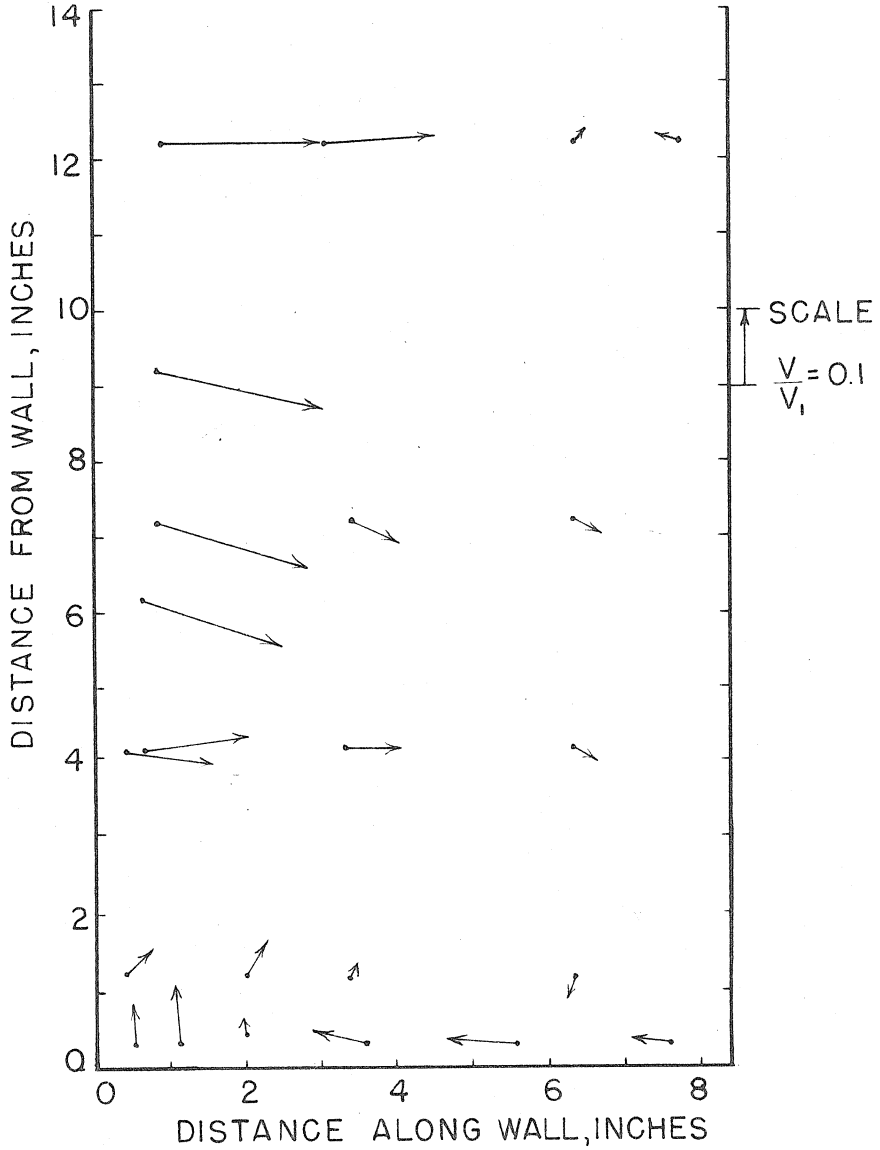

SECONDARY VELOCITY DIAGRAM; ½ C; $\alpha = 13\frac{1}{2}^\circ$

LOW REYNOLDS NUMBER TESTS; Rn = 67,000

FIGURE 79

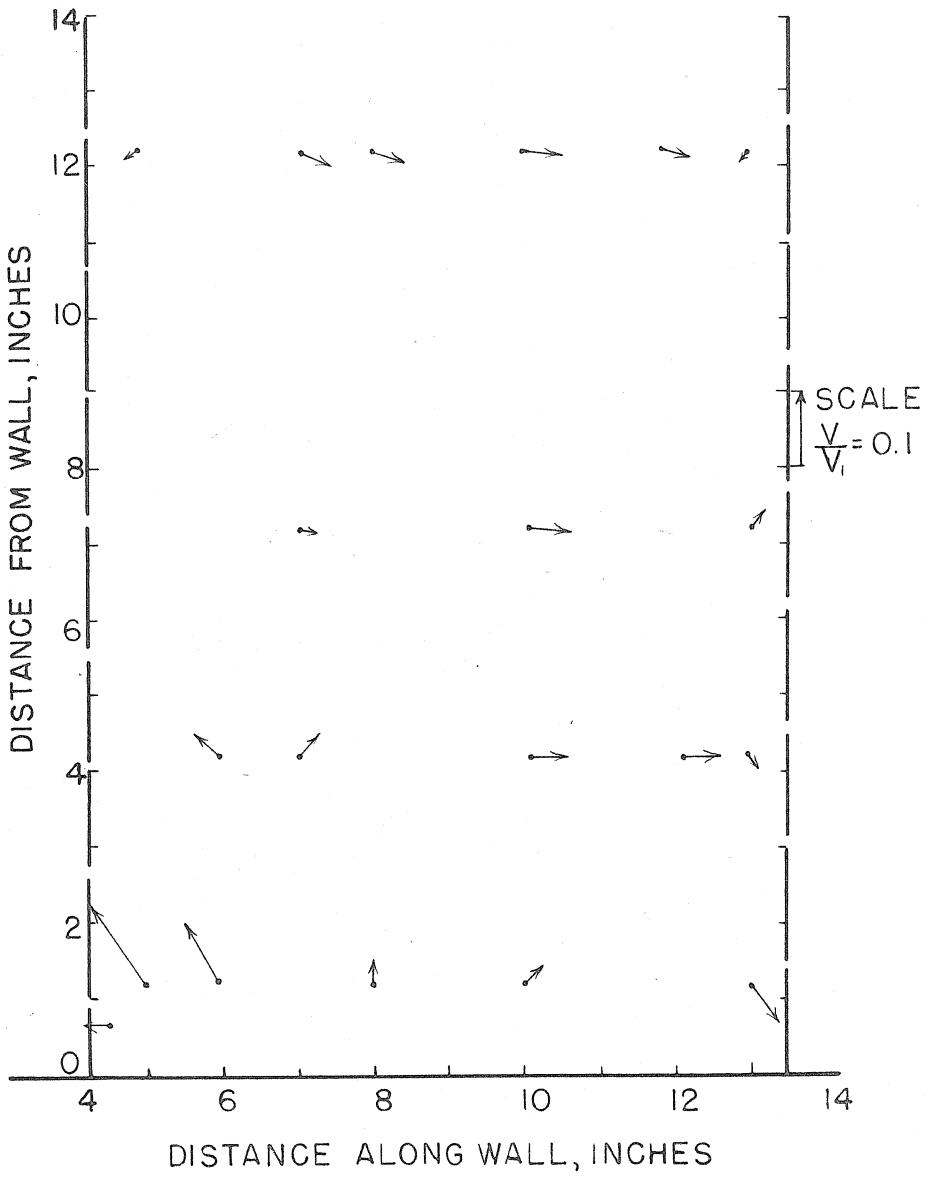

SECONDARY VELOCITY DIAGRAM; IC; $\alpha = 13\frac{1}{2}^{\circ}$

LOW REYNOLDS NUMBER TESTS; Rn = 67,000

FIGURE 80

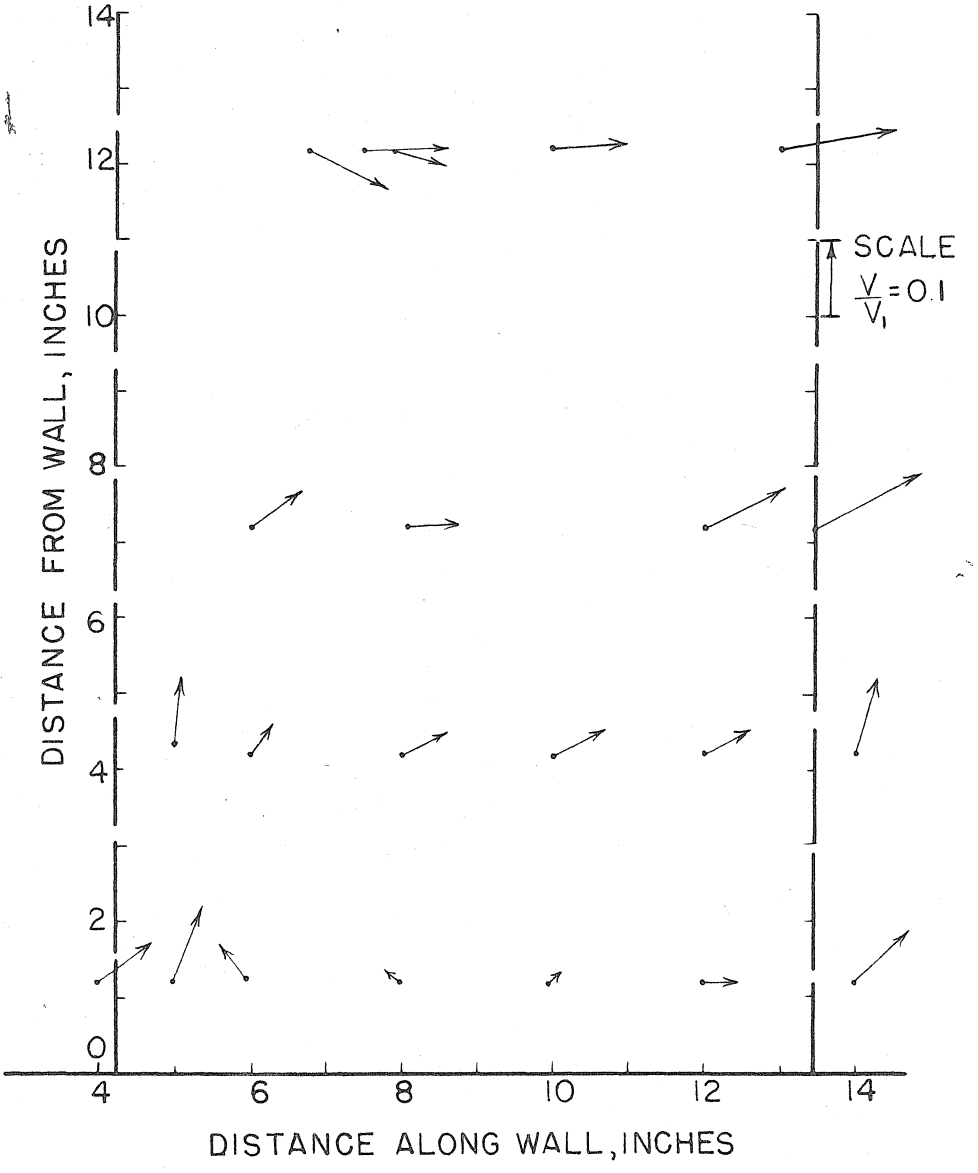

SECONDARY VELOCITY DIAGRAM; 1½C; $\alpha = 13\frac{1}{2}^{\circ}$
LOW REYNOLDS NUMBER TESTS; Rn = 67,000

FIGURE 81

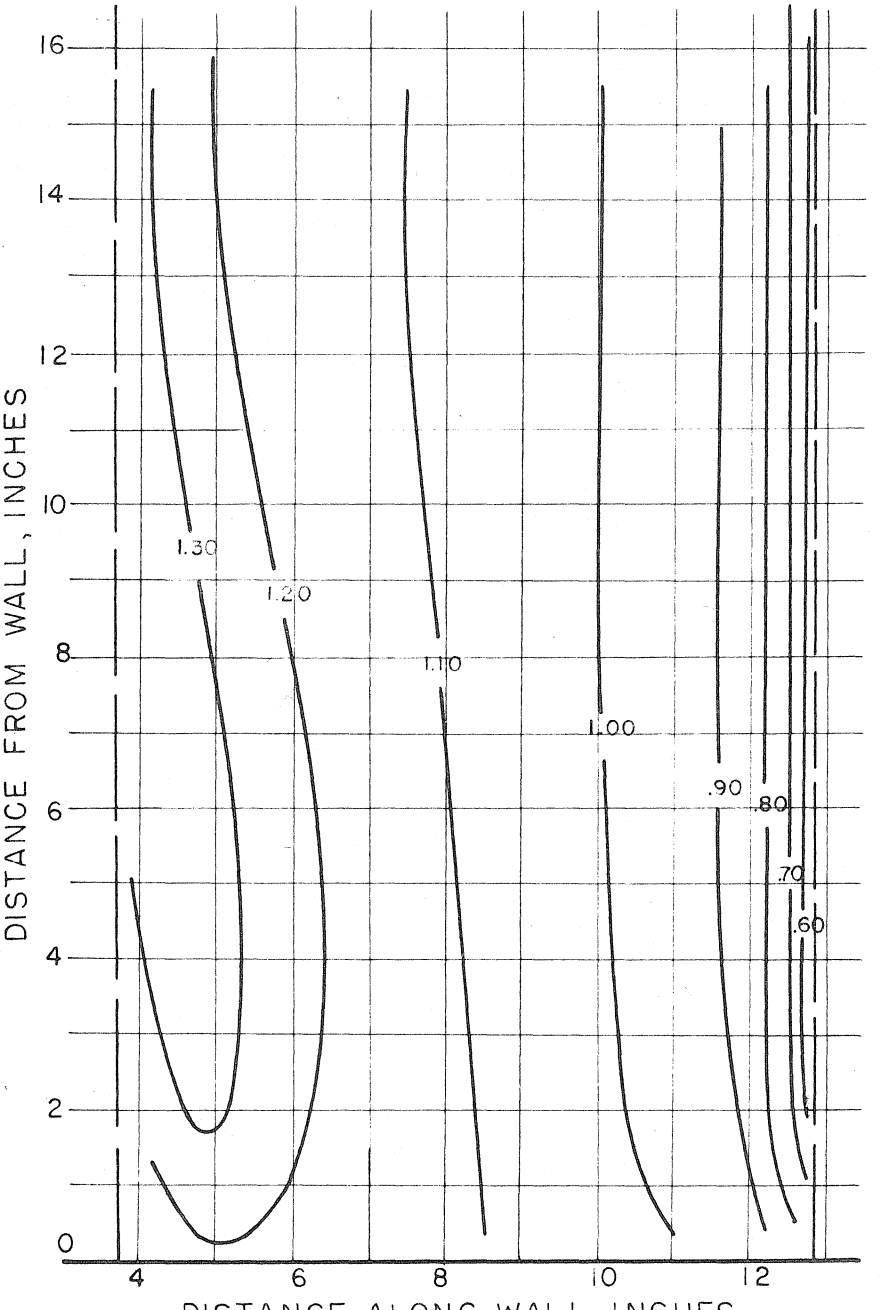

PROFILE MAP OF STATIC PRESSURE DISTRIBUTION; $\frac{P_T - P_S}{Q_1}$

LOW REYNOLDS NUMBER TESTS; Rn = 67,000

OC SURVEY PLANE; $\alpha = 13\frac{1}{2}°$

FIGURE 82

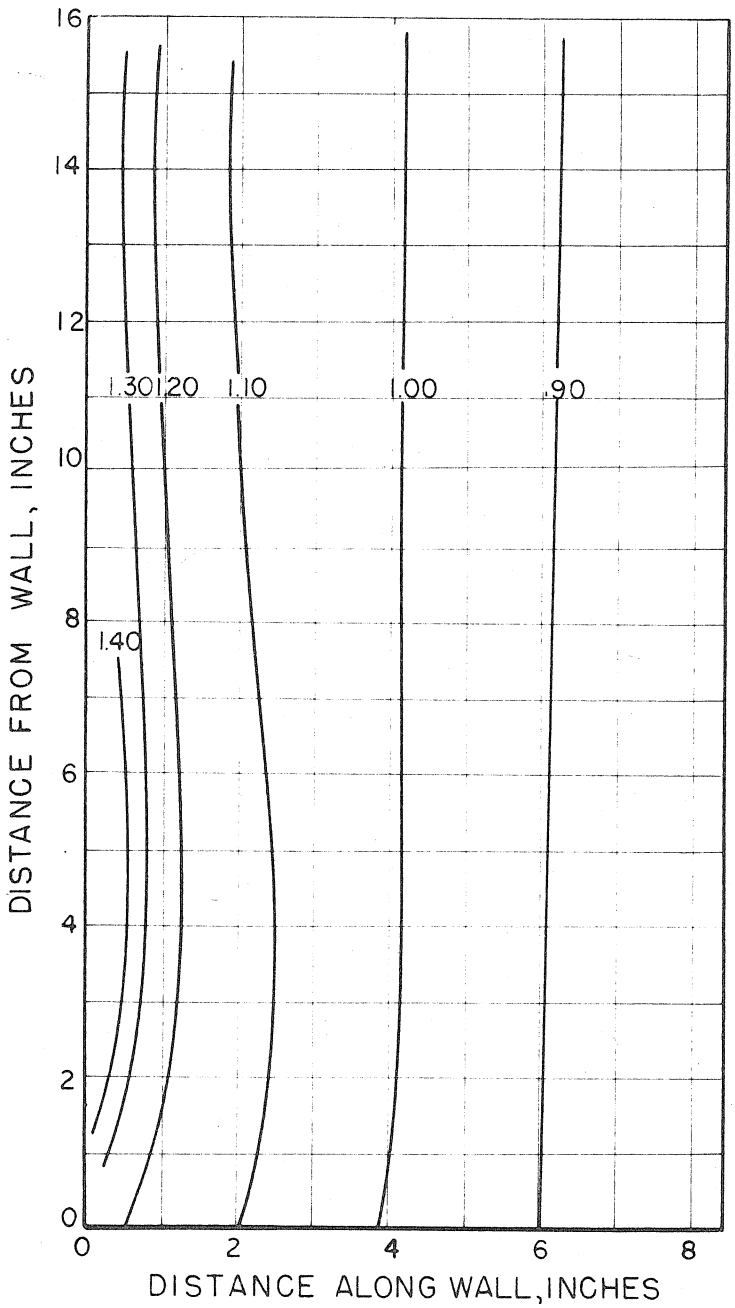

PROFILE MAP OF STATIC PRESSURE DISTRIBUTION; $\frac{P_T - P_S}{Q_1}$

LOW REYNOLDS NUMBER TESTS; Rn = 67,000
½C SURVEY PLANE; $\alpha = 13\frac{1}{2}°$

FIGURE 83

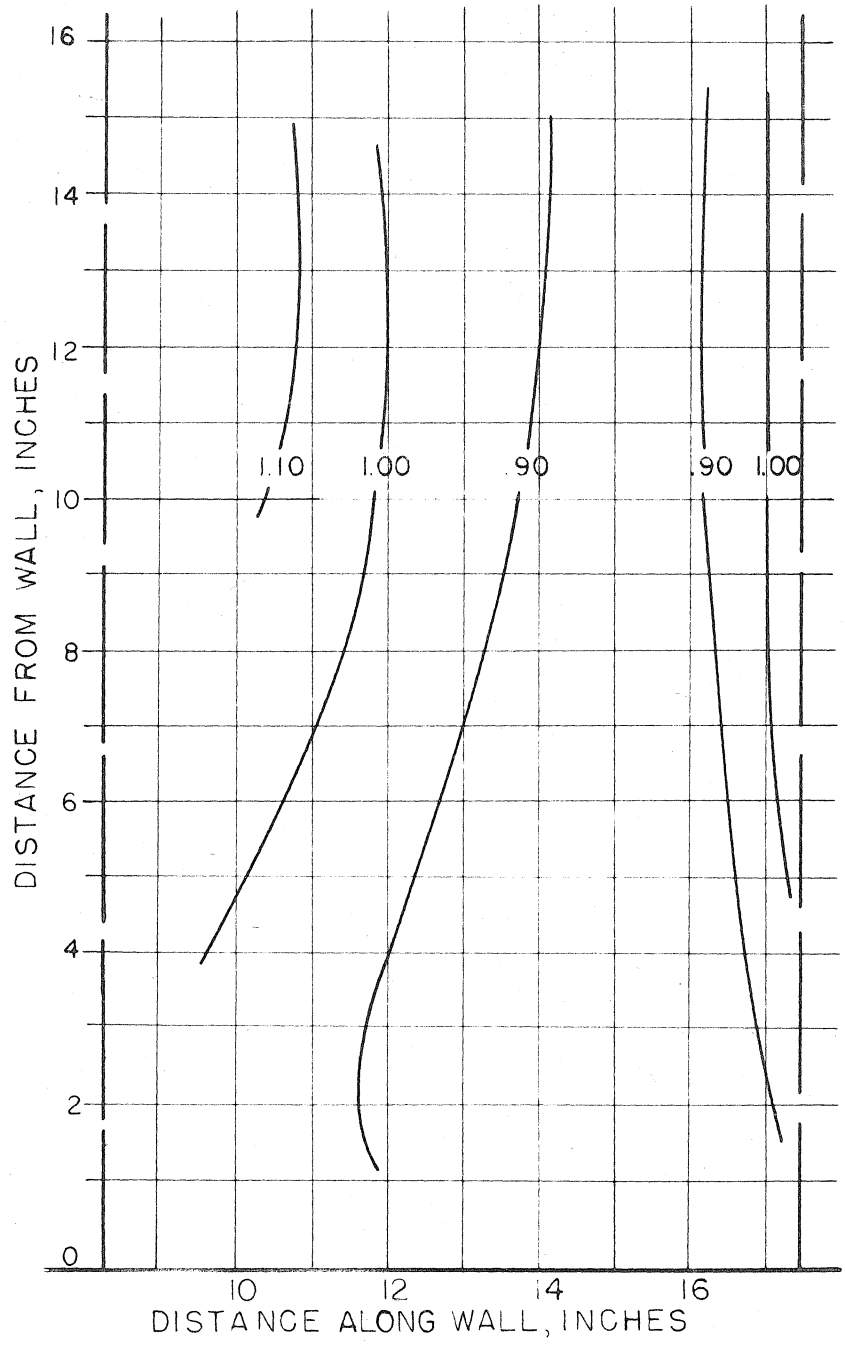

PROFILE MAP OF STATIC PRESSURE DISTRIBUTION ; $\frac{Pr - Ps}{Q_1}$

LOW REYNOLDS NUMBER TESTS; Rn = 67,000

IC SURVEY PLANE; $\alpha = 13\frac{1}{2}^\circ$

FIGURE 84

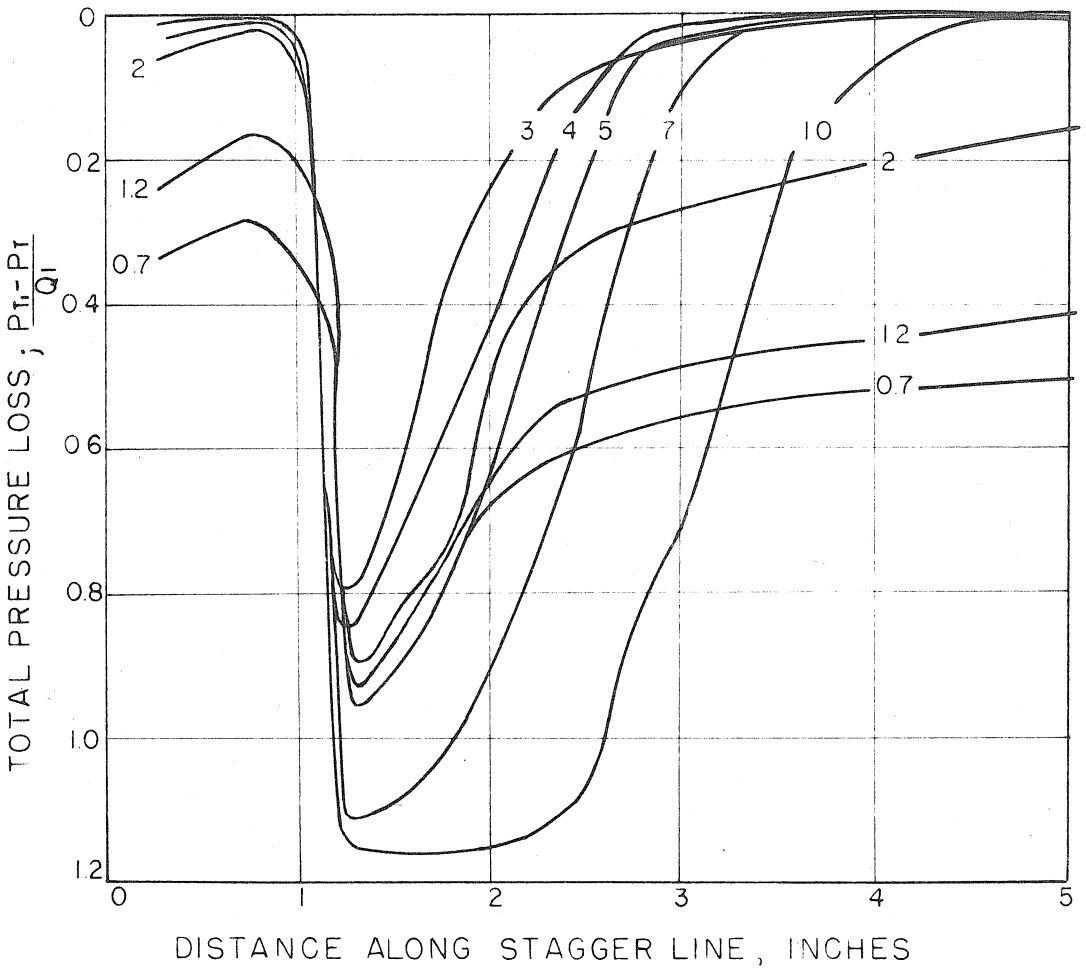

WAKE TOTAL PRESSURE SURVEYS NEAR CRITICAL REYNOLDS NUMBER; Rn = 125,000

DISTANCE FROM WALL; INCHES; IC, $\alpha = 13\frac{1}{2}^\circ$

FIGURE 85

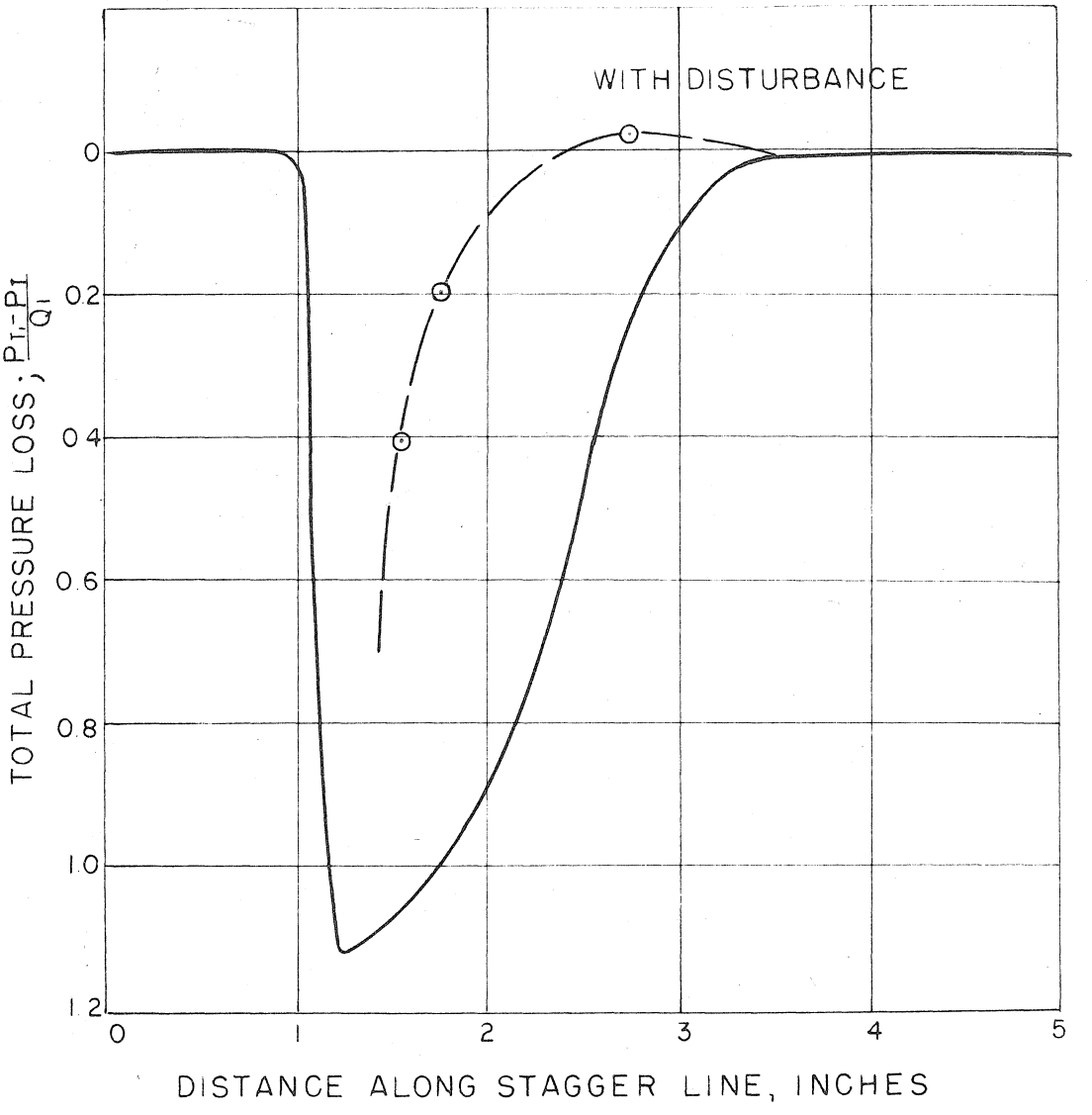

WAKE TOTAL PRESSURE SURVEYS NEAR CRITICAL REYNOLDS NUMBER, Rn = 125,000

SURVEY 7 INCHES FROM WALL; EFECT OF SOUND ON WAKES; IC; $\alpha = 13\frac{1}{2}^\circ$

FIGURE 86

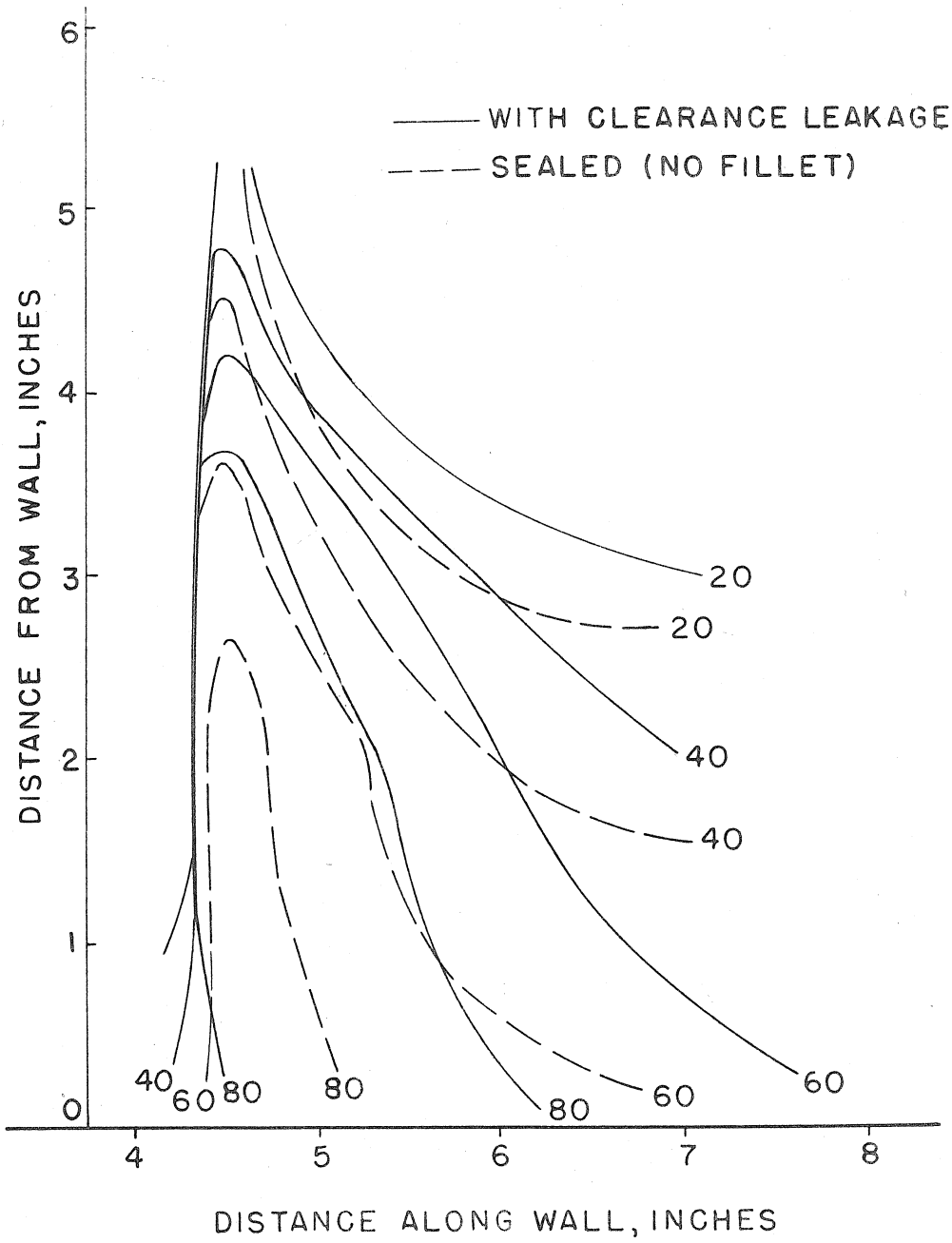

COMPARISON OF TOTAL HEAD DISTRIBUTIONS NEAR CORNER, WITH AND WITHOUT CLEARANCE LEAKAGE

IC, $\alpha = 13\frac{1}{2}^{\circ}$

CLEARANCE = .015

FIGURE 87

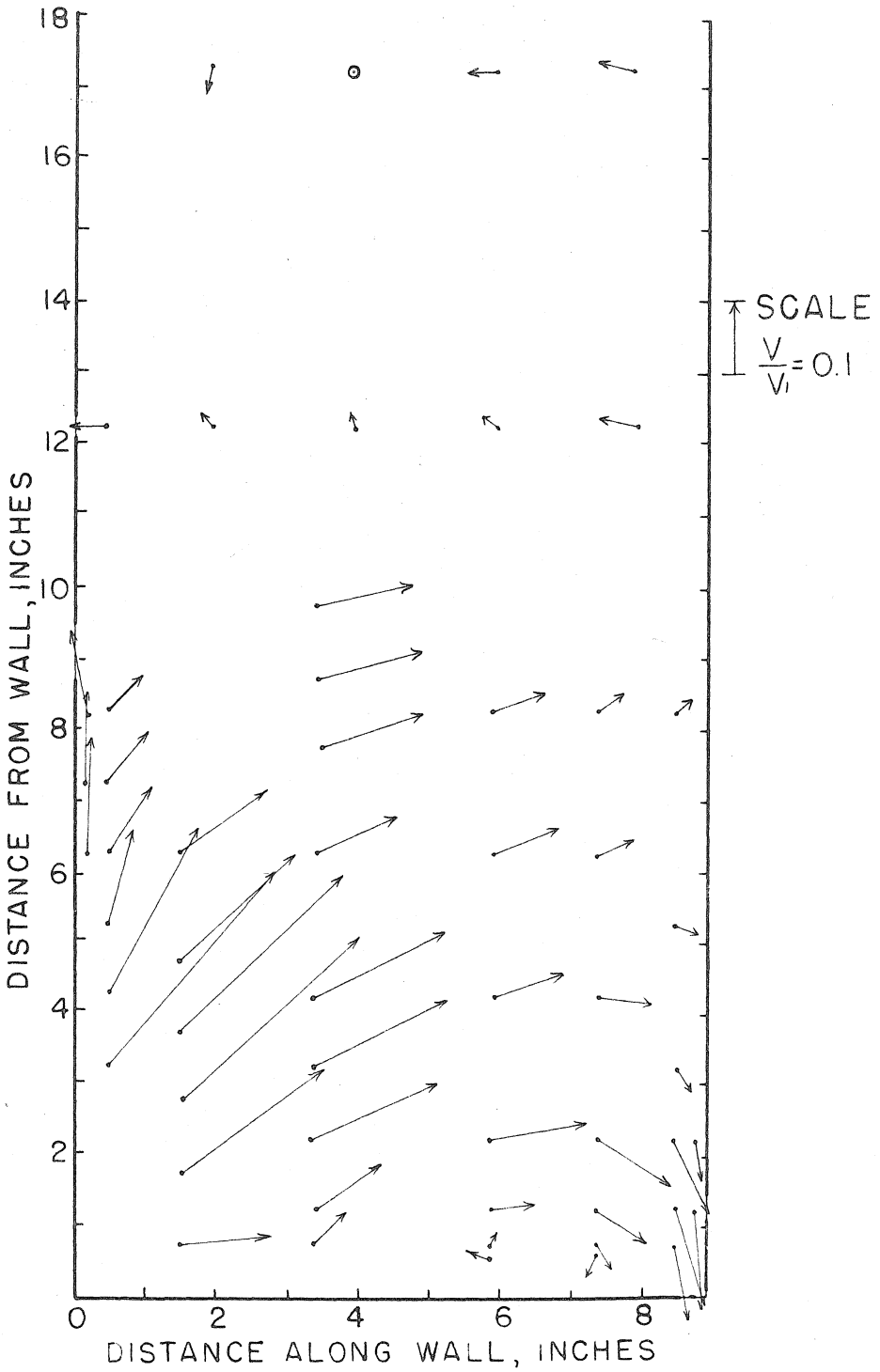

SECONDARY VELOCITY DIAGRAM; $\frac{3}{4}$ C; $\alpha = 13\frac{1}{2}°$
WITH CLEARANCE LEAKAGE

FIGURE 88

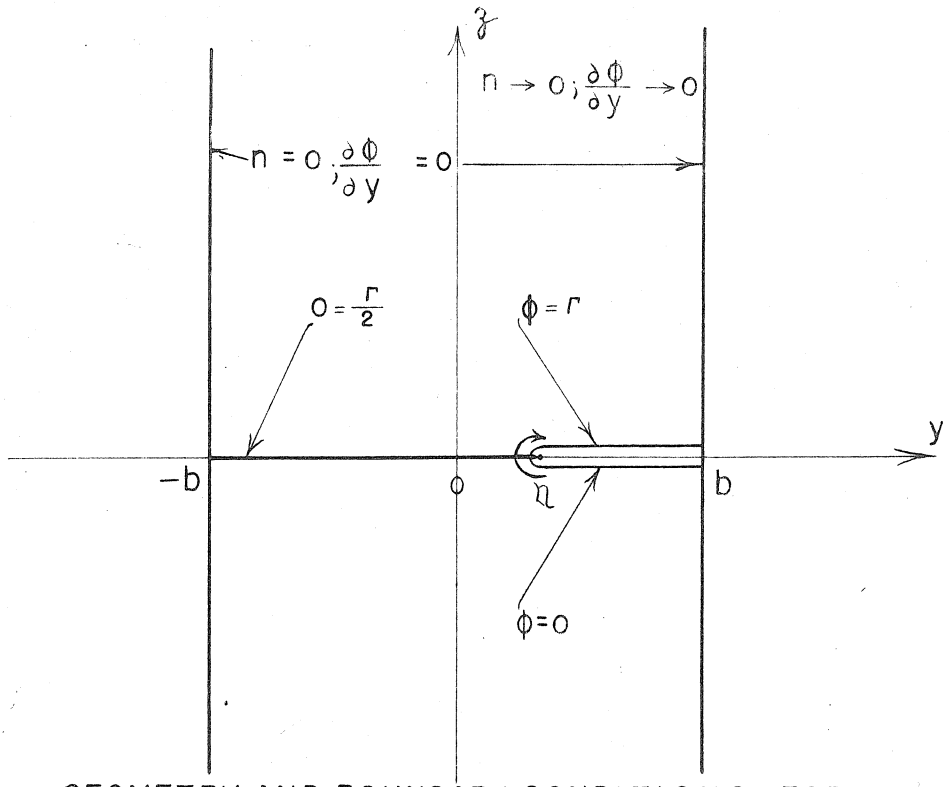

GEOMETRY AND BOUNDARY CONDITIONS FOR VELOCITY POTENTIAL SOLUTION

FIGURE 89

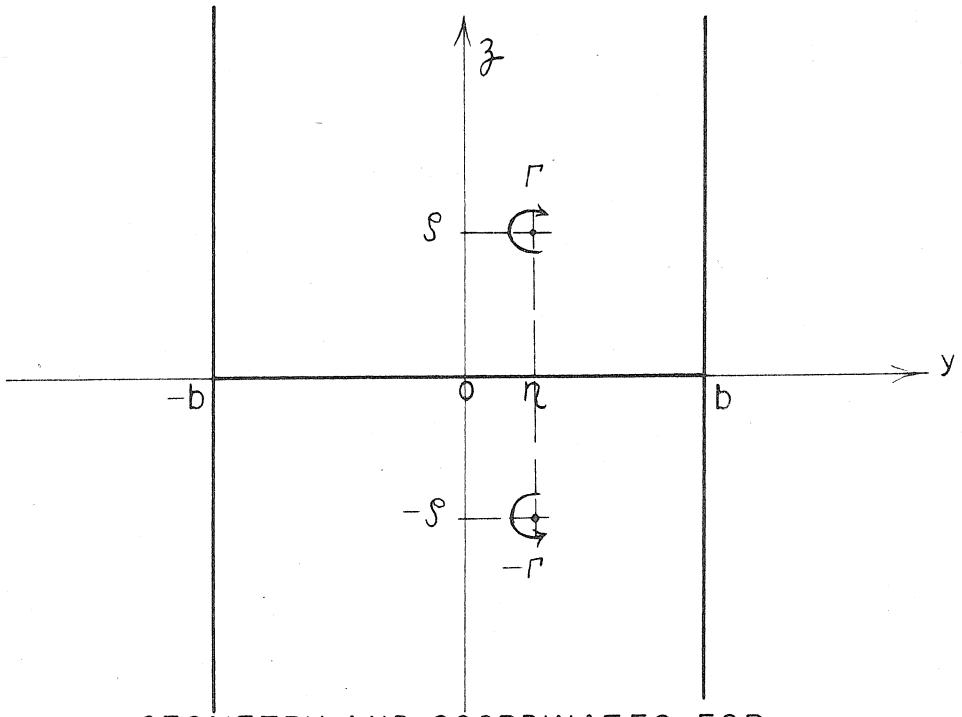

GEOMETRY AND COORDINATES FOR THE VORTICITY GREEN'S FUNCTION

FIGURE 90

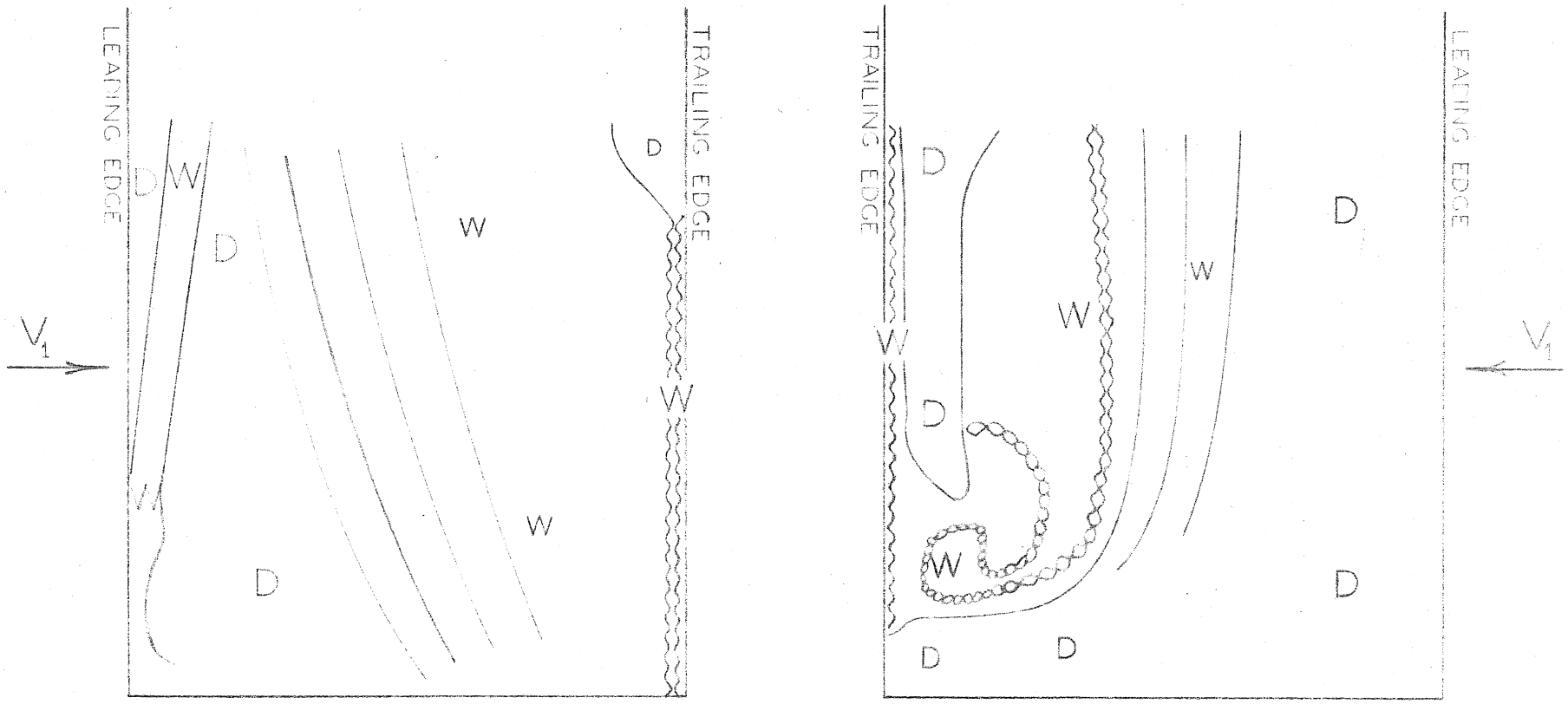

HIGH PRESSURE BLADE SURFACE

LOW PRESSURE BLADE SURFACE

KEY: D = DRY
W = WET
≈≈ = LIQUID BEAD

RESULTS OF LIQUID EVAPORATION TESTS, $\alpha = -1^\circ$

FIGURE 91

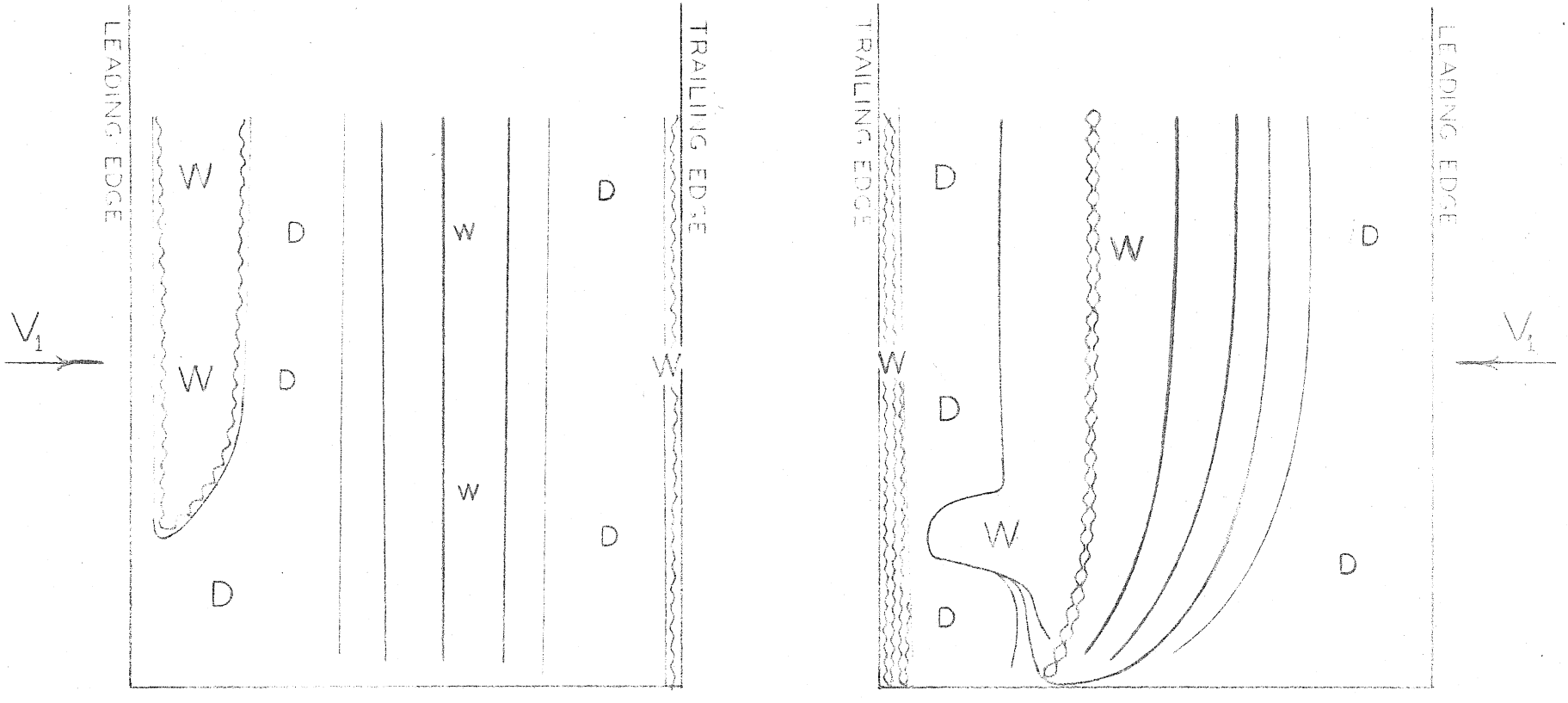

HIGH PRESSURE BLADE SURFACE

LOW PRESSURE BLADE SURFACE

KEY : D = DRY

W = WET

≈≈ = LIQUID BEAD

RESULTS OF LIQUID EVAPORATION TESTS, $\alpha = 5°$

FIGURE 92

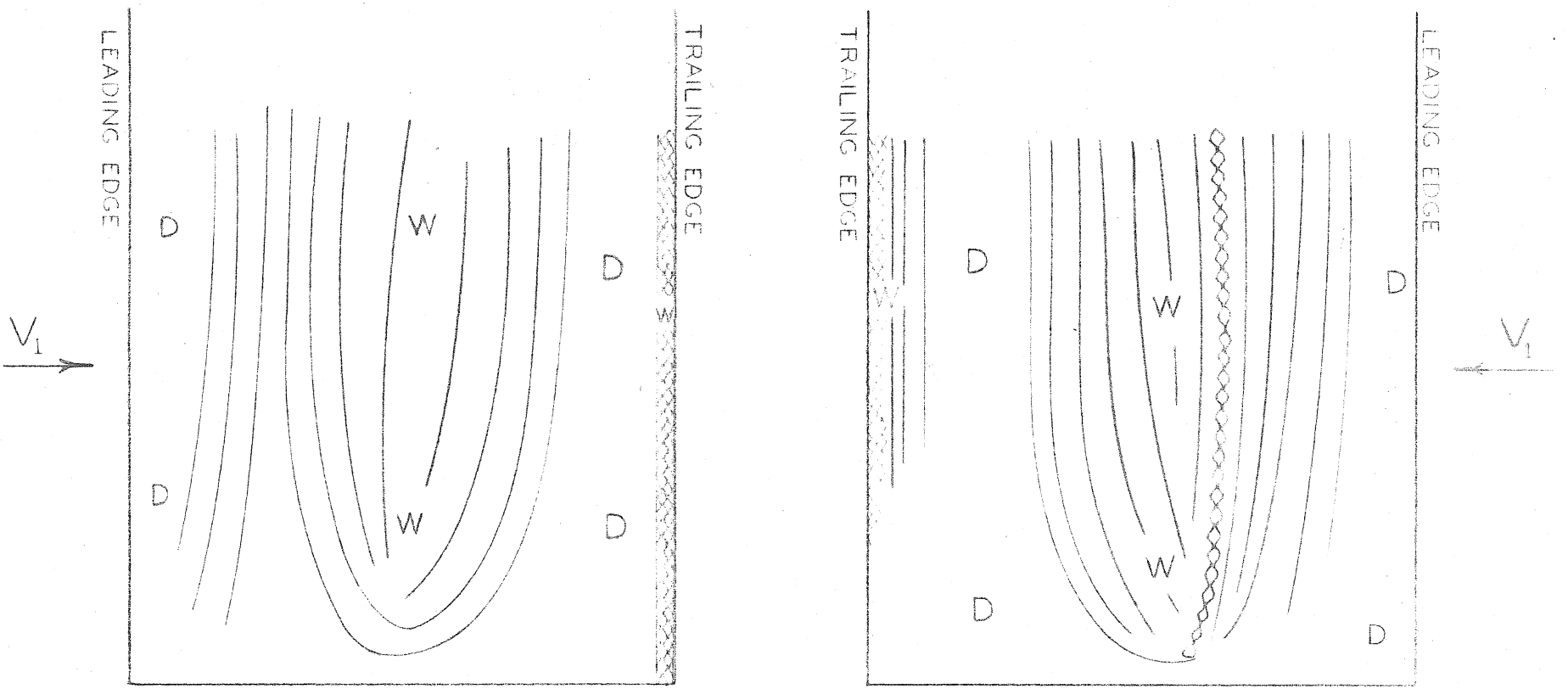

HIGH PRESSURE BLADE SURFACE

LOW PRESSURE BLADE SURFACE

KEY: D = DRY

W = WET

≈≈≈ = LIQUID BEADS

RESULTS OF FLUID EVAPORATION TESTS, $\alpha = 13\frac{1}{2}^\circ$

FIGURE 93

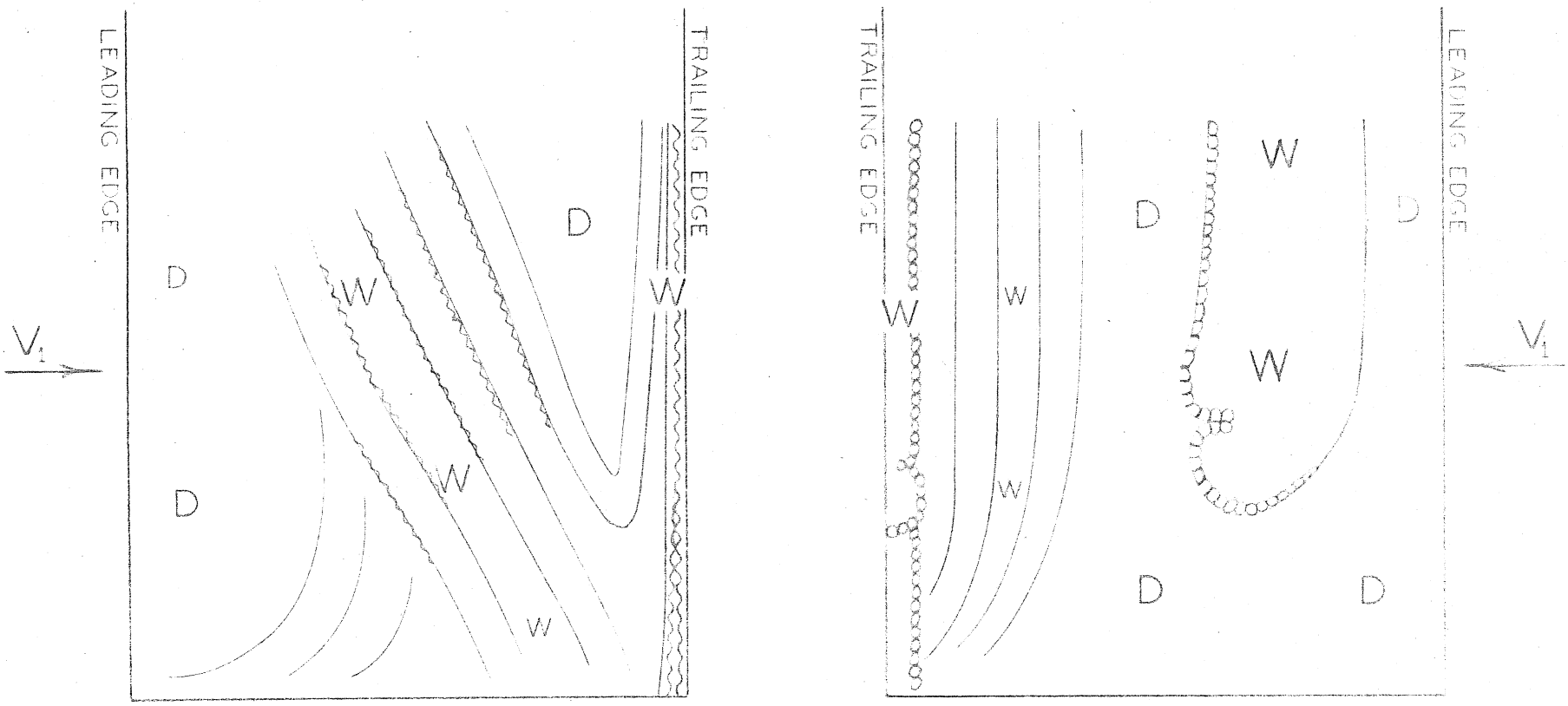

HIGH PRESSURE BLADE SURFACE

LOW PRESSURE BLADE SURFACE

KEY: D = DRY
W = WET
⋈ = LIQUID BEADS

RESULTS OF LIQUID EVAPORATION TESTS, $\alpha = 21\frac{1}{2}^\circ$

FIGURE 24

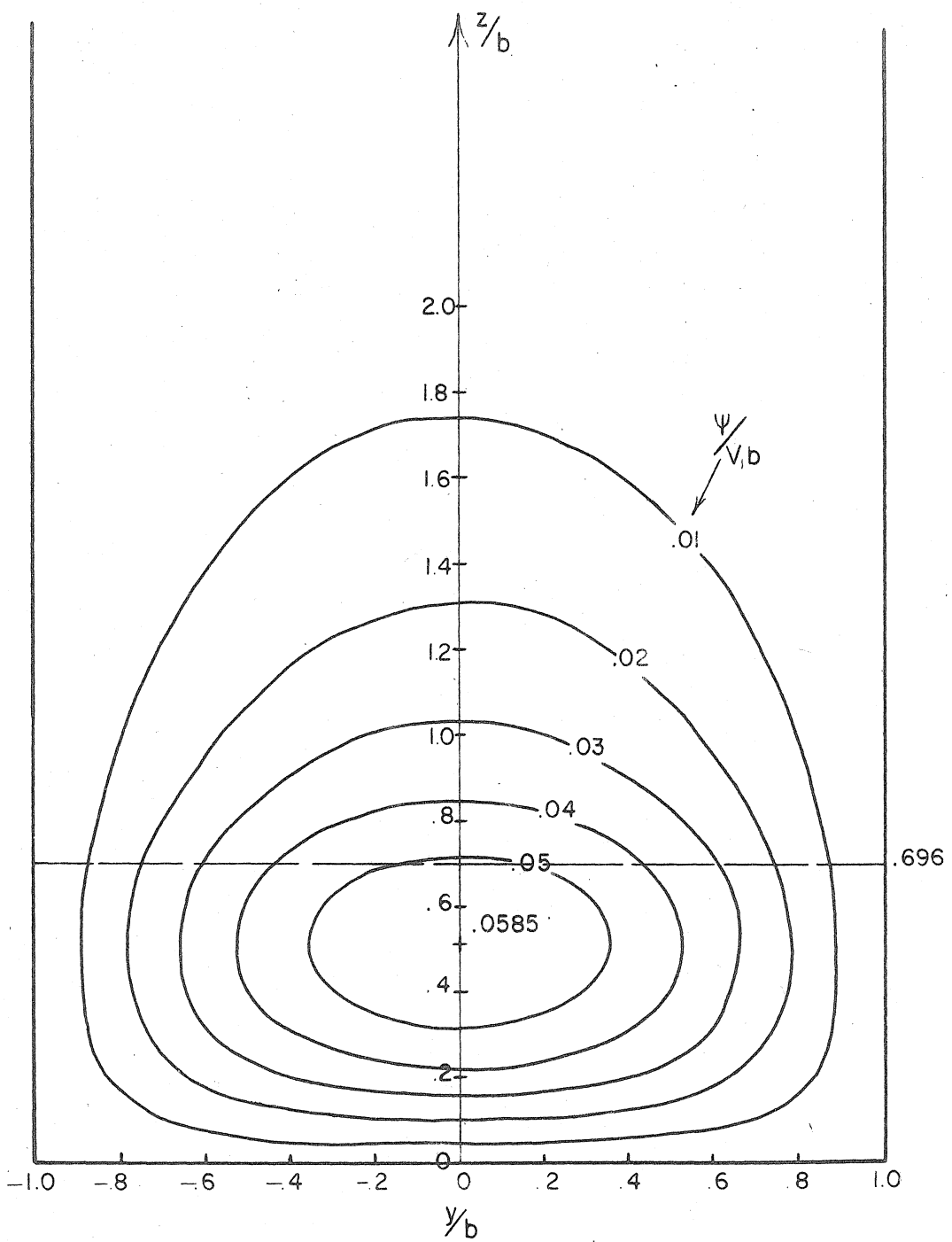

STREAM FUNCTION OF SECONDARY FLOW
FROM ANALYTICAL MODEL

FIGURE 95